

Editor-in-Chief B.E.Paton

Editorial board:

Yu. S. Borisov	V. F. Grabin
A. Ya. Ishchenko	V. F. Khorunov
B. V. Khitrovskaya	I. V. Krivtsun
S. I. Kuchuk	-Yatsenko
Yu. N. Lankin	V. K. Lebedev
V. N. Lipodaev	L. M. Lobanov
V. I. Makhnenko	A. A. Mazur
O. K. Nazarenko	I. K. Pokhodnya
I. A. Ryabtsev	Yu. A. Sterenbogen
N. M. Voropai	K. A. Yushchenko
A. T. Zelnichenko	

International editorial council:

N. P. Alyoshin	(Russia)
U. Diltey	(Germany)
Guan Qiao	(China)
D. von Hofe	(Germany)
V. I. Lysak	(Russia)
N. I. Nikiforov	(Russia)
B. E. Paton	(Ukraine)
Ya. Pilarczyk	(Poland)
P. Seyffarth	(Germany)
G. A. Turichin	(Russia)
Zhang Yanmin	(China)
A. S. Zubchenko	(Russia)

Promotion group:

V. N. Lipodaev, V. I. Lokteva
A. T. Zelnichenko (exec. director)
Translators:
I. N. Kutianova, V. F. Orets,
T. K. Vasilenko, N. V. Yalanskaya
Editor
N. A. Dmitrieva
Electron galley:
I. S. Batasheva, T. Yu. Snegiryova

Address:

E.O. Paton Electric Welding Institute,
International Association «Welding»,
11, Bozhenko str., 03680, Kyiv, Ukraine
Tel.: (38044) 287 67 57
Fax: (38044) 528 04 86
E-mail: journal@paton.kiev.ua
http://www.nas.gov.ua/pwj

State Registration Certificate
KV 4790 of 09.01.2001

Subscriptions:

\$324, 12 issues per year,
postage and packaging included.
Back issues available.

All rights reserved.

This publication and each of the articles
contained herein are protected by copyright.
Permission to reproduce material contained in
this journal must be obtained in writing from
the Publisher.

Copies of individual articles may be obtained
from the Publisher.

CONTENTS

SCIENTIFIC AND TECHNICAL

<i>Makhnenko O.V. and Makhnenko V.I.</i> Prediction of fatigue life of welded assemblies in bridge arched pillars	2
<i>Panin V.N.</i> Experimental-calculation estimation of residual welding distortions in shells of turbine penstocks at hydraulic power stations	7
<i>Fejnberg L.I., Rybakov A.A., Alimov A.N. and Rosert R.</i> Weld microalloying with titanium and boron in multiarc welding of large diameter gas and oil pipes	12
<i>Nazarenko O.K. and Lanbin V.S.</i> Investigation of high-voltage control circuits of welding electron beam current	17
<i>Ostsemin A.A.</i> Influence of surface defect on strength of welded joints with asymmetrical mechanical non-uniformity	21

INDUSTRIAL

<i>Grechanyuk N.I., Kucherenko P.P. and Grechanyuk I.N.</i> New electron beam equipment and technologies of producing advanced materials and coatings	25
<i>But V.S. and Olejnik O.I.</i> Main trends in technology for repair of active pressurised main pipelines	30
<i>Krivtsun I.V., Shelyagin V.D., Khaskin V.Yu., Shulym V.F. and Ternovoj E.G.</i> Hybrid laser-plasma welding of aluminium alloys	36
<i>Pokhodnya I.K., Yavdoshchin I.R., Marchenko A.E., Skorina N.V., Karmanov V.I. and Folbort O.I.</i> Low-hydrogen electrodes for repair of ships, metallurgical industry facilities and pipeline transport	40
<i>Zhadkevich M.L., Pereplyotchikov E.F., Puzrin L.G., Shevtsov A.V. and Yavorsky M.N.</i> Calculation of deposited layer thickness on components of oil-and-gas high-pressure valving	44
<i>Lankin Yu.N.</i> Computer system of monitoring the technological parameters of ESW	48

NEWS	51
------------	----

INFORMATION	57
-------------------	----

Developed at PWI	29, 50, 56
------------------------	------------



PREDICTION OF FATIGUE LIFE OF WELDED ASSEMBLIES IN BRIDGE ARCHED PILLARS

O.V. MAKHNENKO and V.I. MAKHNENKO
E.O. Paton Electric Welding Institute, NASU, Kiev, Ukraine

Fatigue life of welded assemblies in bridge arched pillar was predicted on the basis of the information on a range of loads and rated stresses in their joints.

Keywords: welded assemblies, range of loads, fatigue life of joints, cyclic strength, prediction by calculations

Welded structures are finding now an increasingly wide application in bridge construction. Figure 1 shows schematic of a gas-shielded welded assembly in arched pillar of low-alloy steel 10KhSND (GOST 6713-75), having the form of a shaped box girder and made from plates 32 mm thick. Longitudinal briquettes 20 mm thick are welded to a wall of the girder along axes 1 and 2 with T-joints No. 3 (Table 1) along the entire length, excluding regions between assembly points 82 and 213, and 597 and 433. Corresponding joints Nos. 2 and 22 (Table 1) are used between assemblies 82 and 213, and 597 and 433. Transverse briquettes are welded along axes 3 and 4 with joints Nos. 21 and 20.

It was necessary to estimate fatigue life of welded joints on a condition of initiating fatigue fractures at «hot» spots A and B (see Figures in Table 1), allowing for the corresponding normal rated membrane stresses.

Table 2 gives selected results of numerical analysis of the rated stressed state at the most characteristic points along axes 1-4 in a direction that promotes formation of fatigue cracks at spots A and B. In this case, the values of σ_1^r correspond to the distribution of stresses due to constant rated loads, and stresses σ_{tI}^r and σ_{tII}^r correspond to those due to extra temporary rated loads. Three variants of alternating loading cy-

cles with extreme cycle points can be distinguished from these data on the basis of stresses:

- 1) from $(\sigma_1^r + \sigma_{tI}^r)$ to σ_{tr}^r , $\Delta\sigma_1 = |\sigma_{tr}^r|$;
 - 2) from $(\sigma_1^r + \sigma_{tII}^r)$ to σ_1^r , $\Delta\sigma_2 = |\sigma_{tII}^r|$;
 - 3) from $(\sigma_1^r + \sigma_{tI}^r)$ to $(\sigma_1^r + \sigma_{tII}^r)$,
- $$\Delta\sigma_3 = |\sigma_{tI}^r - \sigma_{tII}^r|,$$

where $\Delta\sigma_j$ is the amplitude of variations of stresses in cycle $j = 1-3$. Maximal and minimal values of σ_{max}^j and σ_{min}^j are determined by the above extreme points depending upon the values of σ_1^r , σ_{tI}^r and σ_{tII}^r (Figure 2).

Longitudinal normal rated stresses along axes 1 and 2, according to the data of numerical analysis, are characterised by the values of $\sigma_1^r = -134.9$ MPa at $\Delta\sigma = 20.8$ MPa, which insignificantly vary over the welded joints along axes 1 and 2. It was necessary to estimate the fatigue life of the welded joints under consideration, proceeding, first, from the most conservative variant of cyclic loading (1) by the set values of Table 2, and then at points where the calculated fatigue life does not meet a requirement of $2 \cdot 10^6$ cycles, and make a more exact calculation on the basis of loading cycle (1) at different fractions α_j of the amount of the j -th component of a range.

Calculation procedure. Procedure developed by the International Institute of Welding for estimation of service life of welded joints of the type given in Table 1, based on initiation of a fatigue crack in the weld to base metal transition zone («hot» spots A or B), was used to determine fatigue life of these welded joints, for which the crack-like defects of the type of lacks of fusion are inadmissible. This procedure generalised a large amount of experimental studies for typical welded joints, which allows formulation of recommendations for each of them on determination of permissible amplitude of rated stresses under regular loading in the following form:

$$[\Delta\sigma] = \frac{FAT f_1(R) f_2(N) f_3(\partial) f_4(T)}{\gamma_M}, \quad (2)$$

where FAT is the class of a joint or permissible amplitude of stresses for a given joint on a base of $2 \cdot 10^6$ regular loading cycles (constant parameters of a load-

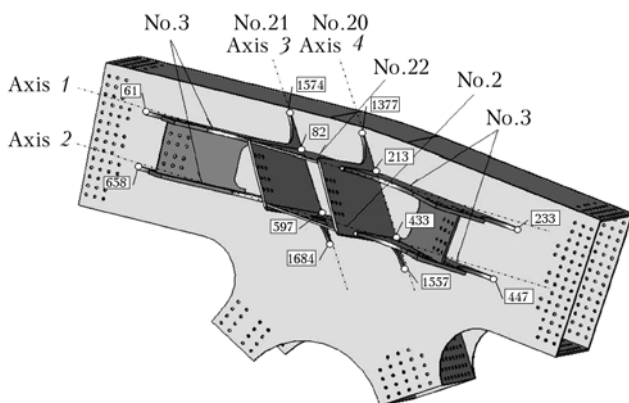


Figure 1. Schematic of welded assembly in an arched pillar with indication of axes 1-4, along which it is necessary to estimate fatigue life of welded joints Nos. 2, 3 and 20-23 (numerals in boxes — reference points, assemblies)



Table 1. Welded joints subject to strength design

Weld No.	Standard	Drawing of welded joint	Characteristics allowed for in calculation	Location of assembly in schematic
<i>Standard</i>				
2	GOST 23518-79		Two-sided welded T-joint with one-sided bevel. Full penetration	Along axis 2; between assemblies 597 and 433
3	GOST 23518-79		Two-sided welded T-joint with two-sided bevel. Full penetration	Along axis 1; between assemblies 61 and 82, and 213 and 233. Along axis 2; between assemblies 658 and 597, and 433 and 447
<i>Non-standard (gas-shielded arc welding)</i>				
20	GOST 14771-76*		Full penetration	Along axis 4; between assemblies 1377 and 1557
21	GOST 14771-76*		Same	Along axis 3; between assemblies 1574 and 1684
22	GOST 14771-76*		»	Along axis 1; between assemblies 82 and 213



Table 2. Initial value of rates stresses in transverse section of the weld along axes 1–4

No.	Axis 1			Axis 2				
	Node No. (FEM)	σ_I^r , MPa	σ_{I1}^r , MPa	σ_{I11}^r , MPa	Node No. (FEM)	σ_I^r , MPa	σ_{I1}^r , MPa	σ_{I11}^r , MPa
1	61	3.4	1.5	1.0	658	3.0	1.2	1.0
2	82	8.4	-12.7	0.5	5220	-53.7	-26.6	-2.5
3	76	-40.0	-25.1	-1.6	672	-53.5	-29.2	-2.8
4	7130	-35.6	-29.4	-1.9	5217	-52.9	-32.2	-3.1
5	77	-39.9	-32.2	-2.9	673	-51.7	-39.3	-3.3
6	7126	-30.5	-34.5	-2.2	5214	-49.8	-35.1	-3.4
7	78	-24.6	33.4	-1.9	674	-47.2	-34.0	-3.3
8	7124	-13.7	-28.1	-1.3	5211	-43.0	-30.7	-3.0
9	79	-6.4	-2.34	-0.7	597	21.4	0.4	0.2
10	213	24.9	4.5	2.7	433	-25.5	-2.6	-1.0
11	233	1.6	0	0	447	5.5	0.5	1.0

Table 2 (cont.)

No.	Axis 3			Axis 4				
	Node No. (FEM)	σ_I^r , MPa	σ_{I1}^r , MPa	σ_{I11}^r , MPa	Node No. (FEM)	σ_I^r , MPa	σ_{I1}^r , MPa	σ_{I11}^r , MPa
1	1574	1.0	0	0	1377	0.7	0.1	0.1
2	1578	11.2	3.5	1.7	1404	43.7	5.3	2.7
3	1657	41.6	1.6	1.5	6773	34.4	4.7	2.7
4	2549	43.6	1.4	1.1	3214	48.2	6.6	2.7
5	2552	43.2	1.6	0.9	3207	49.8	6.7	2.5
6	2555	41.3	1.9	0.7	1403	49.4	6.4	2.6
7	1656	43.3	1.4	1.3	1402	49.7	6.9	2.5
8	1654	42.4	1.7	0.8	1401	48.1	7.1	2.3
9	1653	39.6	2.1	0.8	1399	40.2	7.2	1.6
10	1652	33.3	2.7	5.5	433	-25.5	2.6	-1.0
11	1684	1.8	0	0	1557	1.7	0.3	0.1

ing cycle) at $f_1 = f_2 = f_3 = f_4 = \gamma_M = 1.0$; and γ_M is the safety factor.

The given IIW document* comprises a table of the FAT values for different typical welded joints. The

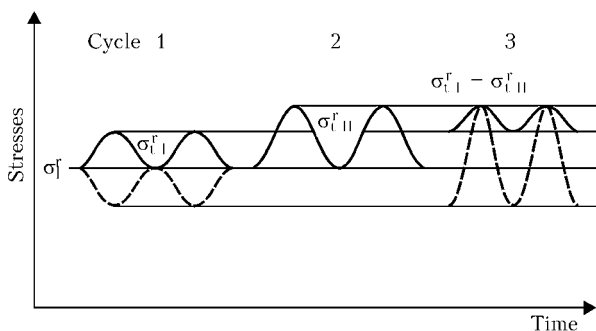


Figure 2. Graphic interpretation of loading cycles (1) at identical (solid curve) and different (dashed curve) signs of σ_I^r

* (2002) Recommendations for fatigue design of welded joints and components. IIW Doc. XIII-1539-96/XV-845-96. 153 p.

joints considered, given in Table 1, provided that they have no lacks of fusion and were made in flat position, correspond to a variant of weld No. 411, for which $FAT = 80$ MPa (Table 3). If the weld to base metal transition zone is not treated, the welded joints correspond to No. 412, and $FAT = 71$ MPa (assume that $FAT = 71$ MPa for the welded joints under consideration).

In expression (2), factor $f_1(R)$ allows for the effect of the loading cycle asymmetry:

$$R = 1 - \frac{\Delta\sigma}{\sigma_{max}} \tag{3}$$

as well as the level of residual stresses in the joining zone.

If residual stresses are not in excess of $0.2\sigma_y$ ($\sigma_y \approx 400$ MPa for steel 10KhSND), then, according to the IIW document:



Table 3. Types of welded joints and corresponding values of FAT for a case of arched pillar

Weld No.	Drawing of joint	Characteristics	FAT, MPa
411		Cruciform or T-joint with K-groove of adjoining elements, full penetration, displacement $e < 0.15t$. Transition zone is treated	80
412		Same as for No. 411, but transition zone is non-treated	71
323		Longitudinal continuous fillet welds, manual welding with or without K-groove (stresses in flange)	90
522		Longitudinal gasket with radius $r > 150$ mm is welded with fillet welds, welds are treated, $c < 2t$, $c_{max} = 25$ mm	90

$$\begin{aligned}
 f_1(R) &= 1.6 \text{ for } R < -1.0; \\
 f_1(R) &= -0.4R + 1.2 \text{ for } -1.0 \leq R \leq 0.5; \\
 f_1(R) &= 1.0 \text{ for } R > 0.5.
 \end{aligned}
 \tag{4}$$

$$f_2(N) = \left(\frac{C}{N} \right)^{1/m}, \tag{5}$$

If residual stresses are higher than $0.2\sigma_y$ (approximately 80 MPa for the case under consideration), or a combination of two- or three-dimensional elements takes place, then $f_1(R) = 1.0$, i.e. the value of factor $f_1(R)$ for relationship (2) is minimal. It can be assumed that $f_1(R) = 1.0$ for the case under consideration.

Factor $f_2(N)$ allows for a limited fatigue. In a range of $10^4 < N < 5 \cdot 10^6$ cycles, according to the IIW procedure (Figures 3 and 4), $f_2(N)$ is determined by the following dependence:

where N is the fatigue life of a welded joint; $C = 2 \cdot 10^6$, $m = 3$ at $10^4 < N < 5 \cdot 10^6$ cycles, and $C = 2.54 \cdot 10^6$, and $m = 5$ at $5 \cdot 10^6 < N < 10^8$ cycles.

Correction for thickness of an adjoining element, where the fatigue crack initiates, is $f_3(\delta) = 1.0$, if thickness $\delta < 25$ mm. At large thicknesses

$$f_3(\delta) = \left(\frac{25}{\delta} \right)^{0.3}. \tag{6}$$

For the joints considered, $f_3(\delta) = 1.0$.

Factor $f_4(T)$ allows for working temperature T in operation of a joint. According to the IIW document, it can be assumed that $f_4(T) = 1.0$ at $T < 100$ °C.

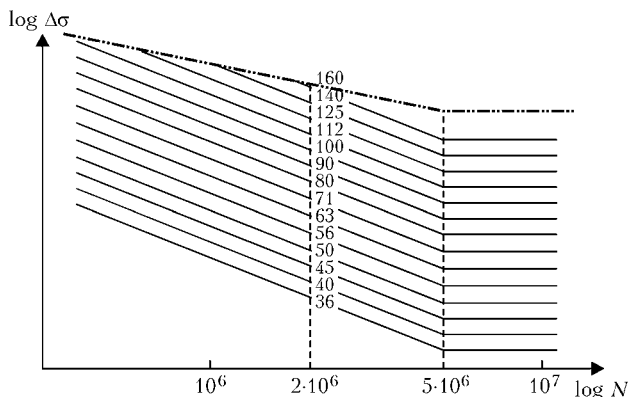


Figure 3. Generalised Weller curves for different FAT (steel) at $m = 3$ for normal rated stresses at $N < 5 \cdot 10^6$ cycles

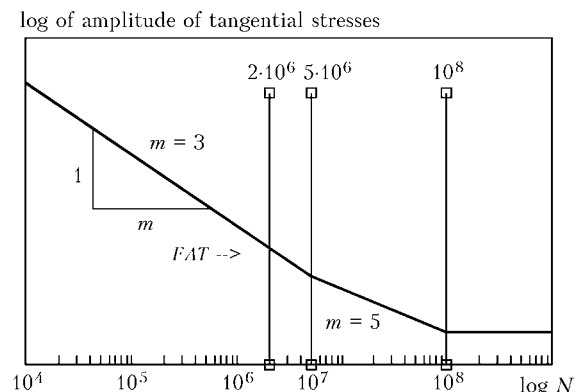


Figure 4. Weller curve for some FAT at $N < 10^8$ cycles



Allowing for the above-said, relationship (2) for the welded joints considered can be written down as follows:

$$[\Delta\sigma] = \frac{FAT}{\gamma_M} \left(\frac{C}{N} \right)^{1/m} \quad (7)$$

Accordingly, limiting fatigue life N_j under regular loading with amplitude $\Delta\sigma_j$ from (7) can be expressed as follows:

$$N_j = C \left(\frac{FAT}{\Delta\sigma_j \gamma_M} \right)^m \quad (8)$$

When selecting safety factor γ_M , it is necessary to take into account that it is recommended that FAT be at a level of 0.95 of the probability of non-fracture according to the experimental data. Therefore, it is recommended in the document that γ_M be selected in a range of 1.0–1.4 ($\gamma_M = 1.4$ corresponds to a case where there is a threat to the human life).

Accordingly, assuming that $\gamma_M = 1.4$ and $FAT = 71$ MPa, it will yield from (8) that

$$N_j = C \left(\frac{51}{\Delta\sigma_j} \right)^m \quad (9)$$

where $C = 2 \cdot 10^6$, $m = 3$ at $10^4 < N_j < 5 \cdot 10^6$ cycles; and $C = 2.54 \cdot 10^6$, $m = 5$ at $5 \cdot 10^6 < N_j < 10^8$ cycles.

Dependence (9) can be used to estimate fatigue life using the most conservative variant of regular cyclic loading (1) from the data of Table 2.

In the case of allowance for a loading range of three regular cycles described by relationships (1), fatigue life N_{range} is determined by linear summation of damageabilities (Palmgren–Mainer method):

$$\sum_{j=1}^M \frac{n_j}{N_j} = 1, \quad (10)$$

where n_j is the quantity of the j -th cycles with amplitude $\Delta\sigma_j$.

If $n_j = \alpha_j N_{range}$, where α_j is the fraction of the j -th load in total loading on a base of N_{range} , it follows from (10) that

$$N_{range} = \left(\sum_{j=1}^M \frac{\alpha_j}{C_j [51 / (\Delta\sigma_j)]^{m_j}} \right)^{-1} \quad (11)$$

As to procedural issues of estimation of cyclic strength of the joints under consideration, along axes 1 and 2 over the welds (see Figure 1), according to the initial data the rated constant stresses $\sigma_{zz}^r = -134.9$ MPa with amplitude $\Delta\sigma^r = 20.8$ MPa are effective along the above axes in a wall of the pillar assembly 32 mm thick, whereto the adjoining elements are welded with welds Nos. 2, 3 and 22. Such loading may induce transverse fatigue cracks. It is suggested that the probability of initiation of such cracks should also be estimated on the basis of FAT for this type of the joints. Far from the ends, the joints considered correspond to No. 323 and have a value of $FAT = 90$ MPa. At the end of the adjoining welded element, having a smooth transition with radius $r > 150$ mm (Table 3), the welded joints correspond to No. 522 and have a value of $FAT = 90$ MPa. It should be noted that high negative stresses σ_{zz}^r do not prevent initiation of the fatigue damage, as high tensile residual stresses (at a level of σ_y of the base material, i.e. approximately 350–400 MPa) are effective in this zone. Therefore, the real loading cycle will take place within the tensile zone at $R > 0.5$, i.e. $f_1(R) = 1.0$ in dependence (2) for the permissible value of $[\Delta\sigma]$.

The similar situation takes place also in transverse loading of the welded joints considered, where (see Table 2) the rated constant stresses in the negative zone amount to -53 MPa. Although the transverse residual stresses in welding rarely exceed $0.5\sigma_y$

Table 4. Calculated fatigue life for points along axes 1–4 (see Table 2)

No.	Axis 1			Axis 2		
	N_1 , cycle	N_2 , cycle	N_3 , cycle	N_1 , cycle	N_2 , cycle	N_3 , cycle
1	$> 10^8$	$> 10^8$	$> 10^8$	$> 10^8$	$> 10^8$	$> 10^8$
2	$> 10^8$	$> 10^8$	$> 10^8$	$6.8 \cdot 10^7$	$> 10^8$	$7.4 \cdot 10^7$
3	$9.1 \cdot 10^7$	$> 10^8$	$9.7 \cdot 10^7$	$4.3 \cdot 10^7$	$8.4 \cdot 10^7$	$4.6 \cdot 10^7$
4	$4.1 \cdot 10^7$	$7.3 \cdot 10^7$	$4.4 \cdot 10^7$	$2.6 \cdot 10^7$	$5 \cdot 10^7$	$2.8 \cdot 10^7$
5	$2.6 \cdot 10^7$	$4.7 \cdot 10^7$	$2.8 \cdot 10^7$	$1.9 \cdot 10^7$	$3.6 \cdot 10^7$	$2.1 \cdot 10^7$
6	$1.9 \cdot 10^7$	$3.3 \cdot 10^7$	$2 \cdot 10^7$	$1.7 \cdot 10^7$	$3.2 \cdot 10^7$	$1.8 \cdot 10^7$
7	$2.2 \cdot 10^7$	$3.8 \cdot 10^7$	$2.3 \cdot 10^7$	$2 \cdot 10^7$	$3.8 \cdot 10^7$	$2.2 \cdot 10^7$
8	$5.2 \cdot 10^7$	$8.8 \cdot 10^7$	$5.6 \cdot 10^7$	$3.3 \cdot 10^7$	$6.3 \cdot 10^7$	$3.6 \cdot 10^7$
9	$> 10^8$	$> 10^8$	$> 10^8$	$> 10^8$	$> 10^8$	$> 10^8$
10	$> 10^8$	$> 10^8$	$> 10^8$	$> 10^8$	$> 10^8$	$> 10^8$
11	$> 10^8$	$> 10^8$	$> 10^8$	$> 10^8$	$> 10^8$	$> 10^8$

Notes. 1. N_1 --- minimal fatigue life of three cycles (1); N_2 --- fatigue life for a range of loads according to variant 2; N_3 --- same according to variant 3. 2. For axes 3 and 4 the values of fatigue life for all the cycles are (N_1 , N_2 and N_3) $> 10^8$.



(~ 170 MPa), cyclic loading at the above values of σ_j^r occurs in the tensile zone.

Results of fatigue design of welded joints in an assembly of arched pillar. Table 4 gives results of calculation of minimal fatigue life N from dependence (9) for variants 1, the initial data for which are given in Table 2. This most conservative variant of regular cyclic loading yields fatigue life N above 10^7 ($1.7 \cdot 10^7$) cycles at all the points of welded joints Nos. 2, 3 and 20–22 along axes 1–4 (see Figure 1). To compare, the Table also gives fatigue life N_{range} from dependence (11) for a range of cyclic loads (1) in each assembly. The values of α_j were assumed to be within the following limits:

- variant 2: $\alpha_j = 0.9$ for $\Delta\sigma_{\text{max}}$, the rest --- 0.05
- variant 3: $\alpha_j = 1/3$ for $j = 1-3$.

It can be seen that the applied loading range schemes yield less conservative results on the calculated fatigue life, compared with the extreme variant of regular cyclic loading (1).

For welded joints Nos. 2, 3 and 22 along axes 1 and 2 (see Figure 1), the fatigue life from the condition of formation of transverse fatigue cracks is determined from (8):

$$N = C \left(\frac{FAT f_3(\delta)}{\Delta\sigma \gamma_M} \right)^m, \quad (12)$$

where $C = 2 \cdot 10^6$, $m = 3$ at $10^4 < N < 5 \cdot 10^6$ cycles, or $C = 2.54 \cdot 10^6$, $m = 5$ at $5 \cdot 10^6 < N < 10^8$ cycles; $FAT = 90$ MPa; $f_3(\delta)$ is determined from (6), i.e. $f_3(\delta) = (25/32)^{0.3} = 0.93$; $\Delta\sigma = 20$ MPa; and $\gamma_M = 1.4$.

Accordingly, the fatigue life from (12) will be

$$N = C \left(\frac{918 \cdot 0.93}{208 \cdot 1.4} \right)^m = 5.5 \cdot 10^8 \text{ (cycles)}.$$

It can be noted in conclusion that the results of calculation of fatigue life of welded joints Nos. 2, 3 and 20–22 along axes 1–4 in a welded assembly of the arched pillar, based on the set loads and recommendations of the International Institute of Welding developed on the grounds of a very conservative generalisation of experimental data generated for typical welded joints, show the following:

- fatigue life of the above welded joints under the effect of transverse rated stresses is not worse than $1.7 \cdot 10^7$ cycles;
- fatigue life of welded joints along axes 1 and 2 under the effect of longitudinal rated stresses is not lower than 10^8 cycles.

EXPERIMENTAL-CALCULATION ESTIMATION OF RESIDUAL WELDING DISTORTIONS IN SHELLS OF TURBINE PENSTOCKS AT HYDRAULIC POWER STATIONS

V.N. PANIN

Open Joint Stock Company «Prometej», Chekhov, Russian Federation

Application of electroslag welding in fabrication of shells of turbine penstocks at hydraulic power stations leads to a change in their shape under the effect of residual welding distortions. Given are the calculated dependencies of changes in shape of the shells, allowing for their geometric dimensions and technological factors.

Keywords: electroslag welding, turbine penstocks, shells, residual welding distortions, sag, calculation of changes in shape

Shells of turbine penstocks are components of water channels of hydraulic power stations, and they are fabricated directly at a work site of facilities being constructed. Schematics of the shells and their geometric characteristics are given in Figure 1 and in the Table. One of the most common technological variants of their fabrication provides for assembly of the shells of separate elements (sections) in the vertical position and subsequent electroslag welding of slot joints.

Application of welding for the fabrication of such structures is known [1, 2] to lead to changes in their shape because of the presence of residual welding distortions. Available calculation diagrams for prediction

of distortions relate mostly to ship structures. Moreover, they are valid for manual arc and automatic submerged-arc welding, where the welding heat input is much lower compared with electroslag welding. As to the shells of turbine penstocks made by electroslag welding, the available data are only of an experimental character.

The purpose of this study was to derive calculation dependencies of changes in shape of the shells upon their geometric dimensions (length, diameter, thickness), as well as technological factors in their fabrication.

Measurements of distortions were made on full-scale shells. Parameters of electroslag welding of slot joints corresponded to the standard technology. In addition, the latter provided for minimisation of the effect of transverse strains formed in a joint during

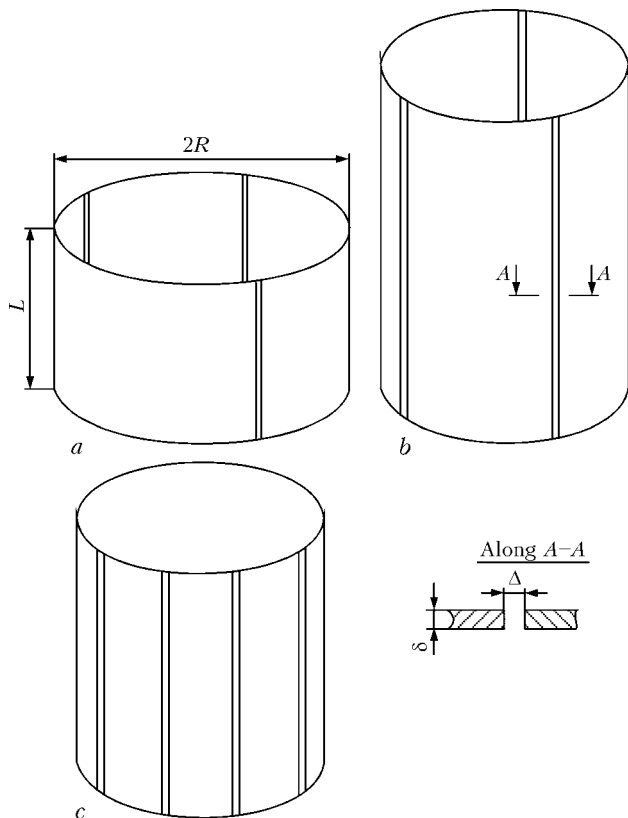


Figure 1. Schematic of experimental turbine penstocks used at hydraulic power stations: *a* — shells with variable L/R and thickness δ ; *b* — link with longitudinal «shell» sections $L/R = 2$, $\delta = 25$ mm; *c* — link with longitudinal sections $L/R = 1$, $\delta = 25$ mm

welding as a result of installing stiffeners in the form of clamps over the entire length of the joint. Therefore, the main changes in shape were caused by the presence of a longitudinal field of stresses and showed up in displacement of the joint out of plane.

Measurements of sags were made before and after welding using a metal ruler and string immediately within the region of the joint, and at a certain distance from it over the preliminarily deposited grid. Difference between these measurements was taken as an actual value of the sag. Welding parameters, as well as sizes of the gaps in a joint before and after welding were thus fixed. Results of the measurements after

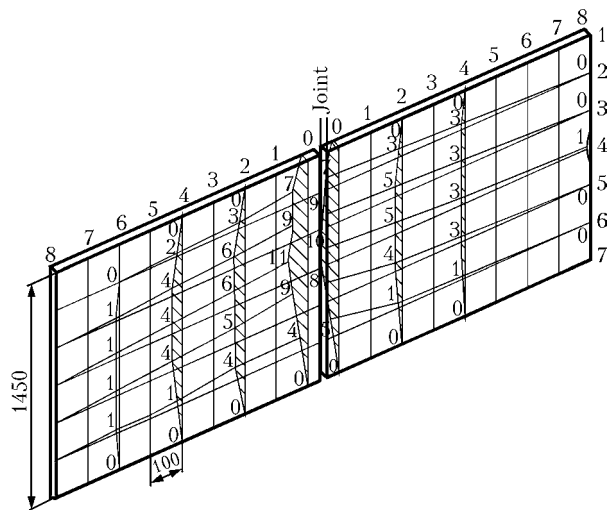


Figure 2. Diagram of distribution of sags in a shell during electroslag welding of a longitudinal joint ($D = 6000$ mm, $\delta = 25$ mm)

processing were presented in the form of a scan diagram of the shell (Figure 2). Results of measurements of 20 sags of the shells with different geometric dimensions were processed by a similar diagram. The resulting data on maximal sags were subjected to statistical processing [3].

The data of calculations of confidence intervals show that the maximal sags vary over rather wide ranges at a mean variation coefficient of 15–30 %. In such a wide range of changes in sags, comparison by the criteria of equality of variances and mean values shows insignificance of the effect by geometric parameters of the shells on the sag values. This is attributable to the fact that in field welding of the shell structures under consideration a substantial effect on the values of the sags is exerted by the main parameters of the welding process, and the energy input in particular. The latter depends upon the heat input in welding, which in turn is determined by the welding conditions (current, voltage, welding speed, etc.). Variations in the welding speed within the ranges under consideration (2.5–4.0 m/h) decreases the sag from 2 to 3 times. At the same time, as found out in the course of the work, the gaps in longitudinal joints vary over substantial ranges (20–32 mm), which ex-

Geometric characteristics of shells and mean sags

No.	Shell size $(D - L) \times \delta$, mm	Average sag size f , mm	Root-mean-square deviation S , mm	Range of sag in 95 % confidence interval $f \pm 2S$, mm
1	$(6000 - 1450) \times 25$	7.6	1.9	4–12
2	$(6000 - 3000) \times 25$	10.2	3.2	4–12
3	$(6000 - 3000) \times 25$	9.4	3.3	3–16
4	$(6000 - 6000) \times 25$	19.3	—	—
5	$(6000 - 2000) \times 22$	7.7	2.1	4–12
6	$(6000 - 1680) \times 36$	8.5	1.6	5–12
7	$(6000 - 2300) \times 32$	7.8	1.0	6–10

Notes. 1. No. 3 was welded using powder additive. 2. D — diameter; L — length; δ — thickness of the shell

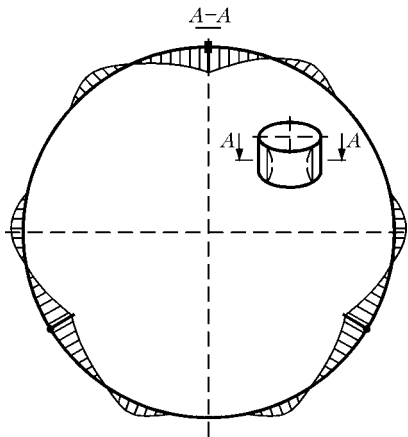


Figure 3. Character of changes in shape of a shell in plane of maximal sags of longitudinal welds on shells of pipeline sections

ceeds the standard requirements for the electroslag welding technology (24 ± 2 mm). In this case the value of the energy input depending upon the gap within the said ranges for a 25 mm thickness of the base metal varies on the average 1.5–2 times. The similar situation is observed with other thicknesses as well.

To increase purity of the experiments, several shells with joints were assembled with the same gaps (26 mm), and welded under identical conditions. In this case the sag varied within 1 mm, and the variation coefficient was 6–7 %, which is 2–4 times lower than the above-mentioned general level of the variation coefficients.

Therefore, the above-noted insignificance of the effect of geometric dimensions of the shells on the sag values is a result of changes in welding energy input, which in turn depends upon the sizes of the gaps in a joint, thickness of the metal welded, and heat input. At the same time, meeting of the standard requirements to preparation of joints for welding leads to stability of the welding energy input over the entire length of a joint, which causes a substantial decrease in the coefficient of variation of residual sags. In the situation of constant energy inputs, the values of residual sags and, hence, variations in shape of the entire shell will be determined by its geometric dimensions.

Also, it should be noted that the said changes in shape of the shell is of a complex character. In the plane of minimal sags, the shell has a curvilinear profile with internal concavity in the region of a joint, with distance from which the sign of residual distortions changes into the opposite (outward convexity), distortions being subsequently decreased to zero (Figure 3). The value of B , which determines the zone of resistance of the shell to changes in its shape, and where the value of the sag changes from maximum (within the joint zone) to zero, as shown by experimental data, is minimal at a maximal sag, and vice versa (Figure 4).

If length L of the shall is smaller than its diameter $2R$, longitudinal shortening of a slot welded joint will be taken up not by the entire section of the shell, but only by its regions lying to the right and left from

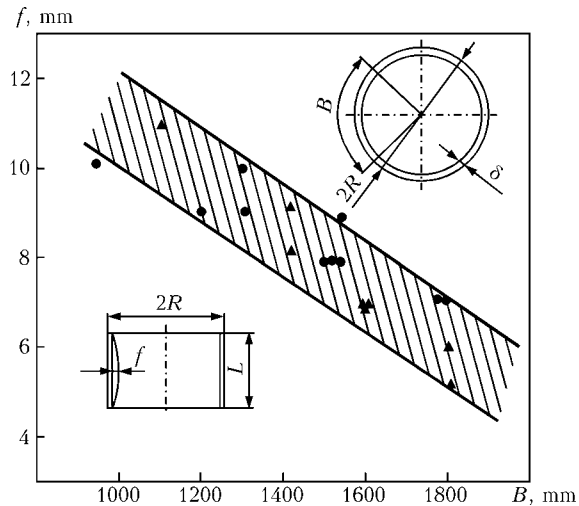


Figure 4. Dependence of sag f upon parameter B for electroslag welded joints in shells: ● — metal thickness 36 mm; ▲ — 25 mm

the welded joint with total length B (Figure 5). In this case, local shortening and bending distortions can be determined using the following formula:

$$f = \frac{\phi L}{8} = \frac{VL^2 z}{8J}, \quad (1)$$

where J is the moment of inertia of an annular section of the shell with width B , which resists bending due to longitudinal shortening of the welded joint, cm^3 ; z is the distance from the centre of gravity of the volume to intersection of the central axis with the internal wall of part of the shell with width b , cm ; f is the sag of a slot in the plane passing through the slot line and cylinder axis, cm ; and V is the running volume of the longitudinal shortening, cm^3 . It holds for structures of low-carbon and low-alloy steels

$$V \cong 3.6 \cdot 10^6 q_p, \quad (2)$$

where q_p is the energy input due to one pass, cal/cm . Using relationship

$$\frac{z}{J} = \frac{30}{\delta R^2 \alpha^3} \quad (3)$$

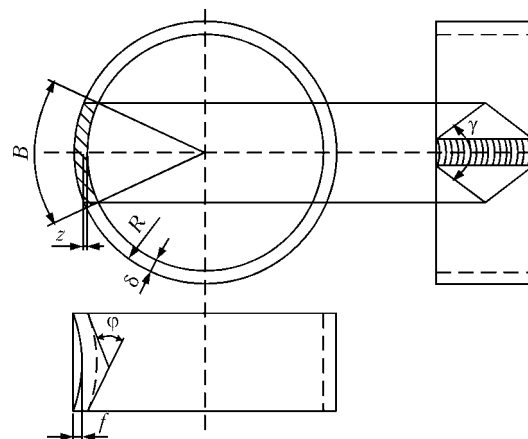


Figure 5. Schematic of width B of the shell resisting bending due to longitudinal shortening of the slot welded joint (see the rest of the designations in the text)



and data of experimental studies, the author of [1] established the following relationship for sag of the slot joints for the case of short shells ($L < 2R$):

$$f = \frac{15}{4} \frac{VR}{K^3 \delta L} \cong 14 \frac{VR}{\delta L}, \quad (4)$$

which is valid on a condition of $\alpha = K \frac{L}{R}$, where $K \cong \cong 0.65$.

Verification of applicability of formula (4) for calculation of sags of the slot welds in the shells considered in the present study shows that the calculation data do not correspond to the experimental ones. Moreover, variations in the calculated and experimental sags are of an opposite character. Analysis of formula (4) shows that the sag grows and tends to infinity with decrease in the L/R ratio. It is likely that the said relationship was derived on the basis of measurements of the shells in a narrow region of variations in their geometric parameters and welding conditions, which will be considered below in more detail.

For further consideration, let us combine formulae (1)–(3) and make some re-arrangement of their terms:

$$f = 13.5 \cdot 10^{-6} \frac{q_p}{\delta} \frac{L^2}{R^2} \frac{1}{\alpha^3}. \quad (5)$$

However, to calculate sag f from formula (5), it is necessary to know variations in angle α depending upon the geometric dimensions of the shell, and length L and radius R in particular. Dependence of angle α upon the above parameters follows from an a priori statement that the longer the shell, the larger the part of its cross section that is involved into resistance to the longitudinal shortening of a welded joint [1]. When solving the inverse problem by substituting mean experimental values of sag f and known values of the L/R ratio, as well as mean values of the used welding energy inputs, it is possible to determine dependence of actual angle α upon L/R , which is shown in Figure 6. It can be seen from the Figure that the trend to increase in angle α persists with increase in L/R . However, in our case the character of variations in the value of α differs from the linear one. The α

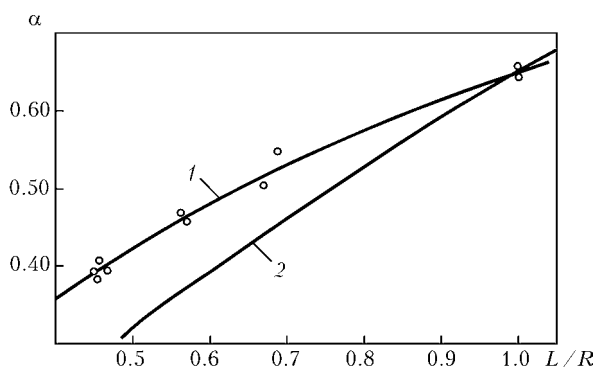


Figure 6. Calculated dependence of angle α upon the ratio of geometric dimensions of the shell L/R : 1 — calculation data of the present study ($\alpha = 0.65(L/R)^{0.63}$); 2 — calculation data of study [1] ($\alpha = 0.65(L/R)$); points — experiment

versus L/R curve is approximated by the following expression:

$$\alpha = 0.65 \left(\frac{L}{R} \right)^{0.63}. \quad (6)$$

By substituting the derived expression to formula (5), after transformation, we obtain the following empirical dependence:

$$f = 49.2 \cdot 10^{-6} \frac{q_p}{\delta} \left(\frac{L}{R} \right)^{0.11}. \quad (7)$$

Analysis of formula (7) shows that the effect on the sag by geometric parameters R and L is negligible, but the sag is determined to a higher degree by specific heat input q_p/δ . The calculation nomogram for determination of maximal sag f depending upon energy input q_p , metal thickness δ and ratio L/R was plotted on the basis of expression (7) (Figure 7). Specific energy input q_p/δ is determined from the known shell metal thickness, ratio L/R and real energy input; and then maximal sag f is determined from ratio L/R . The $q_p/\delta = f(q_p, \delta)$ plot comprises a dashed region that determines energy inputs of the most common parameters of electroslag welding (at electrode feed speed $v_e = 360$ – 430 m/h, electrode diameter 3 mm, welding current $I_w = 650$ – 750 A, and weld edge gap $\Delta = 24$ mm). If the gap size differs from the above one, the value of q_p or q_p/δ should be multiplied by correction coefficient K_Δ (dependence of K_Δ upon the gap is shown in the nomogram).

As seen from the nomogram, the gaps for almost all thicknesses of the shell metal under consideration, with different ratios L/R , change within a narrow interval over the range of the welding conditions used. However, changes of the gap in a joint and, as a result, welding energy input (beyond the standard one) cause a substantial growth of the sag.

As follows from the calculation formula and analysis of the nomogram, the most rational way of decreasing the sag of longitudinal joints in the shells welded by the electroslag method is to decrease the energy input. As in the course of the experiments conducted in this study we used the minimal possible energy inputs for welding with the 3 mm diameter wire, it is almost impossible to decrease the level of distortion on the given shells using the traditional welding technology. However, it can be much decreased by using welding with a larger, i.e. 4–5 mm, diameter wire, by reducing the gap, using powder additive, additional heat sink (sprayer), etc.

It should be noted that dependence (7) can be used with a certain correction also to calculate distortions of the thin shells welded by other welding methods, which is confirmed by comparing the calculation data on the shells given in study [1].

It can be seen from Figure 8 that the calculated values of sags determined from formulae (4) and (7) are very close to the limit of the field of scatter of

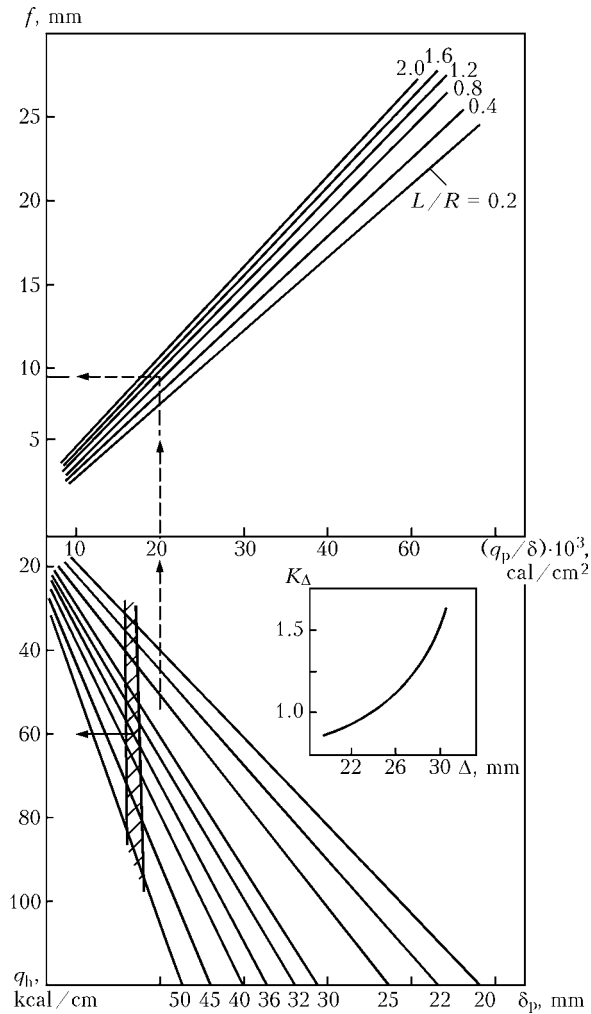


Figure 7. Nomogram for determination of maximal sag f in electroslag welding of a longitudinal joint in the pipeline section shell

experimental values for geometric dimensions of the shells investigated by the author of study [1].

It should be noted in conclusion that the fabrication of shells of turbine penstocks at hydraulic power stations using the standard technology (involving electroslag welding) leads to substantial changes in shape of these structures, caused by welding distortions. The maximal sag of a slot joint due to its displacement out of plane for a range of the shells studied is 3–19 mm, and profile of a shell in the plane of maximal sags is a curvilinear closed line with a concavity formed in a region of the weld, and convexity formed at some distance from it, propagating to a regular circumference.

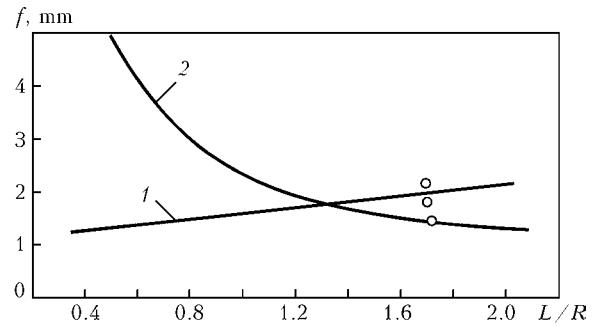


Figure 8. Calculated values of maximal sags f of longitudinal welds in shells 12 mm thick: 1 — using formula (4); 2 — using formula (7); points — experiment

Statistical analysis of the data obtained showed insignificance of the effect of geometric dimensions of the welded shells on maximal sags, which is attributable to a large scatter of experimental data (variation coefficient 15–30 %). The latter is caused by substantial deviations of gaps in the joints from the standard and, as a result, by high variations of welding energy inputs.

When meeting the standard requirements to preparation of joints for welding, variations of geometric dimensions and welding energy inputs have a significant effect on sag of the slot joints, the scatter of experimental data being characterised by a variation coefficient of 6–7 %.

The derived empirical dependence of residual maximal sags of the slot joints, allowing for the effect of welding energy input and rigidity of a shell welded, makes it possible to predict changes in its shape.

Calculation analysis was conducted to study the effect of welding energy input, as well as geometric dimensions of shells on maximal sag of the slot joints. The nomogram was plotted, allowing the maximal sag to be estimated depending upon the variations of the above factors.

As found by the calculations, for shells used in hydraulic engineering the main factor determining changes in their shape is the welding energy input.

1. Kuzminov, S.A. (1974) *Welding distortions of ship hull structures*. Leningrad: Sudostroenie.
2. Panin, V.N. et al. (1982) Evaluation of residual welding distortions of shells of hydroelectric power station penstocks. In: *Welding operations in power construction*, Issue 7.
3. Himmelblau, D. (1973) *Analysis of processes by statistical methods*. Moscow: Mir.



WELD MICROALLOYING WITH TITANIUM AND BORON IN MULTIARC WELDING OF LARGE DIAMETER GAS AND OIL PIPES

L.I. FEJNBERG¹, A.A. RYBAKOV¹, A.N. ALIMOV² and R. ROSERT³

¹E.O. Paton Electric Welding Institute, NASU, Kiev, Ukraine

²OJSC «ARCSEL», Donetsk, Ukraine

³Drahtzug Stein Wire & Welding, Germany

Microalloying of weld metal with titanium and boron in multiarc welding of pipes, performed through a flux-cored wire placed on one of the arcs, was investigated. This process is characterized by the use of neutral and sub-acid fluxes instead of the basic ones, which improves weld formation at increased welding speed. The optimal content of titanium and boron providing a high impact toughness of the weld metal was determined. Industrial tests of the welding process using the developed flux-cored wire of PP-ASF-1 grade yielded positive results.

Keywords: gas-oil pipes, multiarc welding, flux-cored wire, weld microalloying, titanium, boron, fused neutral flux, agglomerated basic flux, impact toughness

In view of increase of the requirements to large diameter gas-oil pipes the problem of improvement of impact toughness of the metal of welds made by submerged multiarc welding is still urgent. Weld microalloying with titanium and boron, which improves the metal structure promoting formation of acicular ferrite inside the grains and suppression of primary ferrite precipitates along their boundaries, remains to be an effective method of its solution. Used for this purpose abroad are agglomerated fluxes of aluminate-basic type AB (EN 760), which limit oxygen content in welds, in combination with welding wire of S3Mo-TiB type or flux-cored wire (FCW) alloyed with titanium and boron. A variant of the second method is a more cost-effective FMI (Fluxcord-Micro-Injection) process, in which alloying of the multiarc weld is performed through FCW (for instance, FLUXOCORD 35.25-3D or 35.25-4D) installed on one of the arcs [1–5]. The disadvantages of these methods are a high cost of imported agglomerated fluxes and relatively low technological properties of most of them in welding of less than 14 mm thick pipes (narrow welds with a high reinforcement).

The purpose of this work is improvement of the welding process by using more cost-effective and adaptable-to-fabrication neutral fused fluxes of the type of AN-67 or AN-47 with achievement of a significant increase of impact toughness ($KCV_{-20} = 60\text{--}80 \text{ J/cm}^2$) of the metal of welds on currently manufactured pipes, made using these fluxes.

It is known [6–10] that balance of titanium, boron, oxygen, nitrogen, as well as active de-oxidizers, namely aluminum, calcium, REMs, is a mandatory condition for producing weld metal with a high level of impact toughness. Suppression of formation of primary ferrite along the grain boundaries is achieved due to the presence of boron remaining after formation

of B_2O_3 oxide and BN nitride. The nuclei for formation of acicular ferrite inside the austenitic grain mainly are dispersed particles of TiO formed as a result of titanium combining with free oxygen.

In welding using basic flux it is recommended for the weld metal to have (wt.%) 0.015–0.030 Ti, 0.002–0.005 B, 0.02–0.04 [O] and not more than 0.006–0.008 [N]. Aluminium content is usually constant at 0.020–0.025 wt.%. Such an element proportion facilitates producing an optimum weld metal structure.

In selection of the weld alloying method application of FCW (FMI process) is preferable for the following reasons:

- use of solid wire of S3Mo-TiB type in combination with neutral fluxes instead of the basic agglomerated fluxes requires increasing its content of boron and titanium, which results in an increase of hardness and rigidity of the wire, which still further aggravates the difficulties arising in its manufacture and application;
- variant with weld metal microalloying through the flux seems to be insufficiently reliable, because of the low metallurgical activity of boron and titanium contained in the fused flux in the form of oxides;
- FCW can be made in small batches, promptly changing its composition, depending on the base metal grade and welding conditions.

At the initial stage of the work, the optimum content of titanium and boron was determined in the welds made on cold-resistant 10G2FB steel, which is used for pipes for critical applications. Reference joints of steel plates 18.7 mm thick were welded from two sides by three or four arcs using fluxes AN-67B and AN-47P (the latter variant is produced by OJSC «Zaporozhstekloflyus»). Heat input of the welding process was equal to 5 kJ/mm. Test FCW with different content of titanium and boron, were placed on the second arc, and cost-effective molybdenum-containing solid wire Sv-08KhM was used for the other arcs.

For comparison purposes, S3Mo-TiB wire and agglomerated fluxes OP 132 (Oerlikon Company) and OK 10.74 (ESAB Company) were used in some ex-



Table 1. Composition (wt.%) of welding wires and base metal

Material	N	Mn	Si	Mo	Ni	Cr	Ti	B	Al	Nb	S	P
Welding wire S3Mo-TiB	0.08	1.3	0.28	0.52	0.05	N/D	0.165	0.0164	0.017	0.013	0.010	0.018
Sv-08KhM	0.10	0.6	0.29	0.61	0.17	1.2	N/D	N/D	N/D	N/D	< 0.025	< 0.030
Sv-08G1NMA	0.09	1.5	0.41	0.70	0.70	0.1	Same	Same	Same	Same	< 0.015	< 0.020
Base metal 10G2FB steel	0.11	1.7	0.32	< 0.03	N/D	N/D	»	»	0.04	0.007	0.016	0.016

Table 2. Flux composition (wt.%)

Flux	Al ₂ O ₃	CaO	MgO	CaF ₂	MnO	SiO ₂	TiO ₂	Fe ₂ O ₃	ZrO ₂
AN-67B	35-40	< 10	--	11-16	14-18	12-16	4-7	< 1.0	--
AN-47P	10-18	12-17	6-10	8-13	10-16	27-30	4-7	0.8-3.0	3.5-5.0
OP 132	23-26	3.5-6.0	20-24	13-16	6.5-8.5	17-20	2.0-3.5	1.3-3.2	--
OK 10.74	21-26	5-7	19-25	16-20	5-7	19-24	< 1.3	--	--

periments. Composition of the base metal and welding consumables is given in Tables 1 and 2.

FCW application did not lead to any essential changes of the welding mode or quality of weld formation. Arcing on FCW was somewhat less stable than on the solid wire, which is attributable to the absence of the copper coating. Impact toughness of weld metal was determined on samples with a sharp notch of IX type (GOST 6996-66), which were cut out of the last weld or point of weld cross-section.

As a result of experiments it was established that in welding with the above fused fluxes, oxygen and nitrogen content in the weld metal varies in the ranges of 0.045-0.700 and 0.0077-0.0110 wt.%, i.e. it is higher than in welding using a basic flux, the aluminium weight fraction being unchanged. Titanium content in the weld metal optimum for improvement of the impact toughness is equal to 0.022-0.038 wt.%, and that of boron --- 0.0025-0.0065 wt.%. At titanium content below 0.018 wt.% the positive effect was absent, and at more than 0.038 wt.% the impact toughness abruptly decreased. As is seen from Table 3, in welding using neutral fused fluxes, microalloying with titanium and boron improves the impact toughness KCV_{-20} of weld metal 2-2.5 times (items 2 and 4) compared to the variants of welding, where it was absent (items 1 and 3).

Increased content of boron right up to 0.01 wt.% did not lower the impact toughness of weld metal. However, in view of the risk of crack formation its limit content was limited to 0.0065 wt.%. Such a value is close to the recommended in [8] optimum boron content at $N \leq 80$ ppm and $O = 330-380$ ppm. It is determined by ratio $B = 0.7N + 15$ ppm, and is equal to 0.0071 wt.% at $N = 80$ ppm.

It is known that when the second (outer) weld of the pipe was made the impact toughness of weld metal of the first (inner) weld decreases by 20-30 % because of dispersion hardening. Due to microalloying a «margin» of impact toughness is created which (despite the lowering of this index at re-heating) provides its

acceptable value for the metal of the first weld and point of weld overlapping. So, for instance, KCV_{-20} of the metal of the last weld made using AN-67B flux was equal to 178 J/cm² (item 2, Table 3), and that of the point of weld overlapping --- 132 J/cm². Here, however, a local lowering of impact toughness can occur in the weld sections, where the re-heating temperature is higher than 750 °C [7].

When basic agglomerated fluxes are used, weld microalloying by titanium and boron is rational in the case, if it is necessary to ensure high impact toughness at the temperature below -20 °C. So, KCV_{-20} of the metal of welds made on steel 10G2FB with Sv-08G1NMA wire using fluxes OK 10.74 and OP 132, with the basicity of 1.4-1.5 did not exceed 153 J/cm² (items 5 and 8, Table 3). Microalloying with titanium and boron increased this index --- $KCV_{-40} > 150$ J/cm².

In view of the lower oxidizing ability of the above fluxes, the optimum content of titanium and boron in the weld metal (and in FCW, respectively) should be lower than in welding using neutral fluxes AN-67B and AN-47P. In our experiments in welding with S3Mo-TiB wire the content of the above elements in the weld metal was equal to 0.024-0.026 and 0.0019-0.0025 wt.%, respectively (items 7 and 9, Table 3). Obtained results (allowing for oxygen and nitrogen content) are not contradictory to the above recommendations for the basic agglomerated fluxes.

When FCW of an uncorrected composition was used in combination with agglomerated fluxes, titanium and boron content in the weld metal was equal to 0.0360 and 0.0053 wt.%, respectively, which exceeded their optimum content and led to an abrupt lowering of its impact toughness (item 6, Table 3).

Composition of weld metals made using OK 10.74 flux with S3Mo-TiB and Sv-08KhM + FCW wires (items 6 and 7, Table 3) differs mainly by the content of titanium and boron. It means that correction of FCW composition by lowering the content of titanium and boron will allow reaching the same high results



Table 3. Composition (wt.%) and impact toughness of the metal of welds made using fluxes

No.	Flux	Welding wire	C	Si	Mn	Mo	Cr	Ti	B	[O]	[N]
<i>Fused</i>											
1	AN-67B	Sv-08KhM	0.09	0.27	1.63	0.14	0.26	--	--	0.045	0.008
2		Sv-08KhM + FCW	0.07	0.30	1.60	0.22	0.37	0.030	0.0044	0.047	0.007
3	AN-47P	Sv-08G1NMA	0.10	0.48	1.63	0.20	--	--	--	0.047	0.010
4		Sv-08KhM + FCW	0.08	0.30	1.67	0.27	0.31	0.028	0.0034	N/D	N/D
<i>Agglomerated</i>											
5	OK 10.74	Sv-08G1NMA	0.06	0.43	1.60	0.30	--	0.011	--	0.037	0.005
6		Sv-08KhM + FCW	0.07	0.41	1.62	0.28	0.36	0.036	0.0053	0.032	0.005
7		S3Mo-TiB	0.07	0.45	1.78	0.22	--	0.026	0.0025	0.022	0.006
8	OP 132	Sv-08G1NMA	0.08	0.30	1.74	0.33	--	0.011	--	0.051	0.008
9		S3Mo-TiB	0.07	0.31	1.67	0.29	0.36	0.024	0.0019	0.048	0.008

Notes. 1. Aluminium content in the weld metal was 0.02–0.03 wt.%, and in the metal of welds made with application of Sv-08G1NMA wire nickel content was from 0.18 to 0.22 wt.%. 2. Samples of IX type for impact bending tests were cut out of the last weld layer.

Table 3 (cont.)

No.	Flux	Welding wire	KCV, J/cm ² , at T, °C		
			0	-20	-40
<i>Fused</i>					
1	AN-67B	Sv-08KhM	N/D	82	49
2		Sv-08KhM + FCW	183	178	135
3	AN-47P	Sv-08G1NMA	76	49	N/D
4		Sv-08KhM + FCW	N/D	122	87
<i>Agglomerated</i>					
5	OK 10.74	Sv-08G1NMA	168	153	111
6		Sv-08KhM + FCW	102	63	N/D
7		S3Mo-TiB	N/D	187	151
8	OP 132	Sv-08G1NMA	147	104	98
9		S3Mo-TiB	216	205	195

in welding with the basic agglomerated fluxes as when S3Mo-TiB wire is used.

Considering the stringent requirements to the content of microalloying elements in the weld metal, it is necessary to very accurately provide the uniformity of FCW composition along its length. After optimizing the technology of FCW manufacture, a series of 12 m deposits on pipes were made with monitoring of the weld metal composition every 0.5 m of its length. Standard deviation of titanium and boron content in the weld metal was equal to ± 0.0010 and ± 0.0002 wt.%, i.e. it was not more than 12.5 % of the range of variation of their optimum content in the weld metal --- 0.016 wt.% Ti and 0.004 wt.% B.

Test batches of FCW were produced in two stages successively in two plants. Initially the billet filled with the flux core was made in Germany in the plant of Drahtzug Stein Wire & Welding Company. Then it was shipped to Ukraine to ARCSEL Company, where finishing operations were performed (heat treatment, drawing, winding on user reels), as well as testing and control of finished wire. During production trials it was established that increase of FCW diameter from 4.0 to 4.5 mm increases the stability of

the process of multiarc welding at more than 800 A current. The difference between the weight of 1 lin. m of FCW of 4.5 mm diameter and solid wire of 4.0 mm diameter is not more than 4 %.

Based on the obtained data FCW of PP-ASF-1-2, PP-ASF-1-3 and PP-ASF-1-4 grades for submerged multiarc welding were developed (TUU 28.7-31206116-008-2003 with Modification 1). Patent of Ukraine and positive decision on an application for a patent were obtained for the above FCW [11, 12].

Development of FCW composition was conducted allowing for the typical plant modes of multiarc welding, which corresponded to certain ranges of the ratios of the sums of solid electrode wire feed rates to FCW feed rate. When solid electrode wires of 4.0 mm diameter and FCW of 4.5 mm diameter placed on the second arc were used, this ratio for three- and four-arc welding was equal to 1.1-1.9 and 1.5-2.7, respectively. Under production conditions taking into account the allowance for FCW composition, change of the composition along the wire length, variations of welding modes, different types of edge preparation and values of weld stirring coefficient, it is recommended for the modes of three- and four-arc welding



Table 4. Dependence of the composition of the metal of welds made on steel 10G2FB using AN-67B flux and solid wire Sv-08KhM on the mode of arcing on FCW

Number of arcs	I, A	U, V	v _w , m/h	Weight fraction of elements, %						
				N̄	Si	Mn	Cr	Mo	Ti	B
1	900	30	38	0.12	0.37	1.89	0.23	0.17	0.118	0.0212
		37		0.10	0.37	1.93	0.21	0.14	0.099	0.0170
3	850	30	80	0.10	0.33	1.63	0.28	0.15	0.027	0.0042
	900	37		0.10	0.33	1.65	0.27	0.15	0.026	0.0044

Notes. 1. I --- arc current, U --- voltage of arc placed on FCW. 2. 3-arc welding mode: I₁ = 1150 A, U₁ = 37 V; I₂ = 850–900 A, U₂ = 30–37 V; I₃ = 45–47 V; v_w = 80 m/h; FCW was placed on the second arc.

to correspond to a more narrow range of the above ratios (1.3–1.7 and 1.8–2.4), this guaranteeing the optimum microalloying of the weld.

In order to widen the range of the welding modes, FCW can be used also on other arcs, in addition to the second one, as limited change of the arcing mode does not have any essential influence on transition of titanium and boron from FCW into the weld metal. For instance, under the conditions of three-arc welding at increase of voltage on the second arc by 7 V (current of 850–900 A), titanium content in the weld metal dropped by 0.001 wt.%, and that of boron practically did not change (Table 4). It is, however, undesirable to place FCW on the first arc, because of excess amount of the deposited metal, which for FCW of 4.5 mm diameter is by 20–30 % higher than for solid wire of 4.0 mm diameter, as well as respective lowering of penetration. In addition, FCW application for the first and last arc is not recommended in view of the possibility of development of weld inhomogeneity [13].

Results of laboratory testing of an industrial batch of FCW 232 of PP-ASF-1-3 grade in three-arc welding of a reference welded joint of 10G2FB steel using AN-67B flux (I₁ = 1220 A; U₁ = 34 V; I₂ = 825 A; U₂ = 38 V; I₃ = 980 A; U₃ = 43 V; v_w = 85 m/h) are given below:

- weld metal had the following composition, wt.%: 0.074C; 0.3Si; 1.6Mn; 0.32Cr; 0.27Mo; 0.027Al; 0.03Ti; 0.0044B;

- average value of impact toughness of the weld metal at testing temperature 0, –20 and –40 °C was equal to 183, 177 and 135 J/cm²;

- weld metal hardness did not exceed HV 237, which satisfies the requirements of the currently valid standard documentation for gas pipes.

Results of weld testing for static tension obtained on samples of type II (GOST 6996–66), are given in Table 5.

In addition to Sv-08KhM wire, PP-ASF wire can also be used in combination with Sv-08GM (S2Mo) wires. Use of wire of Sv-08G1NMA type is unacceptable because of excess increase of manganese content in the weld metal and possible decrease of impact toughness values below the admissible limit.

Welding with application of the developed FCW of outer welds of test batches of pipes from steel of X70 strength class of (1020–1420) × (16–19) mm size made at Khartsyzsk Pipe Manufacturing and Vyksun Metallurgical Plants confirmed the effectiveness of

the considered process, which allowed increasing the weld impact toughness by approximately 2 times. Testing showed that in addition to neutral flux AN-67B (KVC₋₂₀ = 120–180 J/cm²), sub-acid flux of the type of AN-68 (KVC₋₂₀ = 120–180 J/cm²) can be used, the composition of which is equivalent to that of a mixture of fluxes of 50 % AN-67B + AN-60. Use of FCW in combination with acid flux AN-60 did not give any essential effect, because of an increased content of oxygen in the weld metal (0.09–0.11 wt.%).

Metal of welds made by multiarc welding with Sv-08KhM and PP-ASF-1 wires using flux AN-67B on pipes of steel of strength class X70, has a finely-dispersed structure* containing up to 85 vol.% of acicular ferrite practically without intergranular polygonal ferrite (Figure 1, a). Application of AN-68 flux leads to a certain lowering of the share of acicular ferrite and appearance of sparse intermittent interlayers of intergranular polygonal ferrite 2–5 μm thick (Figure 1, b). Weld metal hardness was HV 232–237 in both the cases.

For comparison Figure 2 gives less favourable microstructures of weld metal made with Sv-08G1NMA wires without application of FCW on currently manufactured pipes, using a mixture of fluxes of 50 % AN-67B + AN-60 (Figure 2, a) and AN-67B flux (Figure 2, b). They are characterized by a lower content of acicular ferrite and higher content of polygonal ferrite, the content of intergranular polygonal ferrite being equal to 7–11 vol.%.

At introduction of the process of multiarc welding with application of FCW alloyed with titanium and boron on one of the arcs, the main problem is provision of the above proportion of the sum of solid wire feed rates to FCW feed rate. Considering the wide range of pipes and of welding mode variation, it is rational to use the automatic regulation means for this purpose.

Table 5. Mechanical characteristics of the metal of welds produced at testing by static tension

Sample	σ _y , MPa	σ _t , MPa	σ _y /σ _t	δ, %	ψ, %
1	596.7	751.9	0.79	27.0	66.3
2	594.7	734.8	0.81	24.0	62.3

* Metallurgical analysis of the weld metal structure was made by L.G. Shitova, Leading Engineer.

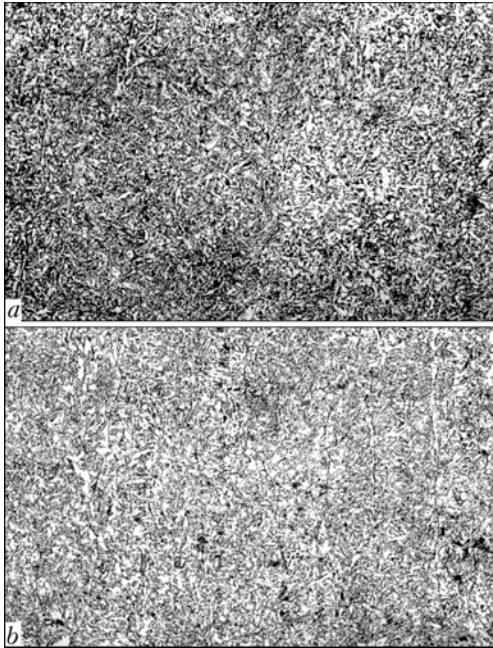


Figure 1. Microstructure of the metal of welds made on pipes from steel of strength class X70 using wires Sv-08KhM + PP-ASF and fluxes AN-67B (a) and AN-68 (b) ($\times 500$, etching in the metal)

In order to implement the above welding process in the mills for welding inner welds it is necessary to ensure the equal strength of the butt joint of FCW ends at replacement of the coils, in view of the high forces, which are generated at wire drawing through the guides up to 15 m long. Solution of this problem requires a special preparation of FCW edges for welding and application of butt welding machines with a programmable cycle.

CONCLUSIONS

1. Weld microalloying with titanium and boron in multiarc welding using neutral or sub-acid fluxes increases their impact toughness 1.5–2.5 times on pipes from steels of 10G2FB type. Optimum content of titanium and boron in the weld metal is equal to 0.022–0.038 and 0.0025–0.0065 wt.%, respectively.

2. Studied was the variant of weld metal microalloying through FCW used for one of the arcs, in combination with solid wires Sv-08KhM used for the other arcs in welding with fluxes AN-67B, AN-68, AN-47P and a mixture of fluxes of 50 % AN-67B + AN-60. Impact toughness KCV_{-20} of the last weld layer is equal to 80–180 J/cm², depending on the flux grade. In addition to Sv-08KhM wire, it is possible to use wire of Sv-08GM type (S2Mo).

3. Ratio of the sum of solid wire feed rates to FCW feed rate should be in the range of values determined by FCW grade and welding conditions.

4. Composition of FCW alloyed with titanium and boron of grades PP-ASF-1-2, PP-ASF-1-3 and PP-ASF-1-4 (TUU 28.7-31206116-008–2003 with Modification 1) was developed for multiarc welding of low-alloyed steels using neutral or sub-acid fluxes in combination with wires of type Sv-08KhM or Sv-08GM, respectively. Application of the above FCW yielded positive results in fabrication of test batches of gas pipes.

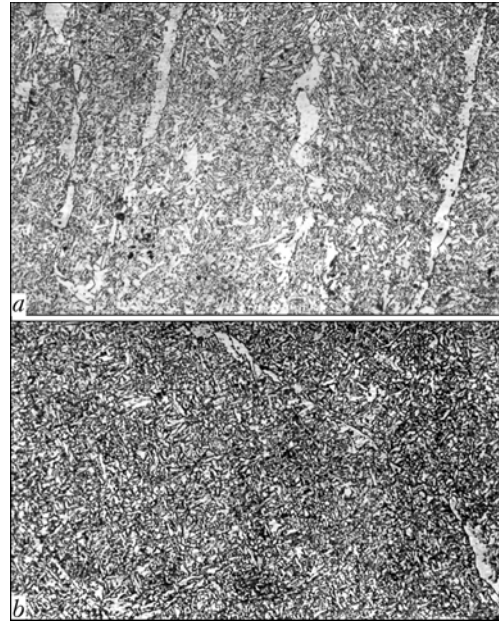


Figure 2. Microstructure of the metal of welds made on pipes of steel of strength class X70 using wire Sv-08G1NMA and a mixture of fluxes of 60 % AN-67B + AN-60 (a) and flux AN-67B (b) ($\times 500$, etching in metal)

5. At a certain lowering of the content of titanium and boron PP-ASF type wire can be applied for welding using the basic agglomerated fluxes to improve the weld impact toughness at the temperature below -20°C .

6. Weld metal microalloying with titanium and boron through FCW placed on one of the arcs, can be accepted for submerged multiarc welding of different structures from low-alloyed steel.

1. Nies, H., Keville, B., Schlatter, B. (1996) Schweißen von Grossrohren mit dem Unterpulver — Mehrdrahtverfahren. *Oerlikon Schweissmitteilungen*, **131**, May, 4–13.
2. Sordi, J., Scholz, E., Schuster, G. (1990) Grossrohren fuer Saergas — Optimierung des UP-Mehrdrahtschweißen mit Fuelldrahtelektroden. *Ibid.*, **122**, February, 11–17.
3. Scholz, E., Weiland, F. (1984) Derzeitige Standssdes UP Schweißens mit mikrolegierten Fuelldrahtelektroden. *Ibid.*, **106**, Okt., 4–14.
4. Engindeniz, E. (1994) Unterpulver — Hohleistungsschweißen mit Fuelldrahtelektroden. *Ibid.*, **130**, April, 11–20.
5. Engindeniz, E. (2000) Unterpulver — Schweißen mit Fuelldrahtelektroden. In: *Jahrbuch der Schweisstechnik*. Dueseldorf, DVS, 11–20.
6. Liu, Z., Lau, T., Noth, T.H. (1987) Deposit properties and the Ti–O–B–N balance in submerged arc welding. *IIW Doc. II-A-713–87*.
7. Horii, Y., Ohkita, S., Wakabayashi, M. et al. (1988) Study on the toughness of large-heat input weld metal for low temperature-service TMCP steel. *Nippon Steel Techn. Rep.*, **37**, April, 1–9.
8. Kawabata, F., Sakaguchi, S., Matsuyama, J. et al. (1987) Measures for toughness improvement of heavy-walled UOE pipe's submerged arc weld metal. *IIW Doc. XII-953–86 II-A-713–87*.
9. Podgaetsky, V.V. (1991) On the influence of the weld chemical composition on its microstructure and mechanical properties (Review). *Avtomatick. Svarka*, **2**, 1–9.
10. Pokhodnya, I.K., Golovko, V.V., Denisenko, L.V. et al. (1999) Effect of oxygen on formation of acicular ferrite structure in low-alloy weld metal. *Ibid.*, **2**, 3–11.
11. Alimov, A.M., Rybakov, A.O., Bat, S.Yu. et al. *Composition of flux-cored wire*. Pat. 74469 Ukraine. Int. Cl. 7 B 23 K 35/368. Publ. 15.12.2005.
12. Alimov, A.M., Rybakov, A.O., Bat, S.Yu. et al. *Composition of flux-cored wire*. Appl. 2004106363/02 RF. Int. Cl. 7 B 23 K 35/368. Publ. 02.03.2004.
13. Engindeniz, E., Berg, B., Linden, W. (2000) Grossrohrfertigung fuer Saergasleitungen aus schweisstechnischer Sicht. In: *Jahrbuch der Schweisstechnik*. Dueseldorf: DVS, 539–524.



INVESTIGATION OF HIGH-VOLTAGE CONTROL CIRCUITS OF WELDING ELECTRON BEAM CURRENT

O.K. NAZARENKO and V.S. LANBIN

E.O. Paton Electric Welding Institute, NASU, Kiev, Ukraine

High-voltage circuits for control of the welding gun beam current were studied using mathematical computer simulation. It is shown that in the case of using an independent control voltage source the spark breakdown in the emission system is accompanied by a long (about 10 ms) full opening of the emission system, this leading to a surge of current violating weld formation. Control of beam current using an automatic offset eliminates such dangerous current surges after spark breakdowns.

Keywords: electron beam welding, control, beam current, high-voltage circuits, emission system, spark breakdown, transient processes, defects, weld formation

The main process of electron beam current control is change of the potential of the control electrode in the welding gun emission system. In this case two schematics of control voltage formation are the most widely accepted:

- use of a self-sufficient voltage source (minus of the accelerating voltage source is connected to the emission system cathode);
- application of automatic bias [1] (an electron tube with grid control is connected to the emission system control electrode [2], and minus of the accelerating voltage source is connected to the emission system control electrode).

In the steady-state mode of the emission system operation beam current is equally well controlled, when using any of the above schematics. In practice, however, application of a self-sufficient voltage source runs into considerable disturbances of weld formation in sheet materials, arising after spark breakdowns in the emission system, which are accompanied by a discharge of the high-voltage circuit capacitances in fractions of a microsecond [3]. The welding process is not interrupted, as protection does not switch off the source, but the weld forms a crater (Figure 1), or an item burn-through may occur. As shown by investigations, value of beam energy required for formation of such a defect, is equal to approximately 300 J. Therefore, defect formation cannot be attributed only to release of the power source stored energy, as its value is less than 10 J [3]. Probability of disturbance of the welding process becomes higher with the use of welding guns moved inside large-sized vacuum chambers, when the high-voltage cable length is up to 50 m, and its inherent capacitance is $1 \cdot 10^{-8}$ F. The weld defect level is the higher, the higher the power of the used power unit of the welding gun-power source. On the other hand, in welding of thick metals such a disturbance practically does not influence weld formation. The above issues were not discussed earlier in technical publications, which led to performance

of several studies, the results of which are given below. This work does not deal with transient processes, which are related to development of arc discharges in the emission system, as in the currently available accelerating voltage source transition of spark discharges into arc discharges is effectively prevented [4].

Simplified diagrams of two high-voltage circuits of beam current control with a self-sufficient source of control voltage (Figure 2, a) and automatic bias (Figure 2, b) allow consideration of the transient processes running in them after spark discharge of the emission system.

Spark discharge of vacuum insulation practically always runs in the accelerating gap of the anode-control electrode, the breakdown current being maintained by a discharge of distributed capacitance of the cable $C2$ and total filter capacitance $C3$, as well as distributed capacitances of the source of accelerating voltage U_{acc} . During the spark breakdown of the emission system, the control electrode is practically shorted to the ground. It is important to note that when a control voltage source is used (Figure 2, a), the discharge of $C3$ capacitance will run through distributed capacitance $C1$ of the cable and filter capacitance $C4$ of the control voltage source U_c . In operation with an automatic bias (Figure 2, b) the discharge current of capacitance $C3$ does not run along the control voltage forming circuits, their operating conditions being improved. After capacitance discharge the spark discharge stops, this allowing restoration of vacuum insulation and charging of the high-voltage circuit capacitances during the time, dependent on the internal resistance of the sources, the capacitances proper, and current-carrying circuit parameters.

It is still not clear how the electrode-cathode potential difference and beam current change during the breakdown and after it.

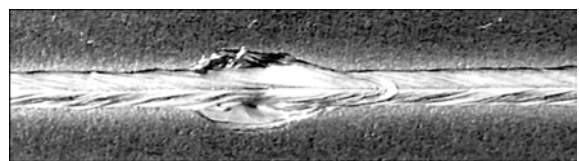


Figure 1. Appearance of weld metal with a defect in the form of a crater due to a short electron beam current pulse with about 300 J energy

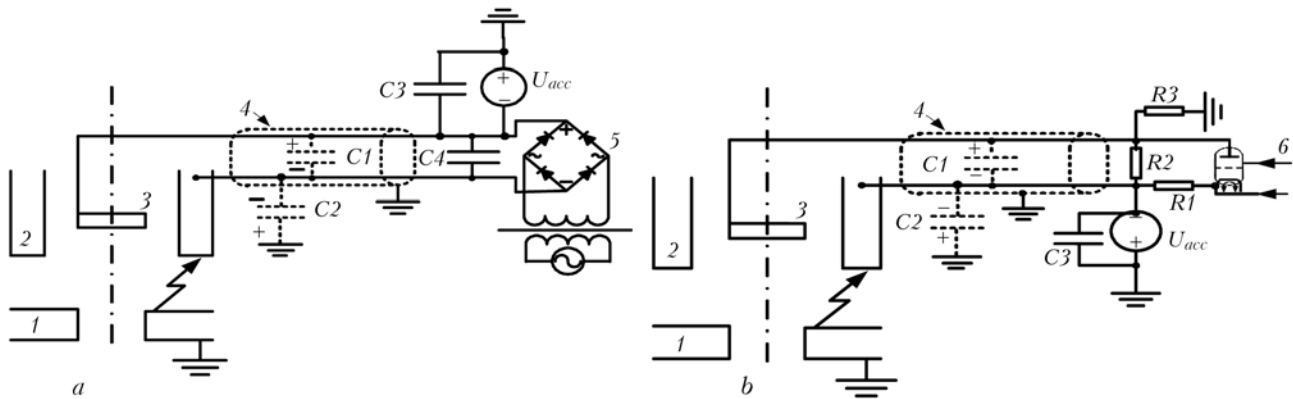


Figure 2. Simplified diagrams of electron beam current control using a self-sufficient control voltage source (a) and automatic bias (b): 1 — anode; 2 — control electrode; 3 — cathode; 4 — HV cable; 5 — control voltage source; 6 — control tube; R1 — feedback resistor in the beam current stabilization circuit; R2, R3 — resistance of HV divider arms; arrows show the main location of the spark discharge of the accelerating gap; for other designation see the text

It is rather difficult to directly record the fast transient processes during the spark breakdown of the emission system with electronic devices, as the studied circuits are immersed into transformer oil and are at a high potential. In addition, the measuring circuits proper at breakdowns are exposed to strong electromagnetic noise, essentially distorting the pattern of the recorded processes. Therefore, we have applied computer simulation of high-voltage circuits of welding current control using one of the known programs OrCAD PCB Designer with Pspice (Cadence Design Systems Company).

At simulation of the diagrams, we assume that in both the cases the same high-voltage cables and emission systems are used, as well as 60 kV accelerating voltage sources of 30 kW power with 5 kOhm internal resistance. Modulation characteristics of emission systems are given in Figure 3. They can be used to assign the value of control voltage and internal resistance of the emission system, corresponding to the selected value of stationary beam current. High-voltage cable 50 m long has three current-conducting wires for powering the cathode and its heater (spiral). Wires are

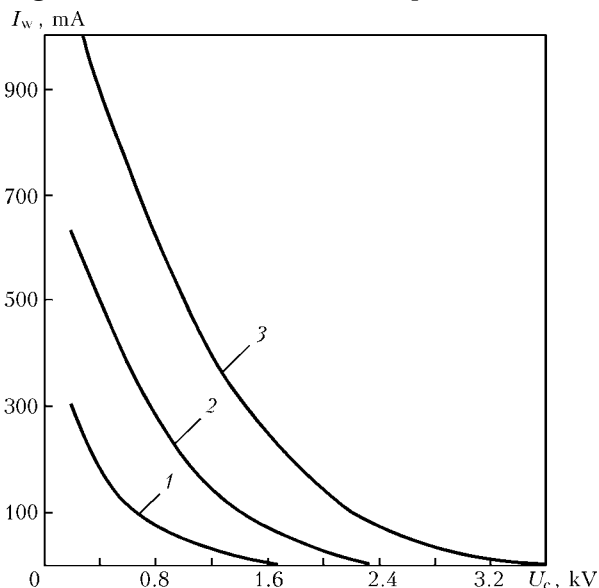


Figure 3. Modulation characteristics of emission systems of 15 (1), 30 (2) and 60 (3) kW power at $U_{acc} = 60$ kV

enclosed into braiding, which is connected to the gun control electrode. Distributed capacitance between the wires is 50 pF/r. m, and 150 pF/r. m between the braiding and external grounded shield. Distributed inductance of the braiding and each of the wires is equal to 1.5 μH/r. m, internal resistance of the control voltage source being 30 kOhm.

Figure 4 shows the graphic windows of a computer mathematical simulator of high-voltage circuits of beam current control with a self-sufficient control voltage source (Figure 4, a) and automatic bias (Figure 4, b) at the initial stationary beam current of 60 mA and other assigned parameters.

Electron conduction of the welding gun corresponding to 60 mA current, is emulated by a resistor with 1 mOhm resistance, connected into a circuit between the ground and current supply to the cathode. Current supply to the control electrode is connected to the contactor emulator closing the control electrode to the ground for 0.5 μs with 100 μs delay after the start of the emulation process. Presentation of the high-voltage cable as one pair of concentrated elements, namely capacitance and inductance, did not fully reveal the resonating nature of the circuit. Therefore, the cable is considered as a long line and is simulated by four links, further increase of the number of links not changing the nature of transient processes, which are revealed by emulation.

Figure 5 gives time changes of the potentials of the control electrode and cathode after a spark breakdown of the emission system with an self-sufficient source of control voltage. It is seen that before the breakdown the emission system forms an electron beam with 60 mA current, and control voltage is 1.6 kV (Figure 5, c). After the breakdown the potentials of both the control electrode and the cathode become equal to that of the ground (Figure 5, b). After that the cathode potential starts changing immediately, and that of the control electrode starts changing with a delay for the time of existence of the short-circuit (0.5 μs) as a result of attenuation of self-excited oscillations, with the frequency of about 1 MHz and amplitude of +60 -- -160 kV. Self-excited oscillations stop approximately after 10 μs; total time

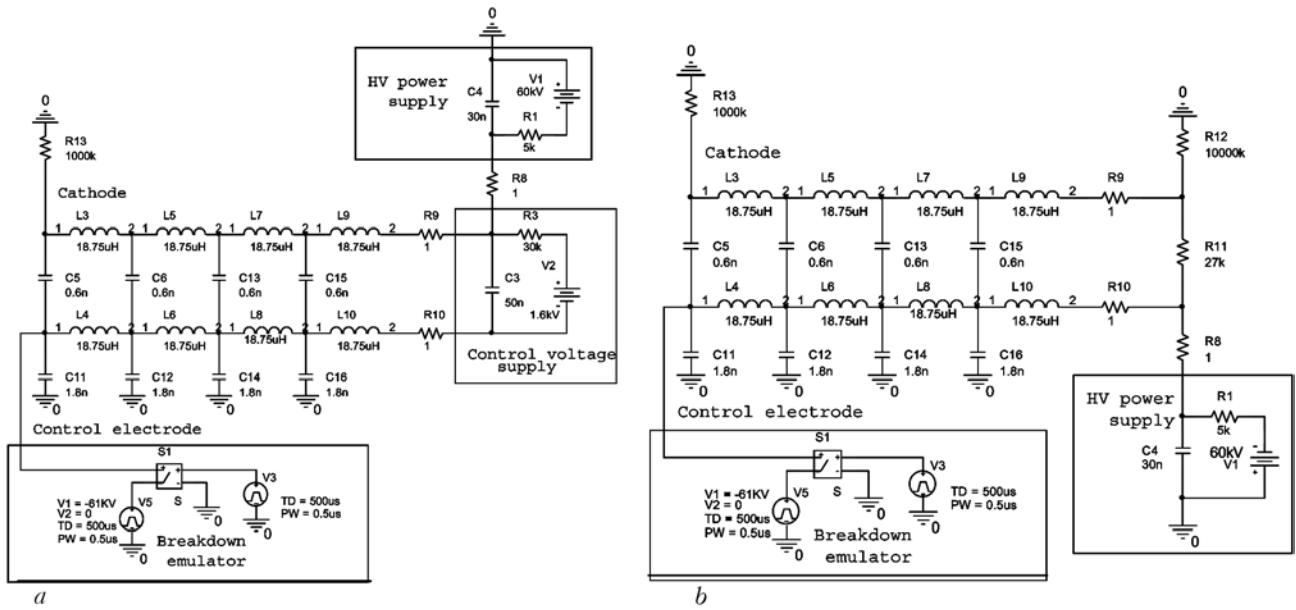


Figure 4. Graphic windows of the computer mathematical simulator for analysis of high-voltage control circuits of 60 mA beam current with a self-sufficient source (a) and automatic bias (b)

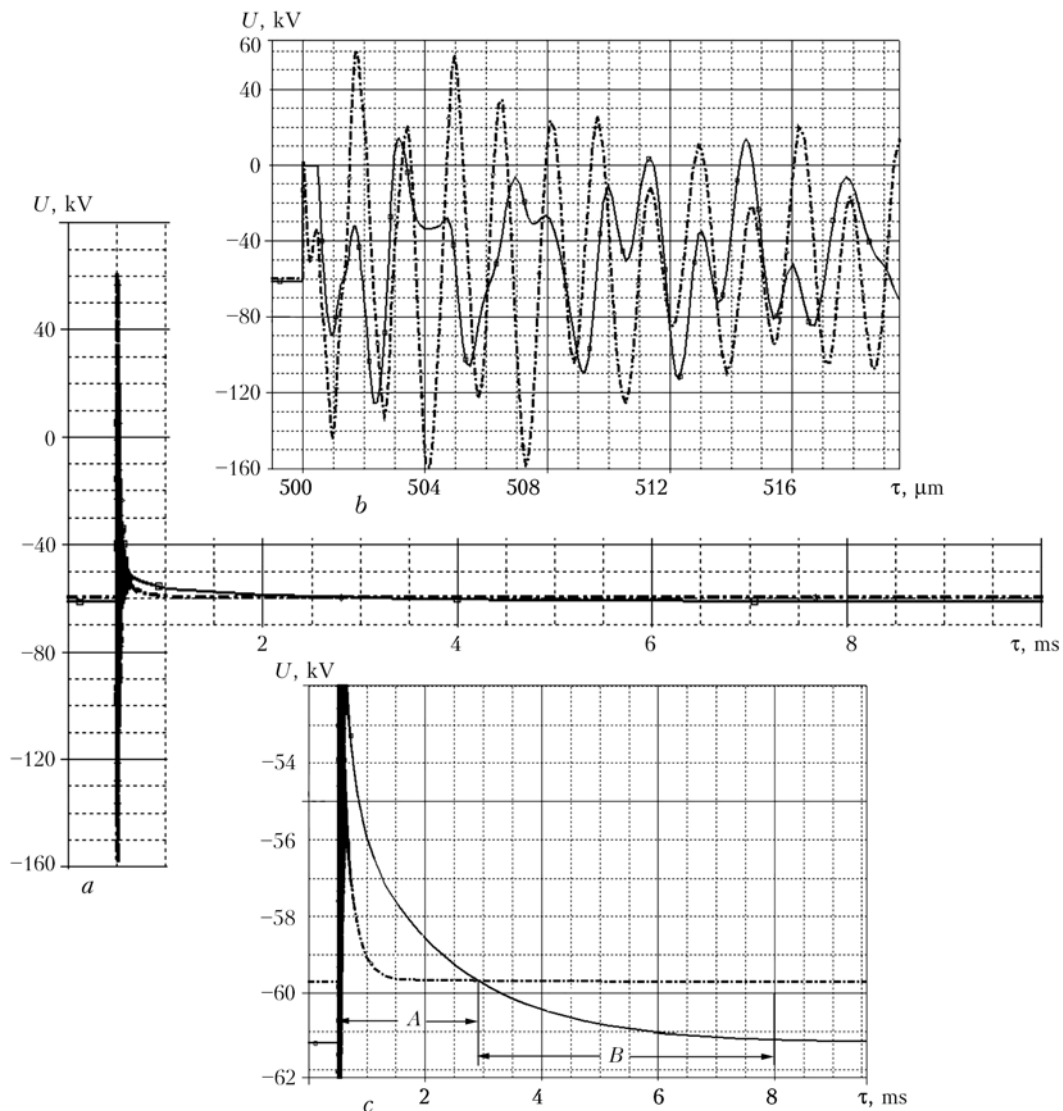


Figure 5. Change of potentials U of the control electrode (solid curves) and cathode (dot-dash lines) after breakdown of the emission system with a self-sufficient source of control voltage: a — general pattern; b, c — spread scales of time and potentials, respectively

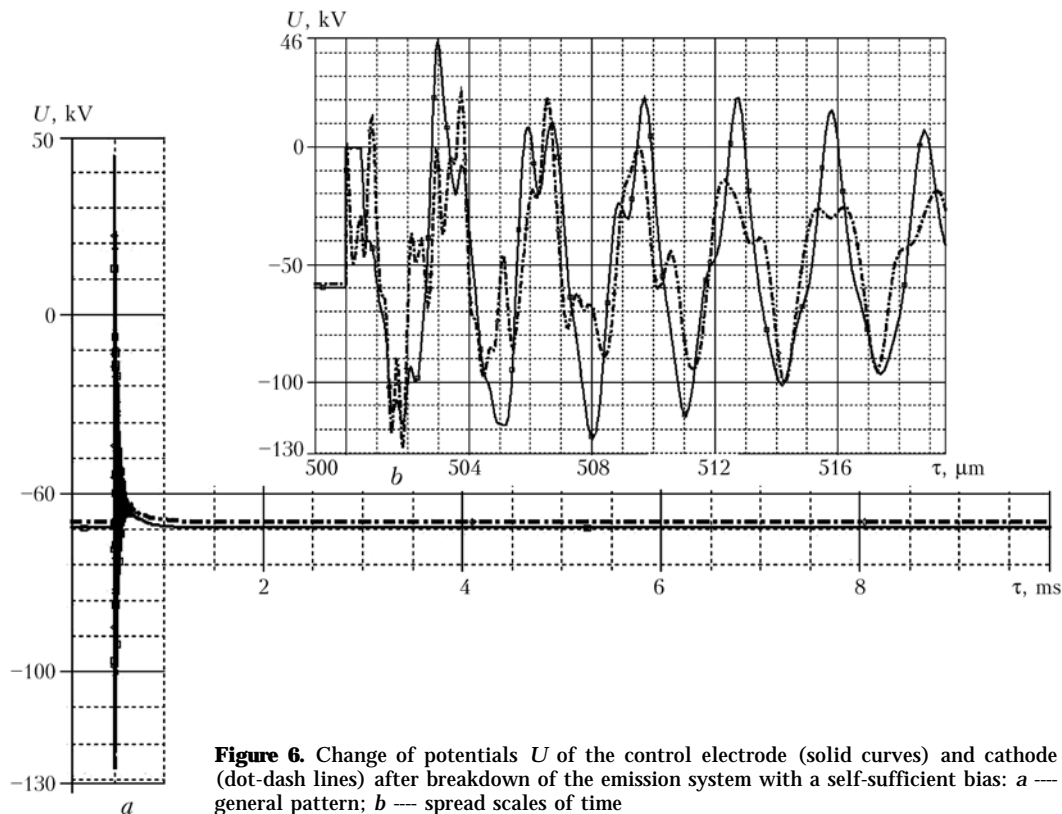


Figure 6. Change of potentials U of the control electrode (solid curves) and cathode (dot-dash lines) after breakdown of the emission system with a self-sufficient bias: a — general pattern; b — spread scales of time

of restoration of the steady state of the circuit is about 10 ms. During this time, the control electrode is under positive potential for 3 ms relative to the cathode (section A in Figure 5, c), i.e. emission system operates in the mode of complete drawing of the cathode current. During this time beam energy of up to 200 J can evolve in the item. From the moment of equalizing of the control electrode and cathode potentials and up to establishment of the initial stationary difference of potentials -1.6 kV (section B in Figure 5, c) not less than 100 J energy of the beam additionally evolves. All together, up to 300 J of energy will evolve on the item during the period of restoration of the high-voltage circuit steady-state condition, which accounts for formation of a crater in the weld (see Figure 1).

At breakdown of the vacuum gap of the emission system operating in the mode of automatic bias, the nature of transient processes differs essentially from the one considered above (Figure 6):

- control electrode potential remains to be negative relative to the cathode potential, this eliminating item damage by excess current;
- time for restoration of the stationary condition of the high-voltage circuit is just 1 ms, i.e. is by an order of magnitude lower;
- amplitude of overvoltages is smaller by almost 25 %, which somewhat lowers the risk of damage of the high-voltage circuit element.

CONCLUSIONS

1. In the case of application of a self-sufficient source of control voltage the spark discharge of the welding gun emission is accompanied by a long-term (about

10 ms) opening of the emission system, the control electrode being under a positive potential relative to the cathode and the emission system operating in the mode of full drawing of current for 3 ms. As a consequence, already after the end of the breakdown the item can be exposed to an electron beam, the power of which is essentially higher than the specified value, this leading to disturbance of weld formation.

2. At control of beam current using automatic bias, the control electrode potential remains to be negative relative to the cathode potential, this eliminating item damage by excess current. Time for restoration of the steady-state condition of the high-voltage circuit is only 1 ms, i.e. it is by an order of magnitude lower than in the case of application of a self-sufficient source of control voltage.

3. Results of computer simulation of high-voltage circuits of welding current control agree well with the experience of their practical application, and are convincing proof of the advantages of beam current control using automatic bias.

The authors feel obliged to express their gratitude to V.E. Lokshin and V.V. Galushka for a fruitful participation in the discussion on the above subject.

1. Bonch-Bruevich, A.M. (1955) *Application of electronic tubes in experimental physics*. Moscow: Gostekhteorizdat.
2. Mayer, R. *Strahlstromsteuerung fuer eine Elektronenstrahl-Schweissmaschine*. Pat. 24 60 424 Deutsche. Int. Cl. H 01 J 37/24. Publ. 17.03.77.
3. Rakhovsky, V.I. (1970) *Physical principles of commutation of electric current in vacuum*. Moscow: Nauka.
4. Nazarenko, O.K., Lokshin, V.E. (2005) Dynamic characteristics of high-voltage power sources for electron beam welding. *The Paton Welding J.*, 1, 31–33.



INFLUENCE OF SURFACE DEFECT ON STRENGTH OF WELDED JOINTS WITH ASYMMETRICAL MECHANICAL NON-UNIFORMITY

A.A. OSTSEMIN

South-Uralsk Scientific-Industrial Center, Chelyabinsk, Russian Federation

On the basis of the plane problem solution method of the plasticity theory the design evaluation of the static strength with asymmetrical mechanical non-uniformity of welded joints with a surface crack-like defect is performed. Stressed state of mechanically non-uniform butt joints with a surface defect is investigated. The proposed methodology for evaluating static strength of welded joints with asymmetrical mechanical non-uniformity allows determining the load-carrying capacity by introduction into the calculation formulas of the mechanical non-uniformity coefficients.

Keywords: arc welding, butt joints, relative thickness, soft interlayer, surface crack, limit tensile force, contact strengthening, asymmetrical mechanical non-uniformity, tangential stresses on the weld fusion line, mechanical non-uniformity coefficients

Welded joints with asymmetrical mechanical non-uniformity of the strength property distribution often occur in practice [1–5]. In the joints from low-alloy steels of main pipelines on both sides of the HAZ metal (areas of the soft interlayer) an area with the highest strength (a weld) and a less strong area (the base metal) are located [1]. The soft interlayer can be easily determined by measurements of hardness.

It is shown in [4] that strength of welded joints in static loading is effected by the kind of mechanical non-uniformity. In the welded joints with asymmetrical mechanical non-uniformity contact strengthening can be really manifested both in static and cyclic loading [5].

In the welded longitudinal joint of a main pipeline the weld is the strongest (CT); the base metal has a lower strength (T); and between them a soft interlayer (M) is located [6]. Such character of asymmetrical mechanical non-uniformity effects, as a whole, properties of welded joints of big diameter pipes [7].

Existing methods of the strength calculation of such joints are based on the theory that the soft interlayer, which weakens a welded butt, is surrounded by a stronger metal with similar mechanical properties [8, 9].

On the basis of experimental investigations of mechanical characteristics of welded joints with asymmetrical mechanical non-uniformity (Figure 1) a calculation was carried out [3] on the basis of averaged value of the mechanical non-uniformity degree of welded joints:

$$K_{tm} = \frac{K_{t1} + K_{t2}}{2},$$

where $K_{t1} = \sigma_t^{\text{N0}} / \sigma_t^{\text{I}}$; $K_{t2} = \sigma_t^{\text{0}} / \sigma_t^{\text{I}}$; σ_t^{N0} , σ_t^{0} , σ_t^{I} are the tensile strengths of the weld, the base and the HAZ metals.

At the same time peculiarities of the combined plastic strain of more strong (CT and T) and less strong (M) metals of the considered joints are not taken into account. In static tensile tests of welded specimens their failure in presence of the plastic strain occurs, as a rule, in the place of minimal hardness of the HAZ metal, which is characterized by a developed structure and chemical and mechanical non-uniformity. In construction works different deviations from the established technology occur and appear such surface defects as lacks of fusion, undercuts, cracks, craters, and defects detected in the HAZ metal (incisions, scratch marks, cracks, scratches, and scores) on the pipelines. The actual task is study of influence of the surface plane defect in the HAZ metal of pipes, where plasticity (relative elongation δ and reduction in area ψ) achieves minimal value.

Influence of the surface defect located in the HAZ metal on static strength in case of symmetrical mechanical non-uniformity is shown in [10], whereby it is established that the main kind of failure of the big diameter pipes are surface cracks adjacent to the weld fusion line. In the failure locus crack-like defects were detected in the form of cracks, scratch marks and

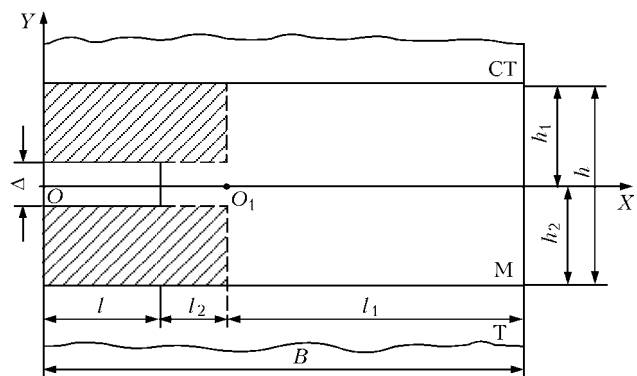


Figure 1. Parameters of soft interlayer with asymmetrical mechanical non-uniformity and surface crack-like defect of a weld (for designations see the text)

This work is supported by the RF grant of 05.08.18179a.

© A.A. OSTSEMIN, 2007



mechanical scratches. All cases of failure of the pipe walls occurred at medium working pressures in the HAZ metal near stress concentrators, that's why theoretical analysis of influence of the surface crack-like defects in the HAZ metal of a weld on static strength of the main industrial pipelines in case of the tough fracture is of great significance. Evaluation of the welding technology and operation reliability of welded joints of the pipes in presence of surface defects and development of recommendations on determining the hazard degree of the crack-like defects is of great practical significance.

For obtaining more accurate theoretical solution the calculation methodology is proposed, based on regularities of mechanical behavior of influence of surface defects of joints with asymmetrical non-uniformity of a weld. In this work, in addition to conventional assumptions and simplifying conditions, which are assumed in theoretical studies of mechanically non-uniform joints [10, 11], the assumption [12] is used, which agrees with the theory of a plastic layer [13] and generalizes known assumption of L. Prandtl — tangential stresses τ_{xy} in a soft interlayer depend upon the distance from plane, on which $\tau_{xy} = 0$ (Figure 1). Method of the investigation is based on theoretical solution of plane problem of the plasticity theory [12, 14].

The goal of this work is determination of the surface crack-like defect influence on static strength of welded joints with asymmetrical mechanical non-uniformity in tough fracture. The peculiarity of the plastic strain character of the welded joints with a crack-like defect is presence of the branching point of the soft interlayer plastic flow O_1 (see Figure 1). It is considered that in the zone between free edge of the interlayer, containing the defect, and point O_1 , above and below the defect (dashed area) plastic flow is absent, which agrees with the result of [15].

In [16] dependence of parameter α upon K_t , which at a low mechanical non-uniformity of the joint ($K_t < 1.5$) may be presented with high accuracy by the expression $\alpha = K_t - 1$, is obtained on the basis of theoretical analysis of stressed state of the mechanically non-uniform welded joint in proximity of the contact surface.

On the contact surface tangential stresses τ_{xy}^{con} don't achieve yield shear strength K_M because of involvement into plastic strain of the base metal and the weld, that's why for high values of x , i.e. for the points remote from axis OY (the flow separation planes) and located near the contact surface, boundary conditions will be as follows [14]:

$$\tau_{xy}^{K_1} = \tau_{xy}(x_1 h_1) = \alpha_1 K \quad (0 < \alpha_1 \leq 1), \quad (1)$$

$$\tau_{xy}^{K_2} = \tau_{xy}(x_1 - h_2) = \alpha_2 K \quad (0 < \alpha_2 \leq 1), \quad (2)$$

where $\tau_{xy}^{K_1}$, $\tau_{xy}^{K_2}$ are the tangential stresses on the contact surfaces CT-M and M-T, respectively; h_1 , h_2 are the distances from the plane, on which tangential stresses equal zero, to the contact surfaces CT-M and M-T ($h_1 + h_2 = h$; h is the soft interlayer thickness), re-

spectively; α_1 , α_2 are the coefficients, which characterize mechanical non-uniformity and dependent upon K_{t1} and K_{t2} , respectively.

Solution for the tangential stress is determined in the following form [11]:

$$\tau_{xy}(x, y) = \varphi(x)y, \quad (3)$$

where $\varphi(x)$ is the odd function, requiring determination.

Knowing parameters α_1 and α_2 , it is possible to find h_1 and h_2 [14]. For this we introduce in turn into the equation (3) $y = h_1$ and $y = -h_2$ and compare obtained expressions with boundary conditions (1) and (2). Then $\alpha_1 h_2 = \alpha_2 h_1$, whence

$$h_1 = \frac{\alpha_1 h}{\alpha_1 + \alpha_2}, \quad h_2 = \frac{\alpha_2 h}{\alpha_1 + \alpha_2}. \quad (4)$$

Position of the neutral line in the interlayer (where $\tau_{xy} = 0$) does not coincide with geometrical axis of symmetry and is shifted in the direction of less strong (T) base metal, which is confirmed by the experimental investigations [5]. The lower is relative thickness χ of the interlayer and the stronger is surrounding it metal, the greater is constraining of plastic strains of the soft interlayer. If the soft interlayer is surrounded by metals with different strength (T and CT), constraining of plastic strains of the soft metal will be manifested to a greater degree on the contact with a stronger metal (CT). That's why the HAZ area, adjacent to the metal with a higher strength (CT), gets stronger and failure is transferred in direction of the metal with a lower strength (T).

Solving approximately system of the plastic equilibrium equations under conditions of Huber-Mises plasticity and using results of [12], we will get:

$$\begin{aligned} \sigma_{x, i} = K_M \left\{ -0.5 \ln \operatorname{ch} \frac{2(\alpha_1 + \alpha_2) [x - (I + I_2)]}{h_i} + \right. \\ \left. + \frac{(\alpha_1 + \alpha_2)^2}{h_i^2} y^2 + \frac{\alpha_1 + \alpha_2}{2\chi} - \right. \\ \left. - 0.5 \ln 2 - \frac{1}{3} (\alpha_1^2 - \alpha_1 \alpha_2 + \alpha_2^2) \right\}, \end{aligned} \quad (5)$$

$$\begin{aligned} \sigma_{y, i} = K_1 \left\{ -0.5 \ln \operatorname{ch} \frac{2(\alpha_1 + \alpha_2) [x - (I + I_2)]}{h_i} + \right. \\ \left. + \frac{(\alpha_1 + \alpha_2)^2}{h_i^2} \frac{y^2}{\operatorname{ch}^2 \left[\frac{2(\alpha_1 + \alpha_2)}{h_i} \chi \right]} + \right. \\ \left. + 2 - 0.5 \ln 2 + \frac{\alpha_1 + \alpha_2}{2\chi} - \frac{1}{3} (\alpha_1^2 - \alpha_1 \alpha_2 + \alpha_2^2) \right\}, \end{aligned} \quad (6)$$

$$\tau_{xy, i} = K_1 \frac{\alpha_1 + \alpha_2}{h_i} y \operatorname{th} \frac{2(\alpha_1 + \alpha_2) [x - (I + I_2)]}{h_i}, \quad (7)$$

where $-h_1 < y < h_2$; $i = 1, 2$.

If $I + I_2 < x < B$ (I is the length of the crack-like defect; I_2 is the plastic layer area; B is the welded



joint width), then in the formulas (5)–(7) $h_i = h_1$ should be assumed. In this case formulas (5)–(7) determine components of the tensor of stresses in the soft interlayer to the right from the branching point O_1 . For the plastic layer zone l_2 , located between apex of the defect and point O_1 , i.e. $l < x < l + l_2$, we assume $h_1 = h_2$. We will get coordinates of the branching point O_1 , if we equate stress values σ_x to the left and to the right from this point: $l_1/h_1 = l_2/h_2$. Then we come to the system of equations for l_1 and l_2 (see Figure 1):

$$l_1 + l_2 = B - l, \quad l_1 = \frac{h(B - l)}{h + \Delta},$$

or

$$l_1 \Delta = h_2 h, \quad l_2 = \frac{\Delta(B - l)}{h + \Delta}, \quad (8)$$

where h is the welded joint thickness; Δ is the defect width.

For welded joints with lack of penetration $\Delta \leq 0.1$ mm shift of the branching point of plastic flow l_2 from apex of the defect is, according to the equation (8), small in comparison with the specimen width B . One may consider that branching point O_1 is on apex of the lack of penetration, and reduction of stresses σ_y from their maximum value σ_y^{\max} down to yield strength of the HAZ metal on free surface of the defects occurs stepwise on small bases $l_2 \rightarrow 0$. Such assumption allows significant simplifying calculation of mean ultimate stresses for welded joints with a surface defect in the HAZ metal.

Having used condition of static equivalence of total stresses σ_y to the external force P and integrated them, we will find mean ultimate stress $\sigma_{y m}$. Then we will get total force:

$$P = P_1 + P_2, \quad P_1 = \int_{l+l_2}^{\beta} \sigma_y(x, h_1) dx, \quad P_2 = \int_l^{l+l_2} \sigma_y(x, h_2) dx.$$

Having calculated the integrals, we will get:

$$P_i = \hat{E}_i I_i \left[-\frac{\alpha_1^2 + \alpha_2^2 + 0.2}{\alpha_1 + \alpha_2} \chi^{**} + \frac{\alpha_1 + \alpha_2}{4\chi^{**}} + 2 - \frac{1}{3} (\alpha_1^2 - \alpha_1\alpha_2 + \alpha_2^2) \right], \quad (9)$$

where $\chi^{**} = \frac{2(h + \Delta)}{B - l}$.

Taking into account formulas (5)–(9), we will get the mean stress for asymmetric mechanical non-uniformity of a welded joint with the surface crack-like defect of l length, using presentations of functions th and \ln , ch in the form of the power series, ignoring small terms, with accuracy 1–2 %:

$$\sigma_{y m}^{K, i} = K_1 \left(1 - \frac{l}{B} \right) \times \left[-\frac{\alpha_i^2 + 0.2}{(\alpha_1 + \alpha_2)} \chi^* + \frac{\alpha_1 + \alpha_2}{4\chi^*} + 2 - \frac{1}{3} (\alpha_1^2 - \alpha_1\alpha_2 + \alpha_2^2) \right]. \quad (10)$$

For the cracks at $\Delta = 0$ we get $\chi^* = \frac{\chi}{1 - l/B}$. Taking into account substitution of K_M for $\sigma_t^M/\sqrt{3}$, formula (10) for surface cracks will assume the form of

$$\sigma_{y m}^{K, i} = \frac{\sigma_t^M}{\sqrt{3}} \left\{ \left[\frac{\alpha_1 + \alpha_2}{8\chi} \left(1 - \frac{l}{B} \right)^2 - \left[1 - \frac{\alpha_1^2 - \alpha_1\alpha_2 + \alpha_2^2}{6} \right] \left(1 - \frac{l}{B} \right) - \frac{\alpha_i^2 + 0.2}{2(\alpha_2 + \alpha_2)} \chi \right] \right\}, \quad (11)$$

where $\chi^* = \frac{h + \Delta}{B - l}$; $\chi = \frac{h}{B}$.

It should be noted that in case of absence of the defect in formula (11) $l = \Delta = 0$, we will get formulas, presented in [14]. We determine from formula (11) allowable range of relative critical sizes of cracks, for which the welded joint is of equal strength with the base metal without a defect, provided $\sigma_{y m} = 2K_M$:

$$\left(\frac{l}{B} \right)^{\text{cr}} = 1 - \frac{2\chi}{\alpha_1 + \alpha_2} \left\{ 1 - \frac{\alpha_1^2 - \alpha_1\alpha_2 + \alpha_2^2}{6} + \sqrt{\left(1 - \frac{\alpha_1^2 - \alpha_1\alpha_2 + \alpha_2^2}{6} \right)^2 + \frac{\alpha_1 + \alpha_2}{2\chi} + \frac{\alpha_i^2 + 0.2}{4}} \right\}. \quad (12)$$

For a symmetrical mechanical non-uniformity at $\alpha = \alpha_1 = \alpha_2$, expression (12) assumes form of the formula obtained in [10]. As mechanical non-uniformity coefficients K_{t1} and K_{t2} reduce, critical value of a surface defect in the HAZ metal decreases.

When $\alpha = \alpha_1 = \alpha_2$, formula (11) turns into the dependence for mean normal stresses $\sigma_{y m}^{K, i}/2K_M$ of welded joints with symmetrical mechanical non-uniformity with a surface defect in the HAZ metal obtained in [10]:

$$\sigma_{y m}^{K, i} = 2K_M \times \left[\frac{\alpha}{2\chi} \left(1 - \frac{l}{B} \right)^2 - \left(1 - \frac{\alpha^2}{6} \right) \left(1 - \frac{l}{B} \right) - \frac{\alpha_i^2 + 0.2}{4\alpha} \chi \right]. \quad (13)$$

In Figure 2 theoretical dependence according to formula (13) and experimental values [17] for titanium alloys (welded joints of $100 \times 95 \times 25$ mm size, $\sigma_t^T = 875$ MPa, $\sigma_t^M = 600$ MPa, $K_t = 1.33$, $\alpha = 0.33$ at $\chi = 0.3$ and $\chi = 0.5$). An external one-sided surface defect was simulated by sharp notches. As relative thicknesses of the soft interlayer χ reduce from 0.5 to 0.3, mean normal stresses $\sigma_{y m}^{K, i}$ increase due to the contact strengthening of the soft interlayer. Good correspondence of new theoretical results and experimental investigations was obtained [17].

New theoretical formulas may be used for estimating straight seam pipes of big diameter with a surface defect, located in the HAZ metal, at the mechanical non-uniformity coefficient $K_t = 1.1$ – 1.2 . To do this it is necessary to substitute in formulas [18] tensile strength σ_t for mean stresses $\sigma_{y m}$ according to formula (11).

Equating $\sigma_{y m}$ according to formula (11) to the value $\sigma_m = 2K_y(1 - l/B)$ of strength of the welded

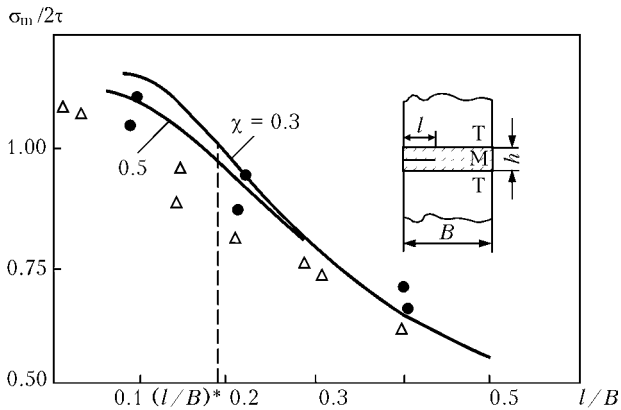


Figure 2. Comparison of theoretical data (solid curves) according to formula (13) at $\alpha = \alpha_1 = \alpha_2$, and experimental data on strength of welded joints at $\chi = 0.3$ (●) and 0.5 (Δ) [17] and $K_t = 1.33$; $(l/B)^* = 0.19$

joint with a defect l/B , we will determine χ_p , taking into account contact strengthening of a welded joint, at which strength of the CT-M-T joint equals strength of the base metal:

$$\chi_{p,i} = \left\{ - \left[\sqrt{3} K_{t,i} + \left(1 - \frac{\alpha_1^2 - \alpha_1 \alpha_2 + \alpha_2^2}{6} \right) \left(1 - \frac{l}{B} \right) \right] + \sqrt{\left[\sqrt{3} K_{t,i} + \left(1 - \frac{\alpha_1^2 - \alpha_1 \alpha_2 + \alpha_2^2}{6} \right) \left(1 - \frac{l}{B} \right) + (\alpha_1^2 + \alpha_2^2 + 0.2) \left(1 - \frac{l}{B} \right)^2 \right]} \times \frac{2(\alpha_1 + \alpha_2)}{\alpha_1^2 + \alpha_2^2 + 0.2} \right\} \quad (14)$$

According to formula (14) at $K_t = 1.33$ ($l/B = 0$) we get $\chi_p = 0.18$, which agrees well with theoretical results ($\chi_p = 0.181$) [7] and experimental data [17].

Proceeding from ensuring of load-carrying capacity of welded joints of big-diameter pipes with asymmetrical mechanical non-uniformity at the level of the base metal strength, optimal ranges of HAZ sizes were established. Range of relative sizes of soft interlayers, at which strength of the welded joint CT-M-T equals the base metal strength, is rather narrow ($\chi_p = 0.15-0.17$), i.e. maximum size of HAZ at thickness of a pipe 22 mm equals 3.74 mm, which does not correspond to sizes of weakened areas of the big diameter pipes ($\chi_p = 0.3-0.5$) [1] because of a wide weld, high welding heat input q/v , and the equipment being used.

If areas CT, T and M of the welded joint are inclined to strengthening, then for determining mean fracture stresses σ_m it is necessary to substitute in formulas (10) and (11) K_M for $(\beta \sigma_t^M)/2$, where β is the parameter that characterizes instability of the process of the welded joint plastic strain (for the ideal elastic-plastic body $\beta = 2/\sqrt{3}$). Carried out theoretical analysis shows that as welding heat input q/v reduces, degree of the weakening K_t and width of weakened area χ decrease, that's why strength of a welded joint σ_{ym} increases due to contact strengthening, and under certain conditions and welding technologies strength balance between the welded joint with asymmetrical mechanical non-uniformity and the base metal may be achieved in tough fracture.

These results can be used in expertise of accidents [18, 19], intrapipe diagnostics of main pipelines, expert evaluation of a weld, and for increasing operation reliability of main gas-and-oil pipelines.

CONCLUSIONS

1. The formulas are obtained for calculating tensor of stresses, ultimate tensile forces, and mean fracture stresses for asymmetrical mechanical non-uniformity of the welded joints with a surface crack-like defect, which are generalizations of respective formulas for symmetric welded joints and agree well with experimental results.

2. Suggested methodology for evaluation of static strength of welded joints with asymmetrical mechanical non-uniformity will allow determining load-carrying capacity by introduction into the calculation relations of the mechanical non-uniformity coefficients K_{t1} and K_{t2} .

3. The area of assumed failure of the straight seam pipes of big diameter in case of the limit pressure excess is the line, located in HAZ adjacent to the weld fusion line.

1. Anuchkin, M.P., Goritsky, V.N., Miroshnichenko, B.I. (1986) *Pipes for main pipelines*. Moscow: Nedra.
2. Pokhodnya, I.K., Shejnkina, M.Z., Shlepkov, V.N. et al. (1987) *Arc welding of position joints of main pipelines*. Moscow: Nedra.
3. Astafiev, A.S., Navoev, V.S. (1965) Welding of heat-hardened low alloy steel. *Svarochn. Proizvodstvo*, **3**, 1-4.
4. Bakshi, O.A., Piksaev, B.P., Kulnevich, T.V. et al. (1968) Evaluation of strength of heat-hardened steel welded joints. *Voprosy Svarochn. Proizvodstva*, **63**, 84-93.
5. Klykov, N.A., Reshetov, A.L. (1979) Strength of welded joints with asymmetrical mechanical non-uniformity. *Avtomatich. Svarka*, **12**, 29-32.
6. Ostsemin, A.A., Shakhmatov, M.V., Erofeev, V.V. (1984) Influence of welding defects, located on fusion line, on strength of welded butt of large diameter pipes. *Problemy Prochnosti*, **8**, 111-116.
7. Ostsemin, A.A., Dilman, V.L. (2004) Evaluation of mechanical non-uniformity effect on strength of large diameter heat-hardened pipes and plates with defects in welds. *Vestnik Mashinostroeniya*, **9**, 23-28.
8. Ostsemin, A.A. (1994) Strength and stress state of interlayer in thin-wall cylindrical vessel under biaxial loading. *Avtomatich. Svarka*, **5/6**, 18-20.
9. Bakshi, O.A. (1985) About taking into account of mechanical non-uniformity factor of welded joints in tensile test. *Svarochn. Proizvodstvo*, **7**, 32-34.
10. Ostsemin, A.A., Dilman, V.L. (2005) Static strength of mechanically non-uniform welded joints with one-sided surface defect in tough fracture. *Khim. i Neft. Mashinostroenie*, **10**, 9-12.
11. Dilman, V.L., Ostsemin, A.A. (1998) Stress state and strength of welds of large diameter pipes. *Ibid.*, **4**, 16-20.
12. Ostsemin, A.A., Dilman, V.L. (1990) About compression of plastic layer by two rough plates. *Problemy Prochnosti*, **7**, 107-112.
13. Unkskov, E.P., Jonson, U., Kolmogorov, V.L. et al. (1992) *Theory of forging and forming*. Moscow: Mashinostroenie.
14. Dilman, V.L., Ostsemin, A.A. (1998) Stressed state strain and strength of welded joints with mechanical non-uniformity. *Svarochn. Proizvodstvo*, **5**, 15-17.
15. Dilman, V.L., Ostsemin, A.A. (1999) Strength of mechanically non-uniform welded joints with slot-like defect. *Ibid.*, **2**, 12-15.
16. Dilman, V.L., Ostsemin, A.A., Voronin, A.A. (2002) Carrying capacity of large diameter straight seam pipes with defects on weld fusion line. *Ibid.*, **3**, 3-7.
17. Shakhmatov, M.V. (1988) Carrying capacity of welded joints with defects in solid and soft welds. *Avtomatich. Svarka*, **6**, 14-17.
18. Ostsemin, A.A., Zavarukhin, V.Yu. (1993) Strength of oil pipeline with surface defects. *Problemy Prochnosti*, **12**, 51-59.
19. Ostsemin, A.A. (1998) Analysis of carrying capacity of active oil main pipeline in presence of defects in longitudinal weld. *Svarochn. Proizvodstvo*, **9**, 11-15.



NEW ELECTRON BEAM EQUIPMENT AND TECHNOLOGIES OF PRODUCING ADVANCED MATERIALS AND COATINGS

N.I. GRECHANYUK, P.P. KUCHERENKO and I.N. GRECHANYUK
SPC «Gekont», Vinnitsa, Ukraine

The paper describes the current achievements of SPC «Gekont» in the field of practical application of the technologies of vacuum melting and evaporation of materials for deposition of thermal barrier coatings of MeCrAlY and other systems on gas turbine blades, producing condensed composite materials for diverse electric contacts, remelting the wastes of metals and alloys to produce sound ingots. Information on development and application of specialized equipment is given.

Keywords: electron beam technologies, melting and evaporation in vacuum, deposition of thermal barrier coatings, condensing composite materials, remelting of metals and alloys, gas turbine blades, electric contacts, specialized equipment

Electron beam impact on the metals leading to their heating, melting and evaporation, as a new technological path in the field of material processing has been intensively developed starting from the middle of XX century [1, 2].

Development of electron beam technology runs along three main paths:

- melting and evaporation in vacuum to produce materials, films, coatings; powerful (up to 1 MW and higher) electron beam units at the accelerating voltage of 20–30 kV are used; power concentration is relatively low (not more than 10^5 W/cm²);
- welding of metals; equipment of three classes has been developed: low-, medium- and high-voltage covering the accelerating voltage range from 20 to 150 kV; unit power is from 1 to 120 kW and higher at maximum power concentration of 10^5 – 10^6 W/cm²;
- precision treatment of materials (drilling, milling, cutting); high-voltage (80–150 kV) low power (up to 1 kW) units are used, providing the specific power of $5 \cdot 10^8$ W/cm².

Improvement of equipment [3, 4], heat sources [5], metal vapour sources [6] and development of equipment for observation, monitoring and control of the process of electron beam impact is performed simultaneously. In development of new processes for growing metal (composite) films, the main attention is given to controlling the metal vapour flows: through energy state of the condensing particles, their molecular composition, intensity, spatial distribution of the flow, etc. It is known that the widely accepted open-type evaporators, including quasi-closed ones, are characterized by instability of the directivity diagram of the vapour flow in time, even at constant temperature. Radiation load on the film growth surface from these sources is sometimes comparable to the energy of vapour flow condensation. Therefore, when they are used, it is quite difficult to produce reproducible

film structures with controllable parameters. Particular difficulties arise at high evaporation rates, when microdrops are usually present in the vapour flow.

SPC «Gekont» is intensively developing the first of the above areas. Special attention is given to development and manufacturing of laboratory and production electron beam equipment for implementation of a number of new technological processes:

- deposition of thermal barrier coatings on gas turbine blades;
- producing composite materials of dispersion-strengthened, microlaminate and microporous type from the vapour phase;
- producing pure refractory metals, special alloys, ferroalloys, polycrystalline silicon for the needs of aerospace and power engineering, and aircraft construction;
- producing complex-alloyed powders of metallic and ceramic types for plasma deposition of coatings.

Protective coatings on gas turbine blades and equipment for their deposition. At SPC «Gekont» protective coatings on gas turbine blades are produced by electron beam evaporation of MeCrAlY (where Me is Ni, Co, Fe), MeCrAlYHfSiZr alloys and ZrO₂-based ceramics stabilized by Y₂O₃. Alongside the traditional single-layer metallic materials of MeCrAlY, MeCrAlYHfSiZr type and two-layer metal/ceramic materials, three variants of three-layer thermal barrier coatings have been developed, the schematics of which are given in Figure 1.

The simplest coating is a three-layer coating with an inner metallic (damping) MeCrAlY, MeCrAlYHfSiZr (where Me is Ni, Co, Fe or alloys on their base), intermediate composite MeCrAlY, MeCrAlYHfSiZr–MeO (where MeO is Al₂O₃, ZrO₂–Y₂O₃), dispersion-strengthened or microlaminate type and outer ZrO₂–Y₂O₃ ceramic layers (Figure 1, a) [7]. The second variant is similar to the first one with the only difference that the outer ceramic layer is made in the form of a zigzag (Figure 1, c). The most interesting is the third variant of the coating, where dispersed particle of refractory borides are added to the outer ceramic layer (ZrO₂–Y₂O₃), which is also made



Outer ceramic layer with a columnar structure	Outer ceramic layer of zigzag type	Outer ceramic layer of zigzag type with «self-regulation» elements
Intermediate high-temperature layer of dispersion-strengthened or microlaminate type	Intermediate high-temperature layer of dispersion-strengthened or microlaminate type	Intermediate high-temperature layer of dispersion-strengthened or microlaminate type
Inner metallic damping layer	Inner metallic damping layer	Inner metallic damping layer
Base	Base	Base
<i>a</i>	<i>b</i>	<i>c</i>

Figure 1. Schematics of thermal-barrier coatings (see the text)

in the form of a zigzag. In operation of products with such a coating, when the outer ceramic layer develops cracks, the boride particles, while oxidizing, form the respective oxides, which heal the developing microcracks. Thus, such a coating has the effect of «self-healing» or «self-restoration».

Two types of production electron beam equipment were developed for implementation of the technological processes of thermal barrier coating deposition on turbine blades [3, 4, 7–10]. Figure 2 shows the general view of a production electron beam unit L-1, which is successfully operated in the science-engineering complex «Zorya–Mashproekt», Nikolaev, Ukraine. When the unit design was developed, a traditional three-chamber schematic of equipment layout was used [7, 9]. The unit working chamber is used for coating deposition proper, and the two auxiliary chambers — for loading-unloading of cassettes with blades. The unit is fitted with eight electron guns of 60 kW power each, of «Gekont» design [7]. Four guns are designed for evaporation of initial materials of 70 mm diameter arranged in a row, the other four guns — for heating the coated items from below or from the top. Maximum overall dimensions of the coated items are as follows: up to 700 mm length, up to 350 mm diameter.

A feature by which the unit differs from those developed earlier [1] is the possibility of conducting not only the technological process of deposition of all the types of thermal barrier coatings, but also obtaining composition materials of the dispersion-strengthened, microlaminate and microporous types in the

form of sheet blanks of up to 800 mm diameter and up to 5 mm thickness. The above equipment can be also used for deposition of superhard wear-resistant coatings on the dies, moulds, special optical coatings (for instance, mirrors from silicon carbide), etc.

At present SPC «Gekont» developed design documentation on fundamentally new electron beam equipment for deposition of protective coatings [3, 4]. The machine (Figure 3) is a vacuum unit consisting of four vacuum chambers (Figure 3, a) connected to each other: main process chamber proper 1, transition chamber 2 and two load chambers (fore chambers) 3. Mounted inside process chamber 1 (Figure 3, b) are water-cooled crucibles 4, which accommodate ingots 5, 6 of evaporation materials. Beams of electron guns 2 evaporate the ingot material, which is condensed on

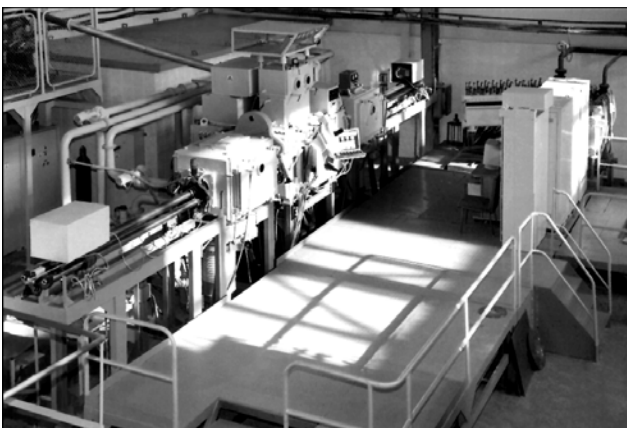


Figure 2. Electron beam unit L-1

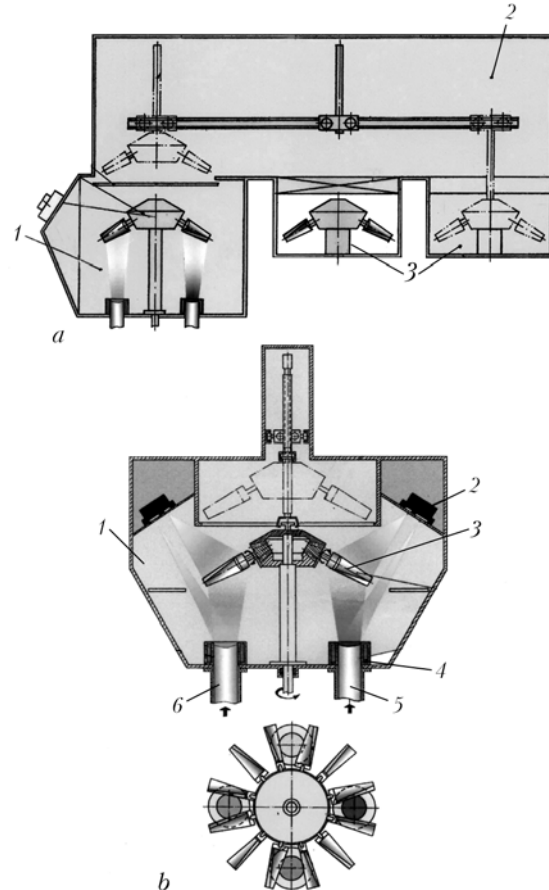


Figure 3. Unit for protective coating deposition (for designations see the text)

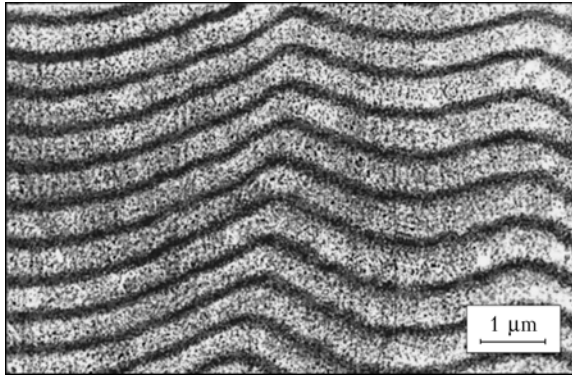


Figure 4. Fine structure of (Cu-Zr-Y)/Mo microlaminate materials

items 3 in the form of vapour. The quantity of the used crucibles can vary, depending on the required composition and design (two-, three-layer, microlaminate) coating. The unit design is fundamentally new [3, 4]. This unit enables deposition of all types of protective coatings, including new types of silicide coatings of microlaminate type.

It should be noted that the Company implemented a closed cycle of coating deposition on turbine blades, including melting of all types of ingots on nickel, cobalt and iron bases in keeping with TU U 27.4-20113410-002--2003, and using ceramic ingots according to TU U 13.2-20113410-004--2003. Production of Ni(Co)CrAlYSi powders of 40–100 μm fraction for plasma deposition of coatings has also been mastered.

Composite materials for electric contacts and equipment for their production. Despite the wide application of the processes of evaporation and condensation for deposition of protective coatings, the unique capabilities of the zonal method for producing fundamentally new materials of dispersion-strengthened, microlaminate and microporous types, functionally-graded materials, etc., did not find application. Development of scientific principles of producing microlaminate materials with less than 0.5 μm thickness of alternating layers at deposition temperatures higher than 0.3 of the melting temperature of the most low-melting of the evaporation materials, is a substantial scientific achievement [11]. It is known that until recently such materials were produced by the method of electron beam evaporation and subsequent condensation of metals and non-metals in vacuum at substrate temperature not higher than 300 °C [12]. These data were the basis for development for the first time in the world practice of a production electron beam technology of producing thick (up to 5 mm) microlaminate materials (Cu-Zr-Y)/Mo (Figure 4) for electric contacts [13]. Condensed materials Cu--(0.08–0.2) % Zr--(0.08–0.2) % Y--(8–12) % Mo are produced in a production electron beam unit L-5 (Figure 5). Technological schematic of producing this material is shown in Figure 6. Condensed materials (Cu-Zr-Y)/Mo are sheets of 1000 mm diameter and up to 5 mm thickness, which are cut up into blanks and soldered onto the contact-holder. Tensile strength and proof stress, depending on the technological condition of production can vary between 645 and 1200 MPa and from 596 to



Figure 5. Electron beam unit L-5

1000 MPa, respectively, relative elongation --- from 2.0 to 8.7 % [14]. New composites, which were named dispersion-strengthened materials for electric contacts» (DSMC), are certified and are produced in keeping with the technical conditions [15].

The main advantages of DSMC materials are as follows:

- absence of silver in their composition, so that they are 1.8–3 times less expensive compared to powder electric contact materials and in terms of operating reliability are 1.5–3 times superior to the existing electrical engineering materials;
- they do not maintain arcing;
- completely replace beryllium bronze;
- can stand switching current of up to 1000 A.

The most effective areas of DSMC application are as follows:

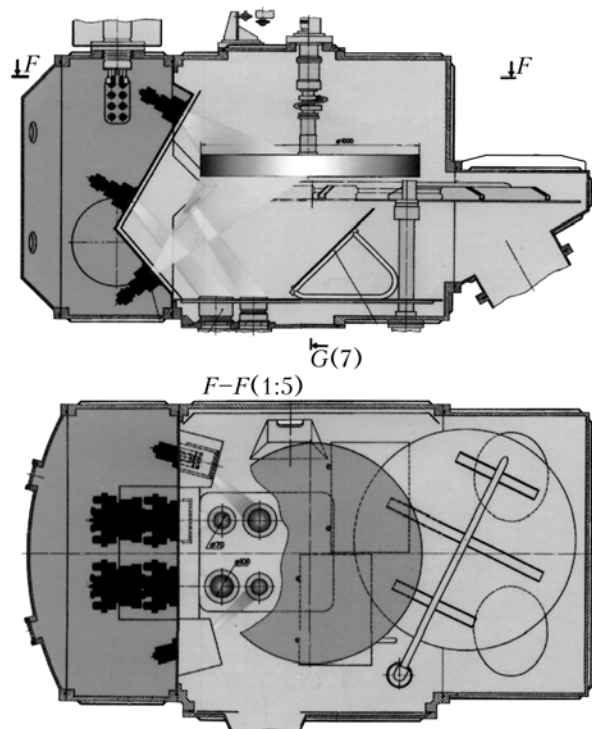


Figure 6. Technological schematic of producing microlaminate materials (Cu-Zr-Y)/Mo



Figure 7. Appearance of a range of electric contacts

- city and long-distance electric transport (contacts used in trams, trolleybuses, trains, metro);
- lift services (passenger and freight lifts);
- port, ship cranes and other hoisting mechanisms;
- electric trolleys of all types;
- mining equipment;
- production and household electrical engineering devices, containing relays, starters, contactors, knife switches, etc.;
- tips for plasma cutting of metals and alloys;
- electrodes of resistance welding machines.

So far according to [16], more than 1.5 mln electric contacts of 370 names have been produced (Figure 7) which are successfully operating in CIS countries, Czechia and Roumania.

Simultaneously with introduction of materials for interrupting electric contacts into industry, the company in co-operation with Institute for Materials Science Problems, of NASU, «Generator» Plant (Kiev), Wrocław Polytechnic Institute (Poland) is working to develop composite materials based on copper, chromium, tungsten, carbon, applied in production of slide contacts, contacts for vacuum blowout chambers (Figure 8).

Production technologies of electron beam remelting of metals and alloys and equipment for their implementation. The Company has mastered the in-



Figure 8. Appearance of contacts for vacuum blowout chambers



Figure 9. Specialized electron beam unit for melting metals and alloys

dustrial technology of electron beam remelting of wastes of high-speed steels and producing finished ingots for subsequent manufacturing of tools from them [17, 18]. The used equipment allows remelting in vacuum the wastes of high-speed steel (used tools, tool production wastes) and producing cylindrical ingots of 60 to 130 mm diameter and ingots of 140--160 mm cross-section and up to 2000 mm length.

Technological and cost advantages are as follows:

- process of ingot remelting and forming occurs in one technological cycle without subsequent thermomechanical treatment (forging, squeezing);
- possibility of remelting lump charge;
- rapid replacement of fixtures for producing ingots of the required dimensions;
- high quality of the produced ingots after vacuum remelting;
- producing small batches of finished ingots;

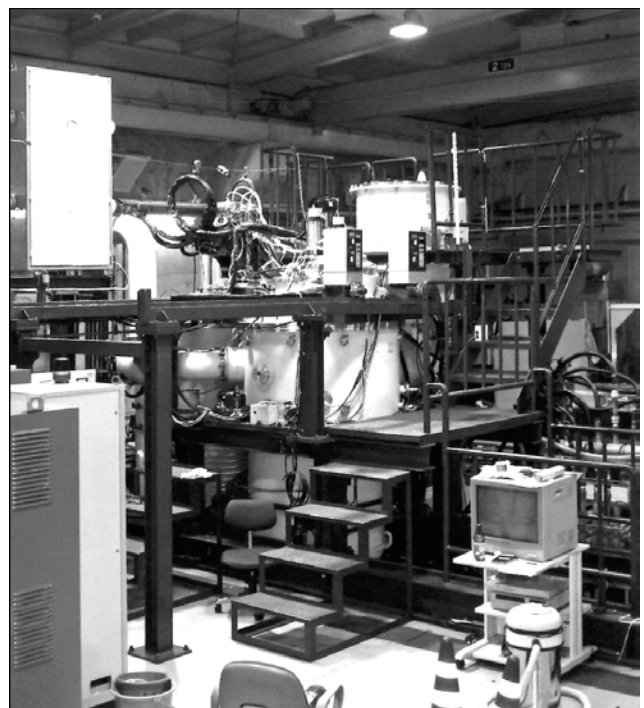


Figure 10. 500 kW electron beam unit for silicon remelting



• cost of finished ingots is approximately 2–3 times lower than that of ingots produced by the traditional technology.

A number of specialized production electron beam units have been developed recently for melting super alloys, refractory metals, titanium and producing finished ingots of the diameter from 60 to 300 mm and up to 2500 mm length. The appearance of a unit of such a type is shown in Figure 9. New high-voltage power sources of SPC «Gekont» design and electron beam gas-discharge guns with a cold cathode developed under the guidance of V.I. Melnik were used in these units for the first time [19].

Special attention is given today to development of new technologies and equipment for melting silicon and ferroalloys. The Company supplied to Japan three electron beam units of 10, 20, 500 kW power for electron beam remelting of silicon (Figure 10).

The above examples of practical application of the processes of melting and evaporation of metals and non-metals in vacuum are a convincing proof of an ever wider application of special electrometallurgy for development of new materials and coatings.

1. Movchan, B.A., Malashenko, I.S. (1983) *Vacuum-deposited heat-resistant coatings*. Kiev: Naukova Dumka.
2. Zuev, I.V. (1998) *Treatment of materials by concentrated energy flows*. Moscow: MEI.
3. Grechanyuk, M., Kucherenko, P. *Installation for electron-ray coating of coatings*. Pat. US 6,923,868 BZ. Publ. 02.08.2005.
4. Grechanyuk, N.I., Kucherenko, P.P. *Installation for electron beam deposition of coatings*. Pat. 2265078 RF. Publ. 12.27.2005.
5. Novikov, A.A. (2003) *Gas-discharge gun and method of its control*. Pat. 60377 Ukraine. Publ. 2003.

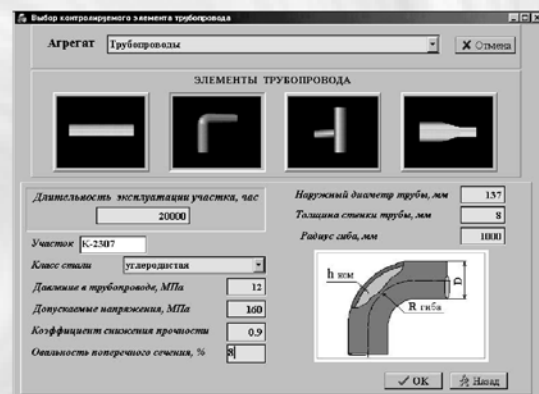
6. Zolkin, A.S. (1992) *Sources of metal vapors for research and technologies*. Novosibirsk: ITF.
7. Grechanyuk, N.I., Kucherenko, P.P., Osokin, V.A. et al. (2000) State-of-the-art and prospects of development of thermal barrier coatings (TBC) for gas turbine blade units and equipment for their deposition. *Novyny Energetyky*, **9**, 32–37.
8. Grechanyuk, N.I., Dyatlova, E.K., Kucherenko, P.P. et al. (2001) *Electron gun with linear thermocathode for electron beam heating*. Pat. 40664 Ukraine. Publ. 2001.
9. Grechanyuk, N.I., Kucherenko, P.P., Osokin, V.A. et al. (2001) *Protective coating for gas turbine blades*. Pat. 42052 Ukraine. Publ. 2001.
10. Grechanyuk, N.I., Osokin, V.A., Shpak, P.A. et al. (2005) Influence of technological parameters on structure of external ceramic layer in two-layer metal-ceramic coatings produced by electron beam deposition in one technological cycle. *Poroshk. Metallurgiya*, **3/4**, 41–48.
11. Grechanyuk, N.I. *Method of production of microlayer thermostable materials*. Pat. 2271404 RF. Publ. 03.10.2006.
12. Iliinsky, A.I. (1986) *Structure and strength of lamellar and dispersion-strengthened films*. Moscow: Metallurgiya.
13. Grechanyuk, N.I., Osokin, V.A., Afanasiev, I.B. et al. *Composite material for electric contacts*. Pat. 34875 Ukraine. Publ. 2001.
14. Borisenko, V.A., Bukhanovsky, V.V., Grechanyuk, N.I. et al. (2005) Temperature dependences of statistical mechanical properties of microlayer composite material MDK-3. *Problemy Prochnosti*, **4**, 113–120.
15. *TU U 20113410.001–98*: Dispersion-strengthened materials for electric contacts.
16. *TU U 31.2-20113410-003–2002*: Electric contacts on the base of dispersion-strengthened materials.
17. Shpak, P.A., Grechanyuk, V.G., Osokin, V.A. (2002) Effect of electron beam remelting on structure and properties of high-speed steel R6M5. *Advances in Electrometallurgy*, **3**, 12–14.
18. Grechanyuk, N.I., Afanasiev, I.Yu., Shpak, P.A. et al. *Method of production of blanks for tools from high-speed steel*. Pat. 37658 Ukraine. Publ. 2003.
19. Melnik, V.I., Melnik, I.V., Tugay, B.A. et al. (2006) Technological equipment for electron beam refusing on the base of glow discharge electron guns. *Elektrotehnika and Elektronika*, **5/6**, 119–121.

COMPUTER SYSTEM FOR EVALUATION OF STRENGTH AND LIFE OF PIPELINES WITH EROSION-CORROSION WEAR

The computer system allows evaluation of residual life and strength of pipeline systems on the basis of information about an object, its material, as well as results of examination of its technical condition.

The system can help to improve reliability of objects in operation, reduce equipment costs and extend the overhaul period.

Application. The computer system is intended for evaluation of strength and residual life of power engineering equipment components (pipeline systems for transportation of steam and hot water, heat exchangers, pressure vessels) with local thinning of walls formed as a result of erosion-corrosion wear. It can be applied for evaluation of performance of power engineering equipment operating at enterprises of power generation and other industries.



Contacts: Prof. Makhnenko V.I.
E-mail: d34@paton.kiev.ua

MAIN TRENDS IN TECHNOLOGY FOR REPAIR OF ACTIVE PRESSURISED MAIN PIPELINES*

V.S. BUT and O.I. OLEJNIK

E.O. Paton Electric Welding Institute, NASU, Kiev, Ukraine

Design approach is proposed to development of repair technologies for pressurised main pipelines having different types of defects in their linear part using arc welding. Design-technological schemes of repair of pipelines and criteria for selection of repair methods, depending upon the character and parameters of defects, are given.

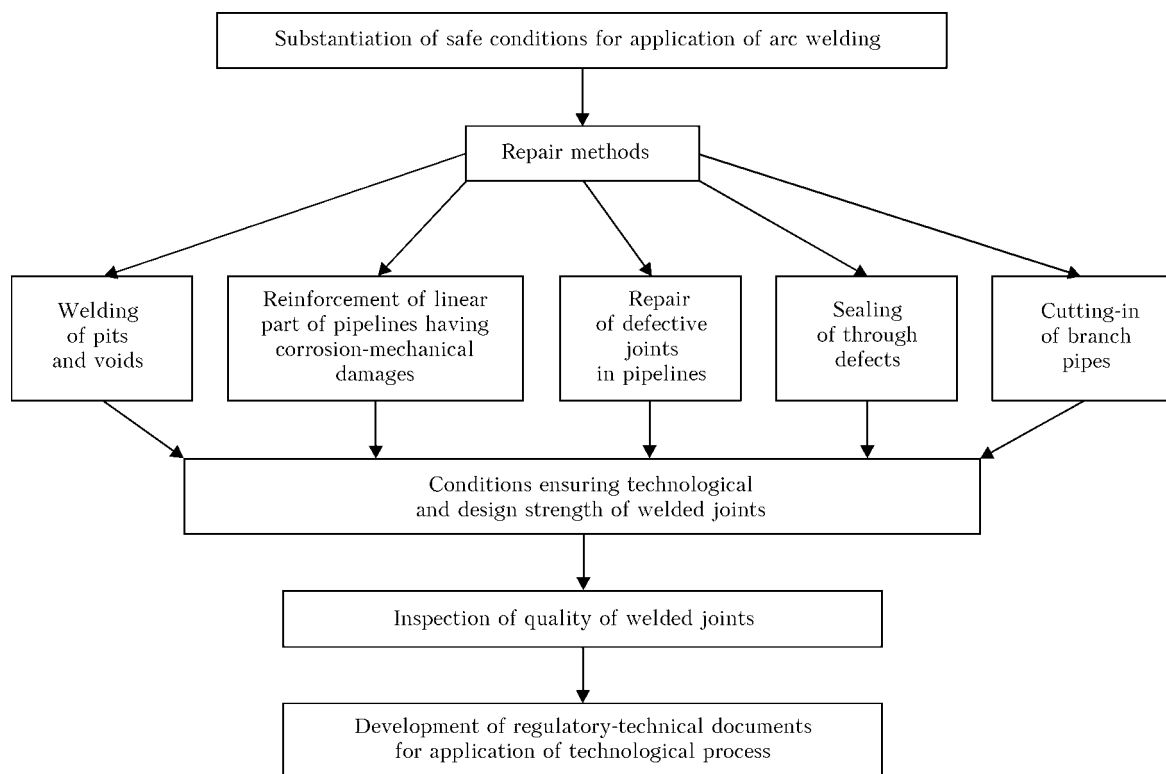
Keywords: arc welding, main pipelines, design-technological repair schemes, geometric parameters of defects

Ukraine has a branched network of pipelines for transportation of natural gas, oil and oil products. Total length of main pipelines controlled by National Joint Stock Company «Naftogaz Ukrainy» is over 45,000 km. These pipelines are composed mostly of main gas pipelines (about 38,000 km), and, in a smaller volume, main oil and product pipelines, the total length of which is 4,700 and 3,400 km, respectively.

Pipeline transport is one of the few industries that continue functioning in the stable manner, despite the crisis phenomena occurring in the economy of Ukraine. Stable functioning of the pipeline transport is pro-

moted by the fact that its capacities are aimed primarily at ensuring export of Russian energy supplies through the territory of Ukraine to third countries: 90 % of export of Russian gas (up to 120 billion cubic metres per year) and annual transit of oil (above 30 million tons) to countries of the Central and Western Europe and Turkey.

Ukraine meets its demands for energy and monetary supplies owing to the sustained operation of gas and oil transportation systems. Despite the fact that Russia explores new routes for its gas export, Ukraine, with its high-capacity system of main gas pipelines, developed infrastructure and highly skilled workers, will remain the key country for transit of Russian gas.



Structure chart of development of repair technologies for pressurised main pipelines

*The article is based on the results of accomplishment of target integrated program of the NAS of Ukraine «Problems of Service Life and Safe Operation of Structures, Constructions and Machine» (2004–2006).

**Table 1.** Selection of repair method depending on the character and parameters of defects

No.	Character of defects and their geometric parameters	Repair method (designation)
Corrosion-mechanical damages		
1	$h_d \leq 20 \% t_r; L_{d,l} \leq L_{cr}$	Grinding (İ 13)
2	External ($20 \% t_r < h_d \leq 50 \% t_r; L_{d,l} \leq L_{cr}$)	Band (İ 1) Composite band (İ 14) Compound sleeve (İ 4)
3	Internal	Leak-proof sleeve (İ 2)
4	$50 \% t_r < h_d \leq 80 \% t_r; L_{d,l} \leq L_{cr}$	Leak-proof sleeve (İ 2) Composite band (İ 14) Compound sleeve (İ 4)
5	$h_d > 20 \% t_r; t_{rem} \geq 5 \text{ mm}$, occasional defects ($S \leq 80 \times 80 \text{ mm}$ at distance of $4t_r$)	Welding up (İ 12) Patch-sleeve (İ 6) Composite band (İ 14) Compound sleeve (İ 4)
6	$L \leq 100 \text{ mm}$ or group of nearby pits $h_d > 40 \% t_r$	Patch-sleeve (İ 6) Composite band (İ 14) Compound sleeve (İ 4)
7	Extended defects in circumferential direction $h_d > 20 \% t_r; L_{d,c} \geq 1/6\pi D_{out}$	Leak-proof sleeve (İ 2) Two-layer sleeve (İ 3)
8	Corrosion-mechanical damages in weld zone of circumferential joint ($h_d > 40 \% t_r$)	Two-layer sleeve (İ 3)
Delaminations		
9	Not escaping to surface	Band (İ 1) Composite band (İ 14) Compound sleeve (İ 4)
10	Escaping to surface	Leak-proof sleeve (İ 2)
11	In weld zone of circumferential joint	Two-layer sleeve (İ 3) Composite band (İ 14)
12	In weld zone of longitudinal (spiral) joints	Composite band (İ 14) Leak-proof sleeve (İ 2) Compound sleeve (İ 4)
13	Protrusion	Two-layer sleeve (İ 3) Volumetric sleeve with filler (İ 5)
Cracks		
14	$h_d < 20 \% t_r; L_{d,l} \leq 2\sqrt{D_{out} t_r}; h_d < 20 \% t_r; L_{d,c} < 1/6\pi D_{out}$	Grinding (İ 13)
15	$L \leq 150 \text{ mm}; h_d > 20 \% t_r$	Branch pipe-sleeve with cutting out of defective region through gate or tap valve (İ 9)
16	$L > 150 \text{ mm}; h_d > 20 \% t_r$	Cutting out of spool
Geometric defects in pipe		
17	Corrugations up to $5 \% D_{out}$ high	Volumetric sleeve with filler (İ 5)
18	Corrugations up to 20 mm high	Two-layer sleeve (İ 3)
19	Nicks to $3.5 \% D_{out}$ deep	Composite band (İ 14) Band with filling of nick (İ 1) Compound sleeve (İ 4)
20	Nicks more than $3.5 \% D_{out}$ deep, inadmissible according to strength design	Branch pipe-sleeve with cutting out of defective region through gate valve (İ 9). Cutting out of spool
21	Nicks of any depth, combined with scratch, crack and loss of metal	Branch pipe-sleeve with cutting out of defective region through gate valve (İ 9) Cutting out of spool
22	Defects in circumferential welded joints, inadmissible according to regulatory-technical documents	Two-layer sleeve (İ 3)
23	Edge displacement in circumferential joint on pipeline. Bevel joint	Two-layer sleeve (İ 3)

Table 1 (cont.)

No.	Character of defects and their geometric parameters	Repair method (designation)
24	Abnormal longitudinal weld on pipeline	Composite band (İ 14) Compound sleeve (İ 4) Band (İ 1)
Through defects		
25	Process holes more than 100 mm in diameter	Patch reinforced with band (İ 7) Branch pipe-sleeve (İ 9) Branch pipe with collar (İ 8)
26	Through defects less than 50 mm in diameter (with no pressure in pipeline)	Chop-pipeline-band (İ 10)
27	Through defects less than 20 mm in diameter (pressurized active pipeline)	Patch-sleeve with sealant (İ 11)
28	Defects not subject to repair, inadmissible design elements or repair structures	Cutting out of spool
<i>Note.</i> h_d --- depth of defect; d_d --- diameter of defect; S --- surface area of defect; $L_{d,1}$ --- length of defect in longitudinal direction; $L_{d,c}$ --- same in circumferential direction; D_{out} --- outside diameter of pipe; t_r --- rated thickness of pipe wall; t_{rem} --- remaining thickness of pipe wall; L_{cr} --- critical length of defect (ANSI/ASME B.31G).		

Structure of gas pipelines of State Company «Ukrtransgaz» [1] is distributed, as to the operation time, as follows: up to 20 years --- 45 %, from 20 to 33 years --- 32 %, and over 33 years --- 23 %. Pipelines with a diameter of not less than 720 mm constitute more than a half of all gas pipelines, the considerable part of which being transit and main gas pipelines with a diameter of 1020–1420 mm (37 % of the total length of pipelines). As to main oil pipelines controlled by Joint Stock Company «Ukrtransnafta», the character of distribution of pipelines as to their operation time is as follows: up to 10 years --- 16.7 % (795.7 km), from 10 to 20 years --- 4.9 % (235.4 km), from 20 to 30 years --- 18.6 % (885.1 km), from 30 to 40 years --- 42.9 % (2044 km), and over 40 years --- 16.9 % (805.9 km). As to diameters, oil pipelines are broken down as follows: 530, 720 and 1020 mm (13.7, 52.9 and 19.5 %, respectively).

Analysis of distribution of pipelines of the gas transportation system, as well as main oil pipelines, as to their operation time and diameters, allows a conclusion that in the nearest future it will be necessary to perform a large scope of repair and renewal work to ensure continuous operation and good working state of the pipelines.

Main pipelines proved to be the most secure, reliable and cost-effective means of transportation of gas and oil to large distances. However, the need to maintain a high level of readiness for emergency conditions is still a priority task, proceeding, in particular, from social, ecologic and economic consequences, which may result from a loss of tightness of a high-pressure pipeline. As the risk of such consequences is potentially run from the moment of pressurising of a pipeline, the readiness for emergency situations is a hot problem during its entire service life. In this connection, in each specific emergency situation, or in detecting inadmissible defects in the linear part of pipelines, it is necessary to develop a repair strategy, which should be based on a number of criteria: selection of a repair method, safety and reliability of a repair structure, effect on environment, ensuring of continuous

transportation of a product, time of repair and its economic expediency. The preference should be given to the repair methods that can be implemented without interruption of operation of a pipeline, causing no decrease in volume of transportation of a product, or an insignificant decrease for a short period of time, and not leading to a substantial material and environmental damage.

Development of advanced repair methods and means, which can be used to renew the carrying capacity of pipes with different defects, as well as remove through defects in active pipelines, has a high potential for raising the efficiency of repair operations. Such operations include welding up of corrosion pits and voids, reinforcing the linear part of a pipeline having corrosion damages with bands or leak-proof sleeves, welding of cathode branch pipes, local repair using patches-sleeves, joining of branch pipelines to connect new users or fields to the main line, installing of girths, joining of looping or replacement of extended defective regions in the active pipeline, removal of defects in welded circumferential joints of the pipeline by arc welding, reinforcing defective circumferential joints with two-layer sleeves, placing of bands and compound sleeves on regions with corrosion-mechanical damages, repair of nicks and corrugations using leak-proof sleeves by filling the pipe space with a self-solidifying solution, cutting out of regions with nicks (under pressure) that hamper passage of cleaning and diagnostic inside-pipe gears, and joining of small-diameter branch pipes by combined arc welding to install the testing and measuring devices.

Arc welding methods play an important role in repair and renewal operations, and in reconstruction of facilities of the linear part of main pipelines. After performing technical diagnostics and revealing of defects, it is necessary to classify them, and then to decide on methods for repair of the facilities. Therefore, one of the primary tasks is to provide performers of welding operations in active pipelines with the departmental regulatory-technical documents prepared on the basis of advanced experience in operation of main pipelines, achievements of the scientific and technologi-


Table 2. Design-technological schemes of repair of pipelines

Designation	Schematic of repair structure	Repair methods with characteristics of defects according to Table 1
İ 1		<p>Band:</p> <ul style="list-style-type: none"> • corrosion-mechanical damages in pipe wall to 50 % of its thickness (item 2); • delaminations not escaping to surface (item 9); • nicks to 3.5 % D_{out} deep (item 19)
İ 2		<p>Leak-proof sleeve with process rings:</p> <ul style="list-style-type: none"> • corrosion-mechanical damages in pipe wall to more than 50 % of its thickness (items 3, 4, 7); • delaminations not escaping to surface (item 10); • delaminations in weld zone (longitudinal and spiral welds) (item 12)
İ 3		<p>Two-layer sleeve:</p> <ul style="list-style-type: none"> • defective circumferential joints and adjoining zones (items 7, 8, 11, 22, 23); • delaminations in weld zone of circumferential joint (item 11); • delaminations with protrusions (item 13); • corrugations up to 20 mm high (item 18)
İ 4		<p>Compound sleeve:</p> <ul style="list-style-type: none"> • major corrosion damages and combined defects in pipeline (items 2, 4-6); • delaminations (items 9, 12); • nicks of 3.5 % D_{out} deep (item 19); • abnormal longitudinal weld (item 24)
İ 5		<p>Volumetric sleeve with filler:</p> <ul style="list-style-type: none"> • corrugations up to 5 % D_{out} high (item 17); • delaminations with protrusions (item 13)
İ 6		<p>Patch-sleeve:</p> <ul style="list-style-type: none"> • groups of local corrosion damages (items 5, 6); • sleeve on existing patch

Table 2 (cont.)

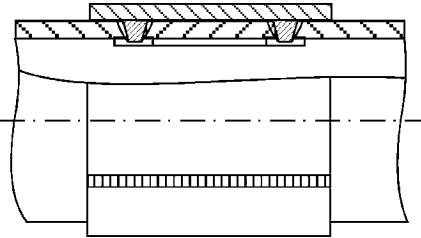
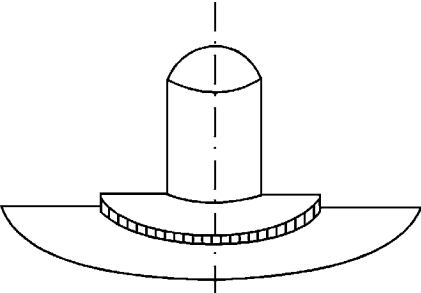
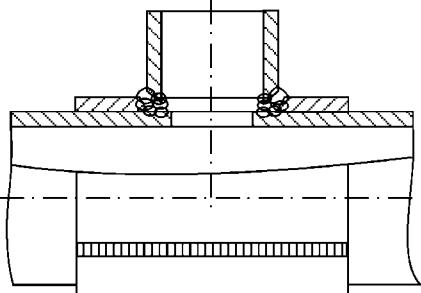
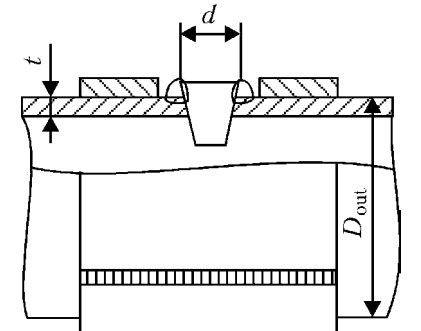
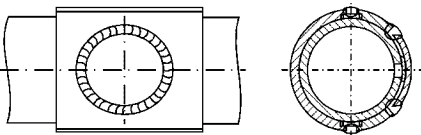
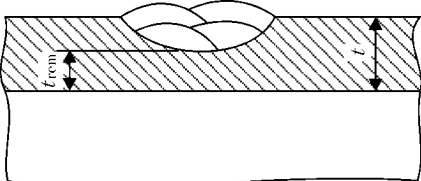
Designation	Schematic of repair structure	Repair methods with characteristics of defects according to Table 1
İ 7		<p>Patch reinforced with band:</p> <ul style="list-style-type: none"> • process holes (item 25)
İ 8		<p>Branch pipe with collar:</p> <ul style="list-style-type: none"> • process holes and incuts (item 25)
İ 9		<p>Branch pipe-sleeve:</p> <ul style="list-style-type: none"> • removal of crack (item 15); • removal of nick (items 20, 21); • removal of process holes (item 25); • joining of branch pipes; • cutting out of regions with cracks (item 15)
İ 10		<p>Chop-pipeline-band:</p> <ul style="list-style-type: none"> • removal of holes (item 26)
İ 11		<p>Patch-sleeve with sealant:</p> <ul style="list-style-type: none"> • through defects under pressure (item 27)
İ 12		<p>Welding up:</p> <ul style="list-style-type: none"> • corrosion pits and mechanical damages (item 5)



Table 2 (cont.)

Designation	Schematic of repair structure	Repair methods with characteristics of defects according to Table 1
İ 13		Grinding: <ul style="list-style-type: none"> • corrosion-mechanical damages (item 1); • surface cracks to depth of 20 % of pipe wall thickness (item 14)
İ 14		Composite band: <ul style="list-style-type: none"> • longitudinally oriented mechanical and corrosion damages in pipes (items 2, 4–6); • delaminations (items 9, 11, 12); • nicks to depth of 3.5 % D_{out} (item 19); • curvilinear surfaces of pipelines (item 24); • abnormal longitudinal weld (item 24)

cal progress in the field of development of new equipment and technologies, as well as international codes and standards. Also, it is necessary to develop a program for training of welding operators and managers, as well as testing to allow them to perform renewal repair using arc welding on pressurised pipelines.

To illustrate classification of defects and their structural distribution, below we give results of diagnostics of a technical state of main gas pipelines controlled by State Company «Ukrtransgaz» (25 % of the entire volume), which was carried out using the «Rozen» intelligence piston [2]. Thus, metal losses of more than 60 % of the pipe wall thickness are equal to 0.9 %; 41–60 % — 5 %, and 20–40 % — 45.5 %. Defects in circumferential welds constitute 10.8 %, those in surface welds — 11 %, in longitudinal welds — 7 %, and in spiral welds — 0.9 %; defects in base metal constitute 11.1 %, non-classified defects — 7 %, and abnormal types of defects — 0.8 %. This shows that metal losses make up the largest quantity of defects. Inadmissible defects, according to codes BCH 006-89 and BCH 012-88, as well as defects formed in construction of main gas pipelines (about 1 % of the total number of revealed defects), were detected in circumferential welded joints. Many surface defects in welds (12 %) and internal defects of the type of delaminations (11 %) in base metal were revealed as well.

The design approach to development of technologies for renewal of carrying capacity of the linear part of pressurised main pipelines using arc welding (Figure) was proposed on the basis of analysis of the character and geometric parameters of the revealed defects. The repair methods shown in the Figure are grouped as to types of defects and target application. Safe conditions for performing arc welding on pressurised pipelines, allowing for their working parameters and physical-chemical properties of environment [3], were defined for each type, followed by identification of conditions for ensuring technological and structural strength of welded joints [4]. Given that

the new type of a welded joint, i.e. overlap-butt joint, is used in the majority of technical solutions, it is necessary to develop the technology for testing such joints on the basis of ultrasonic inspection.

The developed methods for repair of active main pipelines should be regarded as resource-saving technologies, which provide improvement in safety of renewal operations and decrease in technogenic load on the environment through minimising emissions of environmentally harmful carbon compounds. Tables 1 and 2 give design-technological solutions for repair of main pipelines and their application conditions, depending upon the character and geometric parameters of defects.

At present, three technological instructions are in effect at «Ukrtransgaz», and departmental construction codes are available, which regulate repair of the linear part of main oil pipelines. The total economic effect provided by applying some of the repair methods (welding up of pits, installing of leak-proof and compounds sleeves, and reinforcement of defective joints with two-layer sleeves) at active main gas and oil pipelines exceeded 16,000,000 UAH.

Training programs were developed, and 42 welding managers and 80 welding operators were certified at «Ukrtransgaz» and «Ukrtransnafta» to allow them to perform repair operations at pressurised main pipelines.

1. But, V.S., Gretskey, Yu.Ya., Rozgonyuk, V.V. et al. (2001) Validation of new approach to performance of welding works on pressurised pipelines. *Naft. i Gazova Promyslovist*, **4**, 33–39.
2. But, V.S., Vasilyuk, V.M., Fedorenko, Yu.T. et al. (2006) Trends in development of repair technologies for main pipelines under service conditions. In: *Proc. of Sci.-Pract. Seminar on Reliability Control of Systems of Pipeline Transportation* (Kiev, 11 April, 2006), 31–38.
3. Makhnenko, V.I., But, V.S., Velikoivanenko, E.A. et al. (2001) Mathematical modelling of pitting defects in active oil and gas pipelines and development of a numerical method for estimation of permissible parameters of arc welding repair of defects. *The Paton Welding J.*, **11**, 2–9.
4. Makhnenko, V.I., But, V.S., Velikoivanenko, E.A. et al. (2003) Estimation of permissible sizes of welds for mounting T-joints and sleeves on active main pipelines. *Ibid.*, **8**, 6–11.

HYBRID LASER-PLASMA WELDING OF ALUMINIUM ALLOYS

I.V. KRIVTSUN, V.D. SHELYAGIN, V.Yu. KHASKIN, V.F. SHULYM and E.G. TERNOVOJ
E.O. Paton Electric Welding Institute, NASU, Kiev, Ukraine

Technological capabilities of the hybrid laser-plasma welding of aluminium alloys in comparison with plasma and laser welding were investigated. Properties of the welded joints made by hybrid method, as well as their micro- and macro-structure were investigated. It is shown that practical application of laser-plasma welding holds promise for thin-sheet aluminium alloys using lasers with a sharp-focused radiation spot.

Keywords: hybrid laser-plasma welding, aluminium alloys, laser radiation, diode laser, CO₂-laser, filler wire, cleaning, heteropolar pulses, synergetic effect, mechanical properties, metallographic investigations, structure

The need in welding aluminium alloys often occurs in industry, thus stimulating development of a respective technology. There is need in urgent solution of such tasks as welding of thin-sheet honey-comb and stringer panels of the railway cars of high-speed railways, body elements of aviation materiel, ship structures, profile distance pieces for multiple glass units, alleviated bodies of cars, etc. [1]. Different technologies may be used for making welded structures from thin-sheet aluminium alloys. Lately the technologies, in which laser radiation is used, cause the interest [1–6]. Majority of the authors recognize that laser technology holds promise, but at the same time they note a number of problems connected with it.

One of important issues occurring in laser welding of aluminium and its alloys, characterized by high reflection capacity of the surfaces being welded, is the need in using laser radiation of high power (above 2 kW) for transition from the surface to the volumetric heat input [2]. However, increase of the laser radiation power causes increase of the laser equipment cost and, as a result, growth of production cost of 1 m of the weld running length. One of the methods for solution of this issue is increase of absorption capacity of the surfaces being welded. For this purpose laser radiation with a shorter wavelength, for example, diode or Nd:YAG lasers instead of CO₂-lasers may be used [2]. Another method for solution of this issue is application of the combined [4] or hybrid laser-arc [7] technologies that allows combining advantages of separate components of the method and leveling of their shortcomings [8].

Another essential issue occurring in laser welding of aluminium alloys, is removal of the oxide film, so called cleaning. Usually this operation is performed mechanically (for example, by scraping) or by chemical etching in water-alkaline solution. German scientists developed method of laser cleaning of the components being welded from oxide film [9]. For this purpose they used special focusing optics, which split

laser beam into two beams --- a weak cleaning one and a more powerful welding one. Application of special laser units designed for cleaning of the surface being connected, which causes additional expenses, is also possible.

We investigated the method for hybrid laser-plasma welding of aluminium alloys with simultaneous cleaning of their surfaces by applying heteropolar welding current pulses. As laser component of the hybrid welding process the DF 020 HQ diode laser (Rofin-Sinar company, Germany), having power up to 2 kW with 0.808/0.904 μm wavelength, and the LT 104 CO₂-laser [10] with 10.6 μm wavelength, were used. For practical implementation of the hybrid welding process, taking into account the results of previously performed investigations [11], a special integrated plasmatron was developed and made, in which laser radiation acted on the component being welded together with plasma of direct action through a common nozzle. In connection with the fact that the plasmatron was used together with the diode laser, the focusing optics of which has a fixed focus distance 120 mm, development of the scheme for co-axial action of the laser beam and the arc on the weld pool was a failure.

The scheme was adopted, in which axes of the plasmatron electrode and the laser beam were arranged at minimal possible angles to the axis of the plasma-shaping nozzle (21° and 8°, respectively). Appearance and scheme of the plasmatron in section are shown in Figure 1. The design represents a single-electrode plasmatron with a changeable (together with the collet) tungsten electrode of 2.5–3.5 mm diameter, installed in a water-cooled housing. The electrode can travel along its axis with subsequent fixation; its movement in lateral direction is also controlled. Due to special shape of copper nozzle and presence of water channel in it, cooling water can be fed directly to the channel outlet of 1.5–3.0 mm diameter, thus creating maximally favorable conditions for its cooling. Design of the plasmatron allows introducing a focused laser beam into the welding zone at angle 8° to the nozzle axis, for which purpose in upper part of its housing a special unit is envisaged for connection to it of the

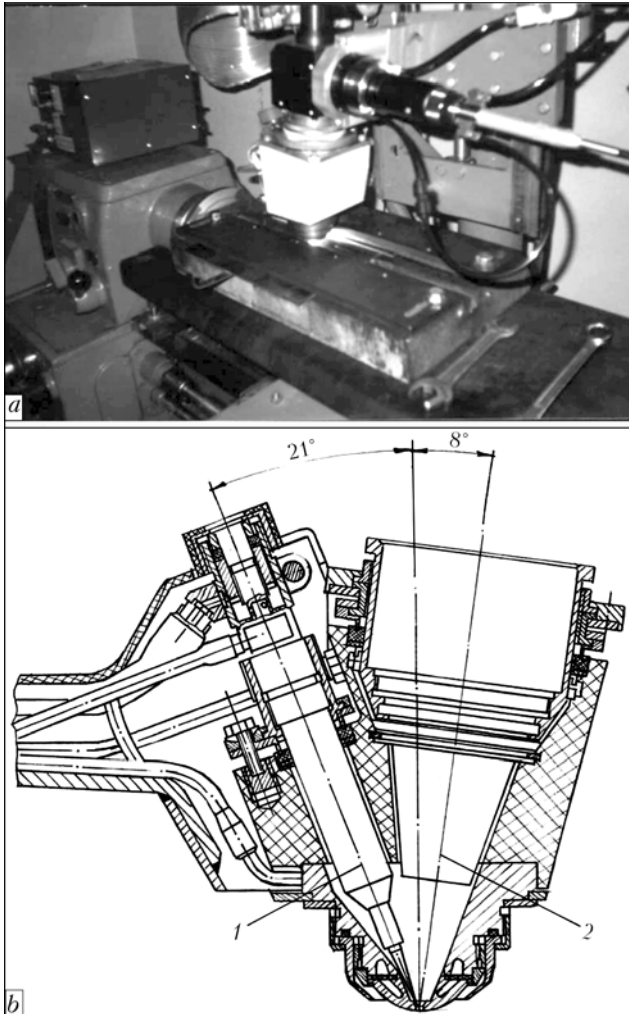


Figure 1. Appearance (a) and cross section (b) of integrated plasmatron for hybrid laser-plasma welding: 1 — cathode unit; 2 — axis of focused laser beam

DF 020 HQ diode laser focusing system with an optic fiber. Possibility of the focusing spot adjustment both relative the laser beam axis and walls of the nozzle outlet channel is envisaged. To prevent soiling of the focusing optics a protection glass with its forced blowing by the plasma gas is envisaged, and for protection of the manufactured from caprolon external body of the plasmatron against possible getting of laser radiation on it the stainless steel cone is available.

For power supply of the plasmatron the plasma arc supply source was developed and manufactured, which allowed performing welding on direct polarity and under conditions of heteropolar current pulses. Used in its development solutions of the schemes (high frequencies of opening and closing the gates and the electrical current conversion frequency) allowed ensuring necessary dynamic characteristics and wide range of the duration adjustment of technological pulses (0.1–99.0 ms). In combination with welding current up to 110 A (straight) and up to 60 A (reversed polarity) this allowed ensuring wide technological possibilities of the plasmatron–power source complex.

For welding diameter of the nozzles varied within 2.0–2.5 mm. Adjustment range of laser power constituted 0.8–2.0 kW, and of the welding current —

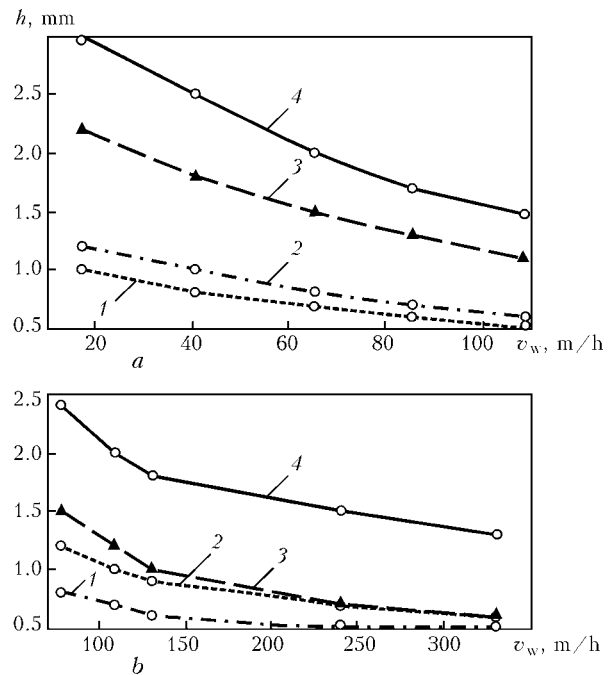


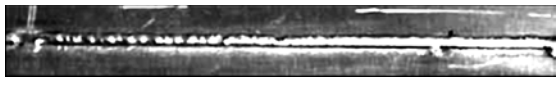
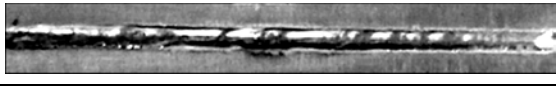
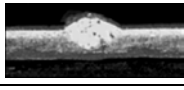
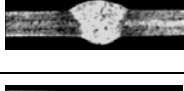
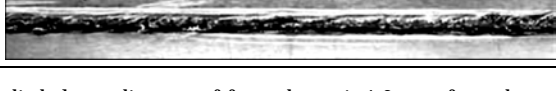
Figure 2. Dependencies of penetration depth h upon speed v_w of laser-plasma welding of aluminium alloys with application of radiation of diode (a) and CO₂-laser (b): 1 — laser welding; 2 — plasma welding; 3 — laser-plasma welding (arithmetic total of h values); 4 — hybrid welding

50–110 A at the voltage about 20 V. Frequency of the welding current pulses achieved 1000 Hz. Materials of the specimens being welded were represented by the AMts, AMg3, AMg5m and AMg6 alloys of 0.5–3.0 mm thickness. In a number of cases filler wire SvAMg6 of 1.2 mm diameter was used.

In the course of experiments deposition of flat specimens and welding of butt and lap joints were performed. Argon-shielded welding, using laser radiation or the direct action plasma and the hybrid method, was performed, whereby diameter of the spot of the diode laser focused radiation constituted 1.2 mm, and of CO₂ laser — 0.5 mm. It is established that in case of the plasma process optimal ratio of the current pulse duration and amplitude in straight and reversed polarity should constitute approximately 1:1 in order to get quality cleaning from oxide film at high speeds (60–330 m/h). This ratio was also later used for the hybrid process. As far as these conditions are not optimal from the viewpoint of the tungsten cathode service life and stability of operation, the measures were taken to improve these parameters, one of which consisted in using the water-cooled plasma-shaping nozzle as the arc anode.

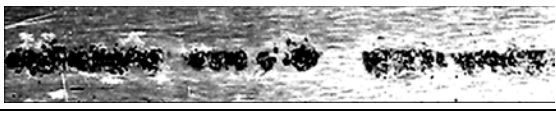
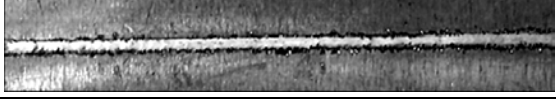
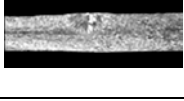
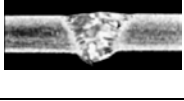
As a result of processing of the data obtained in welding using laser radiation of about 2 kW power, plasma at the 100 A current, and the hybrid method at 50 % power of the plasma component and 1.2–1.5 kW of the laser one, dependencies presented in Figure 2, were plotted. Comparison of curves 1 shows that in laser welding despite big diameter of the focused spot of the diode laser radiation a smaller wavelength allows significant increasing depth of penetration. In the plasma process (curves 2 in Figure 2)

Table 1. Appearance and macrosections of specimens of butt and lap joints of AMg3 alloy 1.5 mm thick produced by laser, plasma and hybrid welding

Laser power, W	Plasma arc current (SP/RP), A	Appearance of weld on face side	Macrosection
2000	--		
--	100/50		
1000	50/50		
1500	100/50		

Note. Welding speed is 108 m/h; DF 020 HQ diode laser; diameter of focused spot is 1.2 mm; focus deepening is 1 mm; plasma arc voltage is 20 V.

Table 2. Appearance and macrosections of butt joint specimens of AMg3 alloy 1.5 mm thick produced by laser, plasma and hybrid welding

Laser power, W	Plasma arc current (SP/RP), A	Appearance of weld on face side	Macrosection
1500	--		--
--	100/50		
1000	60/50		

Note. Welding speed is 130 m/h; LT 104 CO₂-laser; diameter of focused spot is 0.5 mm; focus deepening is 1 mm; plasma arc voltage is 20 V.

monotonous reduction of the penetration depth is observed within the whole range of speeds. Curves 3 in this Figure represent arithmetic total of values of curves 1 and 2. Curves 3 and 4 prove presence of synergetic effect in case of simultaneous welding into common pool by laser and plasma components, whereby in case of using CO₂-laser this effect is manifested more intensively due to a smaller diameter of the focused spot of radiation (higher density of the power). It should be noted here that despite big diameter of the radiation spot of the diode laser (and respectively lower density of the power in comparison with CO₂-laser), a smaller wavelength of radiation and, as a result, higher coefficient of absorption by the aluminium surface, ensures at the same speed of the hybrid welding commensurable in both cases depth of penetration (curves 4 in Figure 2). Reduction of the focused spot diameter increases stability of the

plasma burning at high speed of welding and «ties» it to the laser radiation zone of action.

For visual estimation of different welding methods of the AMg3 aluminium alloy of 1.5 mm thickness in Table 1 appearance of the welds on face side and macrosections of welded butt joints, produced by each of three welding methods at the speed 108 m/h with application of the DF 020 HQ diode laser, is presented, and in Table 2 appearance of deposits on face side and their macrosections, produced by the same method at the speed 130 m/h with application of the LT 104 CO₂-laser, is shown. Radiation of the diode laser of 1.5–2.0 kW power ensures stable penetration at the depth up to 0.5 mm (see Table 1). Radiation of CO₂-laser under similar conditions left on surface of the specimens just discontinuous traces (see Table 2). Penetration by the plasma arc at the speed above 240 m/h is also of unstable and discontinuous character despite high frequency of the welding current

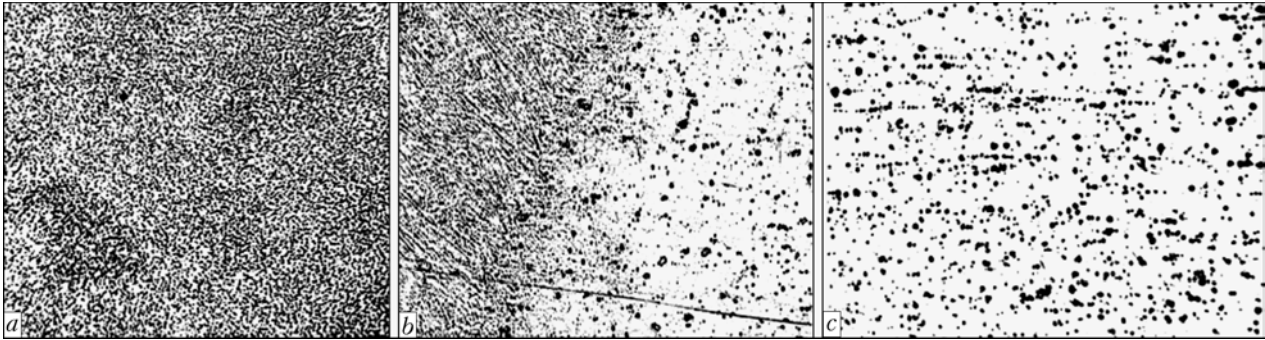


Figure 3. Microstructure of metal of welded butt joint of AMg3 alloy 1.5 mm thick produced by hybrid laser-plasma method: a — central part of weld; b — fusion zone; c — base metal ($\times 150$)

Table 3. Chemical composition (wt.%) of AMg3 alloy welded joint produced by hybrid method of welding with application of diode laser

Object of investigation	Si	Mg	Mn	Cu	Zn	Ni	Ti	Fe	Al
Base metal	0.38	3.5	0.5	0.1	0.18	0.03	0.1	0.4	Base
Weld	0.40	3.2	0.3	0.1	0.12	0.03	0.1	0.4	Base

pulses. The best technological results were achieved in the hybrid method of welding within the whole investigated range of speeds. Complete through penetration of the joint specimen of 1.5 mm thickness with application of the CO₂-laser radiation was ensured at the welding speed 130 m/h and total power of the laser and plasma 2 kW (approximately 1 kW per each). This is explained by the fact that a smaller diameter of the focus spot of the CO₂-laser radiation allows ensuring higher density of energy than radiation of the diode laser. In this case a narrow zone of intensive evaporation of the penetrated metal is formed, which improves conditions of the plasma arc burning, enables its additional constriction and, respectively, achievement of a bigger depth of penetration, stabilization of the process, and «tying up» of plasma to the zone of the laser radiation action, which is confirmed in [12].

Results of investigations of chemical properties of the weld joint, produced by the hybrid method of welding, are given in Table 3. Tensile tests of butt joints from the AMg3 alloy, produced by the hybrid welding with application of the diode laser, showed that strength of the weld metal equaled 232–237 MPa (90–95 % of the base metal strength). It was established on the basis of these investigations that strength of the welded joints, produced by the laser-plasma method with application of the diode laser radiation, constituted approximately 0.9 of the base metal strength. This result allows stating that in regard to strength characteristics the hybrid welding exceeds arc methods of welding and is acceptable for fabrication of the majority of structures.

Carried out investigations of the AMg3 alloy butt joint microstructures (Figure 3) of 1.5 mm thickness produced by the hybrid welding method, prove that structure of the weld metal has dendrite fine-dispersed structure. Precipitation of phases in the weld is of disperse character. The fusion line has no signs of

overheating, except root part of the weld, where continuous chains of precipitates are observed over grain boundaries in HAZ adjacent to the fusion line, which, if necessary, can be removed after welding by machining.

CONCLUSIONS

1. Application of the hybrid laser-plasma welding of aluminium alloys allows increasing 2–4 times depth of penetration in comparison with the laser welding and increasing approximately to the same degree speed of welding in comparison with the plasma welding, whereby an important factor is application of the cathode cleaning of surfaces from oxide film.

2. Manifestation of synergetic effect, tying up of the plasma arc to the laser radiation zone of action and stability of the high-speed hybrid welding process are connected to a greater degree with the level of the laser radiation focusing than with the length of its wave.

3. Chemical composition of the welded joint metal is close to the base metal composition, and their tensile strength constitutes about 0.9 of the base metal strength, which exceeds properties of similar joints produced by the arc methods of welding.

4. Structures of aluminium alloy welded joints, produced by the hybrid method, have more fine dispersity of the weld metal and narrow zone of fusion in comparison with those in arc methods of welding, which brings them nearer to the laser-welded joints.

5. The results of preliminary investigations of technological possibilities of the hybrid laser-plasma welding of aluminium alloys allows drawing conclusion that this method holds promise and it is necessary to perform further deeper experimental and research works in the field of high-speed welding of thin-sheet structures from aluminium alloys.

1. Shibata, K., Iwase, T., Sakamoto, H. et al. (2003) Welding of aluminium car body parts with twin-spot high power Nd:YAG laser. *J. LMWU&C*, 4, 25–34.



2. Tsukamoto, S. (2003) Laser welding. *Welding Int.*, 17(10), 767–774.
3. Katayama, S. (2004) Laser welding of aluminium alloys and dissimilar metals. *Ibid.*, 18(8), 618–625.
4. Volpone, M., Mueller, S.M. (2005) Laser e friction stir welding — due tecnologie di giunzione emergenti. Confronto su vantaggi e limitazioni. *Riv. Ital. Saldatura*, 5, 683–691.
5. Rathod, M.J., Kutsuna, M. (2004) Joining of aluminium alloy 5052 and low-carbon steel by laser roll welding. *Welding J.*, 1, 16–26.
6. (2001) Welding and joining technologies in 21st century. *J. JWS*, 70(3), 6–1.
7. Ishide, T., Tsubota, S., Watanabe, M. et al. (2003) Development of TIG–YAG and MIG–YAG hybrid welding. *Welding Int.*, 17(10), 775–780.
8. Paton, B.E. (1995) Improvement of welding methods — one of the ways to increase the quality and efficiency of welded structures. *Avtomatich. Svarka*, 11, 3–11.
9. Von Beren, J., Seefeld, T., Vollertsen, F. (2004) Laserstrahlschweißen mit prozessintegrierter Reinigung. *Der Praktiker*, 4, 118–120.
10. Garashchuk, V.P., Shelyagin, V.D., Nazarenko, O.K. et al. (1997) Technological LT 104 CO₂-laser of 10 kW power. *Avtomatich. Svarka*, 1, 36–39.
11. Paton, B.E., Gvozdetsky, V.S., Krivtsun, I.V. et al. (2002) Hybrid laser-microplasma welding of thin sections of metals. *The Paton Welding J.*, 3, 2–6.
12. Briand, F., Chouf, K., Lefevre, P. et al. (2002) Soudage hybride arc/laser. *Soudage et Techniques Connexes*, 9/10, 9–13.

LOW-HYDROGEN ELECTRODES FOR REPAIR OF SHIPS, METALLURGICAL INDUSTRY FACILITIES AND PIPELINE TRANSPORT*

I.K. POKHODNYA, I.R. YAVDOSHCIN, A.E. MARCHENKO, N.V. SKORINA,
V.I. KARMANOV and O.I. FOLBORT

E.O. Paton Electric Welding Institute, NASU, Kiev, Ukraine

Principles of formation of coatings for a new generation of low-hydrogen electrodes intended for repair of ships, metallurgical industry facilities and pipeline transport are considered, and their specification is given.

Keywords: arc welding, coated electrodes, repair of structures, alloying system, weld metal, mechanical properties, welding-technological properties

The number of critical facilities that have exhausted their operating resource and need repair or restoration increases continuously in metallurgy, pipeline transport, river and sea shipping. Performance of these works requires electrodes that have high technological characteristics and quality, and are available at a reasonable price to customers. European companies offer electrodes at high prices for these purposes that are in general not affordable to customers.

Low-hydrogen electrodes designed for shipbuilding (ANO-102), for repair of metallurgical industry facilities (ANMK-44.01) and pipeline transport (ANO-38) were developed at PWI during 2004–2006 in accordance with the «Resours» Program. The composition and range of steels, operating conditions of welded structures, as well as peculiarities of repair work performance in the indicated fields of industry, were taken into account when designing these electrodes.

Improvement of welding technological properties of the electrodes and achievement of required mechanical indices of weld metal were the key tasks among those solved when designing the new generation of low-hydrogen electrodes. Gas-and-slag forming part of coatings was upgraded that allowed an essential

improvement of the stability of welding arc burning, weld formation, slag crust detachment, decrease of molten metal spattering, provision of alternating current welding capability.

Optimum manganese content that provides the highest values of weld metal impact toughness at negative temperatures for general-purpose low-hydrogen electrodes is 1.4–1.5 % (Figure 1). At such manganese concentrations the share of acicular ferrite in the weld metal microstructure is equal to 60–70 % and remains the same in spite of variation of silicon concentration in the welds within 0.2–0.9 % [2]. At a lower manganese concentration the fraction of acicular ferrite in the weld metal structure not only decreases, but becomes dependent on silicon concentration in the limits specified by standard documentation (0.2–0.6 %). These are exactly the changes of the acicular ferrite fraction in the weld metal connected with silicon variations that can cause the instability of its impact toughness indices.

Titanium content optimization in weld metal also influences the possibility of providing its high impact toughness. Basicity of the flux or slag-forming base of the electrode coating, welding process, alloying system etc. [3] also influence the optimum titanium content. In accordance with study [4] the optimum titanium content in the weld metal when welding with carbonate-fluorite coated electrode was equal to about

*The article was prepared by the results of performance of purpose-oriented complex program of the NAS of Ukraine «Problems of residual life and safe operation of structures, constructions and machines» (2004–2006).

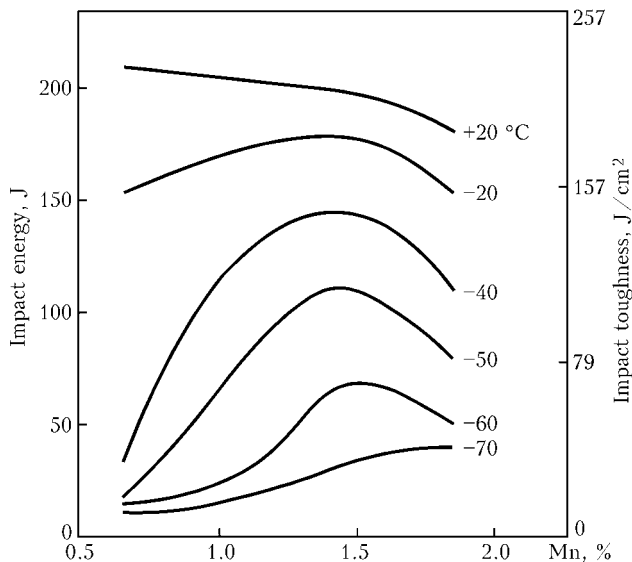


Figure 1. Influence of manganese content on impact energy and impact toughness of weld metal at different temperatures [1]

0.1 %, and in accordance with the study [5] --- 0.2 % (Figure 2). Disbalance of the deoxidation system in a number of electrode grades with basic coating leads to a decrease of impact toughness indices of welds at low temperatures.

The authors have studied the content of titanium in electrode coatings of the basic type (UONI-13/55 type) on impact toughness of weld metal. Titanium content in weld metal was regulated by changing the quantity of ferrotitanium in the studied electrode coatings. A constant level of manganese and silicon in the welds was preserved, and the amount of ferromanganese and ferrosilicon that were added to the coating were varied. Composition of the metal of welds made with the studied electrodes is given in Table 1, results of impact toughness tests of the metal of welds made with these electrodes --- in Table 2. As it is seen from the tabulated data, the highest values of weld metal impact toughness at negative temperatures are provided at titanium content in it on the level of 0.02 %.

Results of the conducted studies were taken into account when developing the compositions of electrode coatings designed for carrying out of repair works.

Electrodes ANO-102. When designing these electrodes, the range of elements concentration in weld metal was optimized, %: 1.2--1.4 Mn; 0.25--0.40 Si; 0.015--0.020 Ti. Corrosion resistance of weld metal in

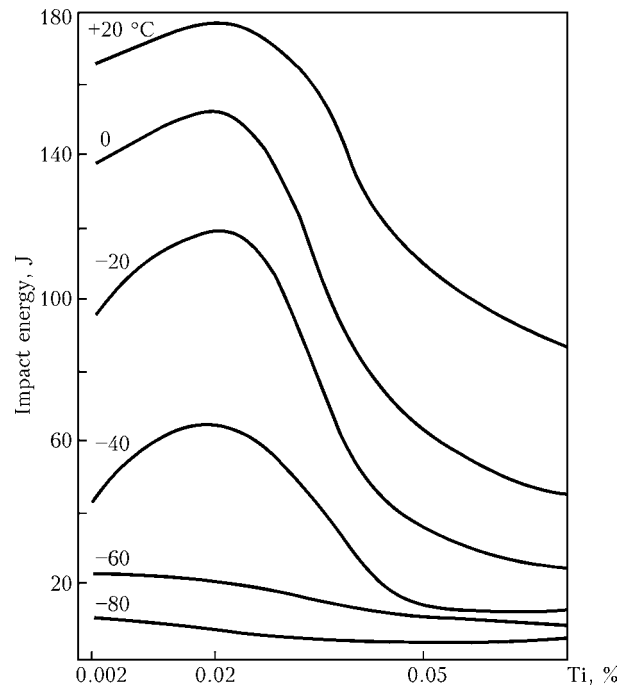


Figure 2. Influence of titanium content in weld metal on impact energy at different temperatures [5]

sea water was provided by adding 0.6--0.8 % Ni and 0.4--0.6 % Cu to its composition. Content of gas-and-slag forming base of ANO-102 electrode coating was designed taking into account the possibility of providing low content of diffusible hydrogen; welding at direct and alternating current; welding and technological properties of electrodes on the level of the best foreign analogs.

Electrodes ANO-102 (E50A according to GOST 9467-75) were designed mainly for application in ship repair and shipbuilding instead of UONI-13/55 electrodes. Their symbolic designation in accordance with the European standard EN 499 is E 46 5 1Ni B 12 H 10.

The electrodes are designed for all-position welding of shipbuilding steels of normal and increased strength with the exception of vertical welds by downward method. Welding can be performed at direct current of reverse polarity or at alternating current from power sources with not less than 65 V open-circuit voltage.

Comparative tests of ANO-102 electrodes with UONI-13/55 electrodes and foreign electrodes OK 73.08 of Swedish company ESAB showed that as to the indices of weld metal impact toughness, ANO-

Table 1. Chemical composition of deposited metal

Electrode index	Ferrotitanium content in coating, wt. %	Element weight fraction in the deposited metal, %					
		C	Mn	Si	Ti	[O]	[N]
T-0	0	0.08	1.3	0.28	Traces	0.047	0.013
T-5	5	0.10	1.0	0.23	0.02	0.044	0.013
T-10	10	0.10	1.0	0.22	0.03	0.038	0.013
T-15	15	0.09	1.1	0.28	0.04	0.038	0.012
T-20	20	0.10	1.1	0.24	0.05	0.037	0.013

Table 2. Impact toughness, J/cm³, of weld metal made by the studied electrodes

Electrode index	Temperature, °C		
	+20	-20	-40
Ò-0	$\frac{217-227}{221.7}$	$\frac{70-134}{112}$	$\frac{64-75}{68.3}$
Ò-5	$\frac{223-257}{239}$	$\frac{141-157}{147.6}$	$\frac{70-75}{73.7}$
Ò-10	$\frac{223-232}{228.3}$	$\frac{102-155}{128.6}$	$\frac{16-61}{31.3}$
Ò-15	$\frac{186-198}{190}$	$\frac{79-107}{94.3}$	$\frac{25-72}{46.6}$
Ò-20	$\frac{196-215}{208.6}$	$\frac{57-151}{104.3}$	$\frac{35-87}{64}$

Note. Here and in Table 3 the minimum and maximum values of impact toughness are given in the numerator, and average values --- in the denominator.

120 electrodes are superior to UONI-13/55 electrodes and not inferior to OK 73.08 electrodes (Table 3).

Testing of welding and technological properties of new electrodes showed that they provide good weld metal formation when welding in different positions, small spattering, easy slag crust removal even at deep edge opening. By these parameters ANO-120 electrodes are superior to UONI-13/55 electrodes.

Melting indexes of ANO-120, UONI-13/55 and OK 73.08 electrodes that were determined when welding with electrodes of 4 mm diameter are given in Table 4. ANO-102 electrodes were tested at Ilichevsk shipbuilding yard where they got good comments from welders. They were approved by Russian Sea Navigation Register.

Application of new ANO-102 electrodes instead of UONI-13/55 electrodes due to the higher corrosion resistance of welds and weld metal impact toughness allowed an essential extension of operating life of welded structures of sea and river ships.

ANMK-44.01 electrodes. Repair works are integral part of production in metallurgy. For almost sixty years they have been done solely with application of welding technologies. Until recently repair of metallurgy complex facilities was done with low-hydrogen DBSK-55 and UONI-13/55 electrodes. Today both electrode grades and their modifications are technically out-of-date and in terms of the key technical indices they are inferior to those of foreign company electrodes that have been introduced in our market.

Table 3. Comparison of impact toughness of the metal of welds made with ANO-102, UONI-13/55 and OK 73.08 electrodes of 4 mm diameter

Electrode grade	Impact toughness KCV, J/cm ² , at temperature, °C			
	+20	-20	-40	-60
ANO-102	$\frac{186-204}{198}$	$\frac{168-192}{181}$	$\frac{94-98}{96}$	$\frac{72-84}{78}$
UONI-13/55	$\frac{181-192}{187}$	$\frac{82-104}{96}$	$\frac{28-74}{52}$	$\frac{12-32}{24}$
OK 73.08	$\frac{190-224}{212}$	$\frac{170-196}{185}$	$\frac{90-102}{96}$	$\frac{76-88}{81}$

New ANMK-44.01 electrodes are designed for metallurgical complex facilities. They correspond to E50A type (GOST 9467-75) by mechanical properties of the weld metal. Their symbolic designation according to the European standard EN 499 is E 46 4 B 52 H10, and according to ISO 2560 --- E 515 B 130 24 (H).

Coating gas-and-slag forming base belongs to CaCO₃--CaF₂--SiO₂ (TiO₂) system. The system of deposited metal deoxidation involves ferroalloys available in Ukraine (medium-carbon ferromanganese of FMn 88 and FMn 90 grades, ferrosilicon of FS-45 grade, ferrotitanium of FTi 35 C5 or FTi 35 C8 grades).

Technical characteristic of ANMK-44.01 electrodes: deposition efficiency 9.5--11.5 g/(A·h); deposited metal yield 120--130 %. Composition of the deposited metal is as follows, %: ≤ 0.1 C; 1.0--1.3 Mn; 0.25--0.35 Si; ≤ 0.03 S; ≤ 0.03 P; 0.02--0.03 Ti (optional). Mechanical properties of weld metal: σ_y ≥ 440 MPa; σ_t = 510--610 MPa; δ₅ ≥ 22 %; φ ≥ 65 %; KCV₊₂₀ = 200--250 J/cm²; KCV₋₄₀ = 80--100 J/cm².

Increased content of iron powder (up to 40 % in dry mixture) and thicker coating compared to previously designed electrodes (ratio D_c/d_r = 1.8; K_{c.m} = 85 %) is a distinguishing feature of new electrodes coating, resulting in a high efficiency and productivity of the electrodes (K_{d.y} = 135 %, a_d = 9.5--11.0 g/(A·h)). At the same time the electrodes of up to 4 mm diameter inclusive retain the possibility of welding in all positions with the exception of vertical welds made by the downward method.

The designed electrodes completely meet the code requirements to the repair works that are carried out at metallurgical complex facilities, and essentially exceed local analogs (electrodes of UONI-13/55, DBSK-55 grades) in terms of key technical indices, including efficiency --- by 15--30 %; deposited metal

Table 4. Melting characteristics of ANO-102, UONI-13/55 and OK 73.08 electrodes (direct current, reverse polarity)

Electrode grade	Deposition efficiency, g/(A·h)	Spattering coefficient, %	Metal yield, %	
			Sound	Deposited
ANO-102	9.2--9.6	0.8--1.9	70.1--70.5	107.9--108.3
UONI-13/55	8.1--8.6	3.2--4.8	68.4--69.4	91.4--94.5
OK 73.08	10.0--10.5	0.9--2.1	72.4--72.8	120--135

**Table 5.** Comparison of technical and economic characteristics of ANMK-44.01, UONI-13/55 and DBSK-55 electrodes

Electrode grade	Deposition efficiency, g/(A·h)	Metal yield, %		Possibility of welding at alternating current	Fraction of active arc burning, %	Electrode consumption per 1 kg of deposited metal
		Sound	Deposited			
UONI-13/55	9	60	90	Impossible	50	1.7
DBSK-55	10	73	105	Admissible	40	1.5
ANMK-44.01	9.5–11.5	70	125–130	Possible	75	1.4

yield by 20–40 %; time of active arc burning by 1.5–1.9 times. Electrode consumption per 1 kg of deposited metal decreases by 10–20 % (Table 5).

The electrodes permit welding at alternating current in site, which enables avoiding the magnetic blow and formation of weld defects connected with it. At present the electrodes are in the process of experimental-industrial trials at potential customer facilities.

Electrodes ANO-38. Gas and transport system (GTS) of Ukraine is one of the biggest and at the same time one of the oldest in Europe [6, 7]. Only one GTS of OJSC «Ukrzazprom» in 2002 consisted of 34.5 ths km of the main gas pipelines. All together 47.9 ths km of pipelines that exhausted their depreciation term. i.e. operate for more than 33 years have been on the balance sheets of gas transport enterprises of Ukraine up to now.

By the data of survey services of OJSC «Ukrzazprom», 1400 km of gas pipelines today require immediate reconstruction taking into account complete physical wear and in the future the annual requirement for restoration of the linear part of gas pipelines will be 500 km. Actual volumes of performed work on capital repair, reconstruction and technical refitting of the main pipelines that have been observed during the last 15 years are essentially lower than

required, in particular, because of unsatisfactory level of technical equipment and technology of repair work performance, as well as lack of the necessary welding consumables.

One half of GTS failures are determined by the low quality of pipes and welding operations, i.e. they are caused by defects that had already existed in pipelines before the beginning of operation. Not revealed by the hydraulic acceptance tests, after some time they have reached a critical state and as a result they became the source of destruction.

Repair welding operations should not by any means affect the performance of the repaired gas pipelines in comparison with that state, which is typical for pipelines in construction. ANO-38 electrodes meet these demands. They are designed for one-side welding of site (position) joints in construction and repair of the main pipelines, including welding in all positions of the root, hot pass, filling layers and facing layer (vertically oriented welds are welded by «uphill» method). Welding is carried out at direct current of reverse polarity. Welding can be conducted at alternating current, if required.

Compared with UONI-13/55 electrodes, ANO-38 electrodes guarantee higher quality of root passes, including root reinforcement formation. They have

Table 6. Hydrogen content in the metal deposited by ANO-102, ANMK-44.01 and ANO-38 electrodes

Electrode grade	Diameter, mm	Current strength, A	[H] _{diff} , ml/100 g	Country and manufacturer
ANO-102	4.0	165	4.2–5.2	Ukraine, PWI
ANMK-44.01	3.0	125	5.0–5.2	Same
	4.0/6.8*	165	5.3–5.5	
	4.0/7.2*	165	5.0–5.7	
ANO-27	3.0	125	4.8–5.4	Ukraine, Badm. Ltd
	4.0	165	5.9–6.0	
DBSK-55	3.0	125	6.2–7.0	Ukraine, Badm. Ltd
	4.0	165	7.1–8.3	
ANO-38	3.0	125	3.0–4.6	Ukraine, PWI
	4.0	165	2.8–3.2	
ANO-TM/SKh	3.0	165	4.4–5.7	Israel, ZIKA
Z-7	4.0	95	4.2–4.8	
ASB-255	3.0	125	3.7–4.6	Turkey, ASKAINAK
	4.0	165	5.9–6.0	

* Diameter of electrode coating is given in the denominator.



greater versatility, are characterized by lower hydrogen content in the deposited metal compared to ANO-TM/SKh, LB-52U, Fox EW 50 Pipe and are local analog of Israel company ZIKA Z-7 electrodes that are imported to Ukraine.

ANO-38 electrodes correspond to E50A type (GOST 9467-75) as to mechanical properties of the deposited metal. Technological strength and mechanical properties of the welds, adequate to those required, are guaranteed on the pipes from steels used in construction of pipelines during all previous years.

Electrodes symbolic designation corresponding to GOST 9467-75 is $\frac{E50A-ANO-38d-UD}{E5614-B26}$.

Full specification of ANO-38 electrodes is as follows: deposition efficiency 8.5-9.0 g/(A·h); deposited metal composition, %: ≤ 0.11 C; 0.9-1.2 Mn; 0.45-0.75 Si; ≤ 0.02 S; ≤ 0.03 P; 0.02-0.03 Ti (optionally), weld metal mechanical properties: $\sigma_y \geq 440$ MPa; $\sigma_t = 530-680$ MPa; $\delta_5 \geq 22$ %; $\varphi \geq 65$ %; $KCV_{-30} = 130-200$ J/cm²; $KCV_{-50} = 60-90$ J/cm². At present ANO-38 electrodes are being tried out by potential customers.

Code documentation has been developed for ANO-102, ANMK-44.01 and ANO-38 electrodes. Technology of these electrode manufacture allows for the capabilities of local electrode enterprises-manufacturers and available raw materials in Ukraine. Data on hydrogen content in the metal deposited with these electrodes are given in Table 6.

CONCLUSIONS

1. Designed low-hydrogen electrodes of the new generation for ship repair (ANO-102), repair of metallurgical complex facilities (ANMK-44.01) and pipeline transport (ANO-38) are superior to local analogs by welding-technological properties of weld metal.

2. Code documentation was designed for ANO-102, ANMK-44.01 and ANO-38 electrodes. ANO-102 electrodes were approved by Russian Register of Sea Navigation.

3. Manufacturing of the new electrodes at the Ukrainian enterprises will allow avoiding purchase of expensive foreign electrodes.

1. Evans, G.M. (1980) Effect of manganese on the microstructure and properties of all-weld-metal deposits. *Welding J.*, 59(3), 67-75.
2. Evans, G.M. (1986) The effect of silicon on the microstructure and properties of C-Mn all-weld-metal deposits. *Metal Construction*, 18(7), 438-444.
3. Abson, D.J., Pargeter, R.J. (1986) Factors influencing the as-deposited strength, microstructure and toughness of manual metal arc welds suitable C-Mn steel fabrications. *IIW Doc. II A-683-86*.
4. Sakaki, H. (1960) Effect of alloying elements on notch toughness of basis weld metals. *J. JWS*, 29(7), 539-544.
5. Ramini de Rissone, N.M., Rissone H.A., Zuliani, J.L. et al. (1985) Effect of titanium on the properties of manual multipass weld. *IIW Doc. II A-665-85*.
6. Belenky, D.M., Geroev, A.E., Oganezov, L.P. (2000) Improvement of the quality of linear gas pipeline section. *Neftegaz. Tekhnologii*, 4, 15-18.
7. Shcherbak, O.V. (1998) Technical condition of gas and transport systems needs constant attention. *Svarshchik*, 1, 8.

CALCULATION OF DEPOSITED LAYER THICKNESS ON COMPONENTS OF OIL-AND-GAS HIGH-PRESSURE VALVING

M.L. ZHADKEVICH¹, E.F. PEREPLYOTCHIKOV¹, L.G. PUZRIN¹, A.V. SHEVTSOV² and M.N. YAVORSKY³

¹E.O. Paton Electric Welding Institute, NASU, Kiev, Ukraine

²«IF ELTERM» company, Kiev, Ukraine

³SE «Ukrgazdobycha», Kiev, Ukraine

Serviceability of the shut-off unit components of the direct-flow high-pressure production Christmas tree valves is ensured by deposition on their working surfaces of the chrome-nickel alloys, doped by carbon, boron and silicon, using the plasma-powder surfacing method. It is shown that for reliable operation of the shut-off units of these valves a layer of the deposited metal should have a guaranteed thickness. It is established that for operation at up to 70 MPa pressure minimum thickness of the deposited layer should be 1.5 mm, and allowing for a possible repeated grinding — up to 2.0 mm.

Keywords: plasma-powder surfacing, high-pressure valving, wear, direct-flow valves, shut-off unit components, concentration of stresses, deposited layer thickness

The most important element of the production Christmas tree (PCT), which operates on oil and gas fields, are valves. They, mainly, ensure safety of the personnel and the well-head equipment, because uncontrolled outburst of the produced by the flow method

combustible product can cause impact on environment and occurrence of fires.

In PCT, designed for almost continuous flow of liquid or gas, preference is given to the direct-flow valves [1-3]. Such valves (Figure 1) have strong steel housing 1 with two, located on the same axis fitting pipes arranged jointly with the housing and the connecting flanges. Shut-off unit of the valve is located



in the housing and consists of a gate 2, which can move upwards and downwards between tightly pressed to it seats 3. In the seats and lower part of the gate holes are made, the size of which corresponds to channels of the valve fitting pipes. In the lower position the gate blocks oil or gas flow and is pressed to the seat by the full working pressure. In the open valve holes in the gate and seats are aligned and the product flows freely without changing its speed and direction. Due to this direct-flow valves ensure low hydraulic resistance with the coefficient not more than 0.2 (in block valves this coefficient is 2--5 and higher) [4].

In the high-pressure direct-flow valves shut-off units with the «metal-metal» sealing are used, airtightness of which depends on careful fitting of the rubbing surfaces of the gate and the seats. For reliable operation their contacting surfaces are ground in up to the surface finish with the roughness height not more than 0.2 μm .

Wear of working surfaces of the gates and the seats is stipulated by a number of reasons, in particular, action of solid particles of the rock, which get from the product being produced on the rubbing surfaces, and contained in the product corrosion-active impurities, such as CO_2 and H_2S . In addition, when a valve is opened and closed, high-velocity turbulent flow of the product occurs, which causes erosion wear of the working surfaces.

For PCT valves long stay of the gate in the «open» or «close» position is characteristic. As shows experience, if corrosion resistance of the working surfaces is insufficient, the gate may get attached to the seats as a result of formation in separate places of common corrosion products, and the valve gets unserviceable.

For preservation of the machining quality, working surfaces of the shut-off unit components should have both high hardness and resistance against corrosion and erosion action of the product being produced. Fulfillment of these requirements is achieved by application in the valve shut-off units of the composite components. Working surfaces of the gate and the seats, made from steel, are coated with special alloys characterized by high hardness and resistance against corrosion and erosion.

The best combination of hardness, resistance against scores, corrosion, and erosion is achieved in plasma-powder surfacing of components of the valve shut-off unit by chrome-nickel alloys containing carbon, boron, and silicon [5, 6]. Technology of plasma-powder surfacing, developed in PWI, is successfully used in manufacturing of the shut-off unit components of the PCT direct-flow valves designed for 70 MPa pressure [7].

An important peculiar feature of design of the PCT direct-flow valves is the fact that edges of the passage holes on working surfaces of the seats are sharp and don't have facets for reducing hydraulic resistance and probability of getting between the gate and the seats hard particles from the product being produced. When the valve is closed, stresses, that occur in the

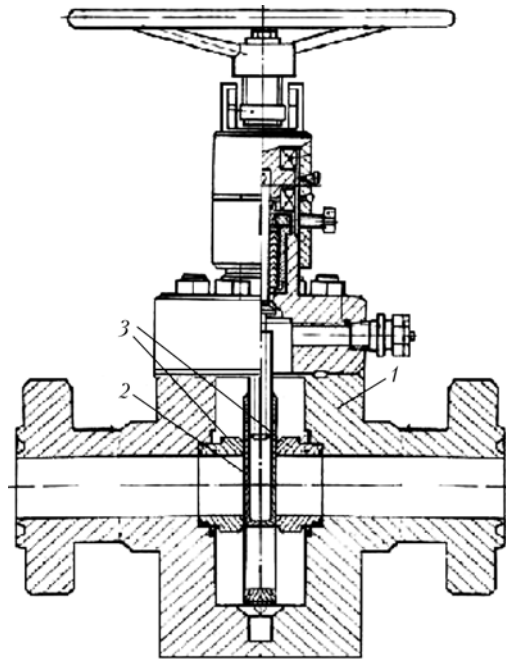


Figure 1. Scheme of production Christmas tree direct-flow valve: 1 — housing with flanges; 2 — gate; 3 — seats

place of contact of the sharp internal edge of the seat with the gate, are with a certain approximation similar to the stresses near the sharp edge of a rigid press tool pressed to a deformed component (Figure 2). Specific pressure near sharp edge of the press tool (seat) in the point with coordinate x is described by the expression [8]

$$q = P/\pi \sqrt{a^2 - x^2}, \quad (1)$$

where P is the linear force acting on the press tool of a single-unit thickness, N/mm ; a is the half of the press tool width, mm .

According to (1), specific pressure on edge of the press tool tends to infinity at $x \rightarrow a$. However, in

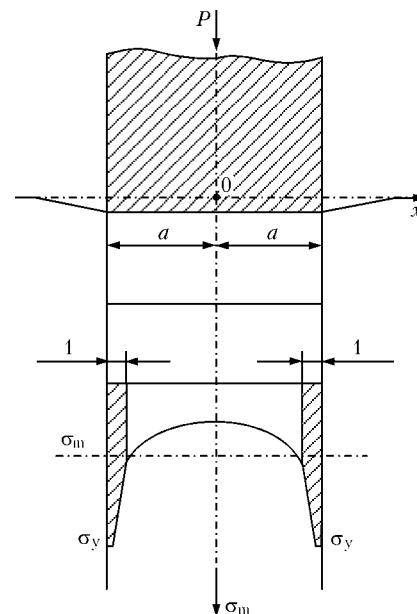


Figure 2. Scheme of compression stress distribution under rigid press tool

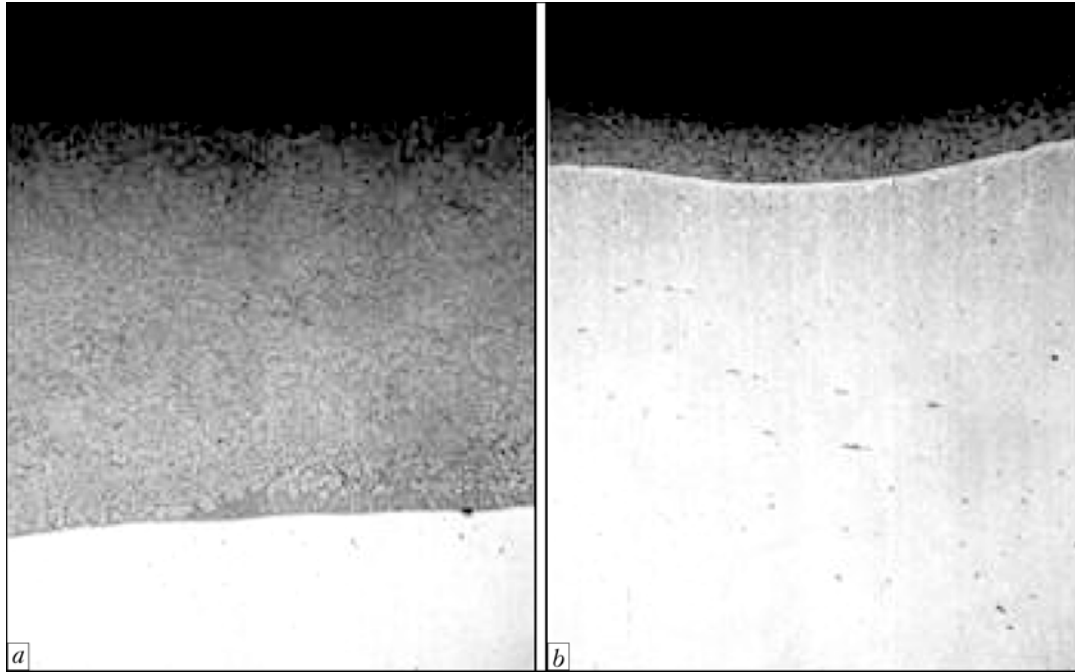


Figure 3. Macrostructure of coating under imprint in Brinell hardness test with coating thickness 2.5 (a) and 0.5 (b) mm ($\times 30$)

practice value of this pressure can achieve only compression yield strength of the component material [8].

In surfacing of the layers with high hardness and respectively high yield strength, in case of compression in the stress concentration area near sharp edge of the seat a situation may occur, in which stresses that achieve base metal of the gate with undoubtedly lower yield strength will cause in it a certain compression plastic strain. In this case hard layer of the coating may get additional bend strain and fail because of its low plasticity. This process is aggravated by the fact that during opening and closing of the valve near sharp edge of the seat a traveling wave of the bend stresses occurs in the gate. These stresses, occurring near sharp edge of the seat, are similar to stresses in a resilient body from the force applied to its surface along the line. They have maximum value near the body surface and reduce in its deep layers [8]. That's why it is possible to prevent hazard of failure of the hard coating layer by increasing its thickness up to the value, at which stresses under the coating get below yield strength in compression of the gate steel base.

On the basis of these ideas an approximate estimation of minimum thickness of the deposited layer, which guarantees reliable operation of the shut-off

components of PCT valving, was made. For calculating minimal thickness of the coating, able to withstand stresses near sharp edge of the seat, dependence of the compression stress inside a semi-infinite resilient body at the distance δ from its surface, caused by the distributed per unit of its length linear load p_s applied to the resilient body surface, was used [8]:

$$\sigma_s = 2p_s/\pi\delta, \quad (2)$$

where p_s is the linear load on the gate, N/mm, applied to the area of 1 mm width along sharp internal edge of the seat, within which stresses sharply increase up to the yield strength when material of the coating is compressed; σ_s are the stresses equal to the yield strength, when steel under the coating is compressed, MPa. Then δ will turn out to be equal to δ_{\min} , i.e. to the minimal thickness of the coating in millimeters, at which stresses in the steel will not exceed its compression yield strength:

$$\delta_{\min} = 2p_s/\pi\sigma_s. \quad (3)$$

Such approximate calculation of the coating minimal thickness has right for existence because elastic modulus of the coating material and of the steel base coincide and constitute about $2.1 \cdot 10^5$ MPa [9]. For approximate estimation of the compression pressure, which acts on the edge area of 1 mm thickness, mean value of the pressure was accepted for it. In this area it sharply increases from approximately mean specific pressure (quotient from division of general force of compression of the components by the whole area of the contacting surfaces) up to the compression yield strength of the coating material. Mean specific pressure of the gate on the seat in the valves with nominal diameter Dn 80 is about 10 MPa at working pressure 70 MPa. Compression yield strength of the coating brittle material

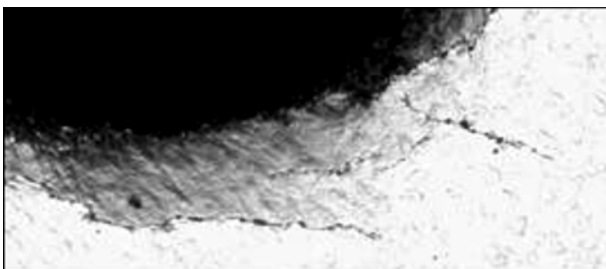


Figure 4. Macrostructure of coating of 0.5 mm thickness in Brinell hardness test with crack near imprint ($\times 30$)



with high hardness ($HB\ 555$) is close to its tensile strength, which constitutes approximately 1900 MPa [10, 11]. Then linear load on the gate on the side of a strip of 1 mm width along sharp internal edge of the seat constitutes in case of change in it of the compression stress from the mean one to the compression yield strength after multiplication by width of the strip equal to 1 mm:

$$p_s = 110 + (1900 - 110) / 2 \sim 1005\ \text{N/mm}.$$

Plastic steels, from which components of the shut-off unit are made, for example steel 40Kh, are characterized by coinciding by the value tensile and compression yield strengths [10]. Value of tensile and respectively compression yield strength of such steels was determined by the value of their Brinell hardness [12]:

$$\sigma_s = 0.367\ HB - 24\ \text{kgf/mm}^2.$$

Hardness of steel 40Kh in the HAZ metal of the deposit is $HB\ 179$, and according to [4] its yield strength equals approximately 420 MPa. Calculated on the basis of these data according to (3) minimal thickness δ_{\min} of chrome-nickel coating with carbon, boron and silicon on the shut-off unit components of the PCT direct-flow valves, designed for operation at the pressure up to 70 MPa, is approximately 1.5 mm.

Ability of thicker coatings in contrast to the thinner ones to withstand without failure concentrated loads is confirmed by measurement of their Brinell hardness. Hardness of the deposited layers of 2.5 and 0.5 mm (after machining of layer 2.5 mm thick) thickness was measured, whereby influence of the stirring zone on properties of the deposited metal layer of 0.5 mm thickness was brought to minimum.

As showed our investigations, in plasma-powder surfacing by mentioned alloys distribution of the alloying elements over thickness of the layer is uniform, and the deposit metal has at the distance above 0.1 mm from the fusion line the same structure and hardness as all over the deposited layer section. That's why measured Rockwell hardness of the layers of 2.5 and 0.5 mm thickness was the same and constituted $HRC\ 47$. In measurements of hardness of the coating surface of 2.5 mm thickness, using standard Brinell method, imprints of 2.6 mm diameter were formed, which corresponded to the hardness $HB\ 555$, and deformation of the coating in this case did not occur (Figure 3, a). When, under the same conditions, hardness of layer of 0.5 mm thickness was measured, imprints of 3.45 mm diameter were formed, whereby thin coating experienced sag (Figure 3, b), and around the imprints annular and radial cracks were formed (Figure 4).

Plasma-powder surfacing of components of the PCT valve shut-off units is performed within one pass by a layer of 3 mm thickness. In ready components the deposited layer is brought after careful treatment to the 2 mm thickness. Such thickness of the hard deposited layer is necessary, first of all, for guaranteed

ensuring of the valve operation under high pressure without destruction of this layer. In addition, a certain reserve of thickness in comparison with the designed one ensures possibility for repair of the valve shut-off unit components by repeated grinding of their working surfaces.

It follows from the mentioned above that in the PCT direct-flow valves only coatings of sufficient thickness can be used, which have high density and strong adhesion to the base metal. Because of this reason thin coatings, produced by plasma, vacuum or detonation spraying, are not used in components of the PCT direct-flow valves of the shut-off units, which is confirmed by numerous unsuccessful attempts of using these methods in practice.

High resistance of the shut-off unit components after plasma-powder surfacing of their working surfaces is confirmed by long positive experience of operation of the valves, produced by «IF Elterm» company, on gas fields of Ukraine.

CONCLUSIONS

1. Plasma-powder surfacing of the components of the shut-off units of high-pressure oil-and gas PCT direct-flow valves by chrome-nickel alloys, containing carbon, boron and silicon, ensures due to high hardness and resistance against corrosion and erosion wear their high serviceability and reliability.

2. It is established by the calculation that for proper operation of the components of the PCT valve shut-off units at 70 MPa pressure the deposited layer from chrome-nickel alloys, containing carbon, boron and silicon, should have thickness not less than 1.5 mm.

1. Vajsberg, G.L., Rimchuk, D.V. (2002) *Flow safety: Questions. Answers*. Kharkiv.
2. Guliantz, G.M. (1991) *Borehole blowout preventer equipment resistant to hydrogen sulphide*: Refer. book. Moscow: Nedra.
3. Artemov, V.I., Kanakov, V.V., Maksymov, Yu.V. et al. (2001) Christmas tree for pressure up to 70 MPa. *Naftova i Gazova Promyslovist*, **3**, 25–28.
4. Gurevich, D.F., Shpakov, O.N. (1987) *Reference book of designer of pipeline fitting*. Leningrad: Mashinostroenie.
5. Gladky, P.V., Pereplyotchikov, E.F., Rabinovich, V.I. (1970) *Plasma cladding in power armature engineering*. Moscow: NIIinformtyazhmash.
6. Pereplyotchikov, E.F. (2004) Plasma-powder cladding of wear- and corrosion-resistant alloys in valve manufacturing. *The Paton Welding J.*, **10**, 31–37.
7. Shevtsov, V.L., Majdannik, V.Ya., Khanenko, V.M. et al. (2001) Production of Christmas tree for deep oilers and gassers by methods of electroslag casting and plasma-powder cladding. *Svarshchik*, **4**, 8–9.
8. Bezukhov, N.I. (1968) *Principles of theory of elasticity, plasticity and creep*. Moscow: Vysshaya Shkola.
9. Knotek, O., Lugscheider, E., Eschnaner, H. (1975) *Hartlegierungen zum Verschleiss*. Duesseldorf: Schutz.
10. (1993) *Resistance of materials to deformation and fracture*: Refer. book. Part 1. Ed. by V.T. Troshchenko. Kiev: Naukova Dumka.
11. Tin Ming Wu (1964) *Untersuchungen ueber das Auftragschweissen von gesenken fuer schmiedestuecke aus Stahl*. Forschungsberichte des Landes Nordrhein. No.1349. Westfalen.
12. Markovets, M.P. (1979) *Determination of mechanical properties of metals by hardness*. Moscow: Mashinostroenie.

COMPUTER SYSTEM OF MONITORING THE TECHNOLOGICAL PARAMETERS OF ESW

Yu.N. LANKIN

E.O. Paton Electric Welding Institute, NASU, Kiev, Ukraine

The computer system for acquisition, processing, display and storage of the data on technological parameters of the ESW process is described.

Keywords: electroslag welding, parameter control, computer system, research automation

The system is designed for acquisition, displaying, saving and processing of technological parameters of welding, as well as producing the protocol of the electroslag welding (ESW) process, and is used for automation of research of this process in the laboratory, while being easily adaptable to production conditions.

Block-diagram of the above system is given in Figure 1. Welding machines of the last generation, for instance AD-381, have separate drives 3, and independent welding sources 1 for each electrode. In keeping with that the following parameters of the welding process mode are controlled: current of the first I_1 and second I_2 electrodes; voltage on the first U_1 and second U_2 electrodes; feed rate of the first v_1 and second v_2 electrodes; carriage displacement speed (welding speed) v_w and carriage position L_{car} .

Parameters measured during welding are displayed in the digital form and in the form of real-time oscillograms (Figure 2, a). At the same time, they are recorded into a binary file on the computer hard disc. Electric parameters of the ESW process, and even more so the electrode feed rate and welding speed change relatively slowly. Only in rare cases, for instance, when studying the process of transfer of molten metal drops at electrode melting, the frequency component of current (voltage) of more than 10 Hz is investigated. In most of the cases it is sufficient for the measurement period to be not more than 1 Hz, which is implemented in this system.

An eight-channel module of analog input I-7017 of ICP DAS (Taiwan) with a 16-channel ADC was used as the converter of analog signals into digital form (see Figure 1, position 8). To reduce electromagnetic pick-up in the measuring wires this module as a component of block 1 is located near welding current

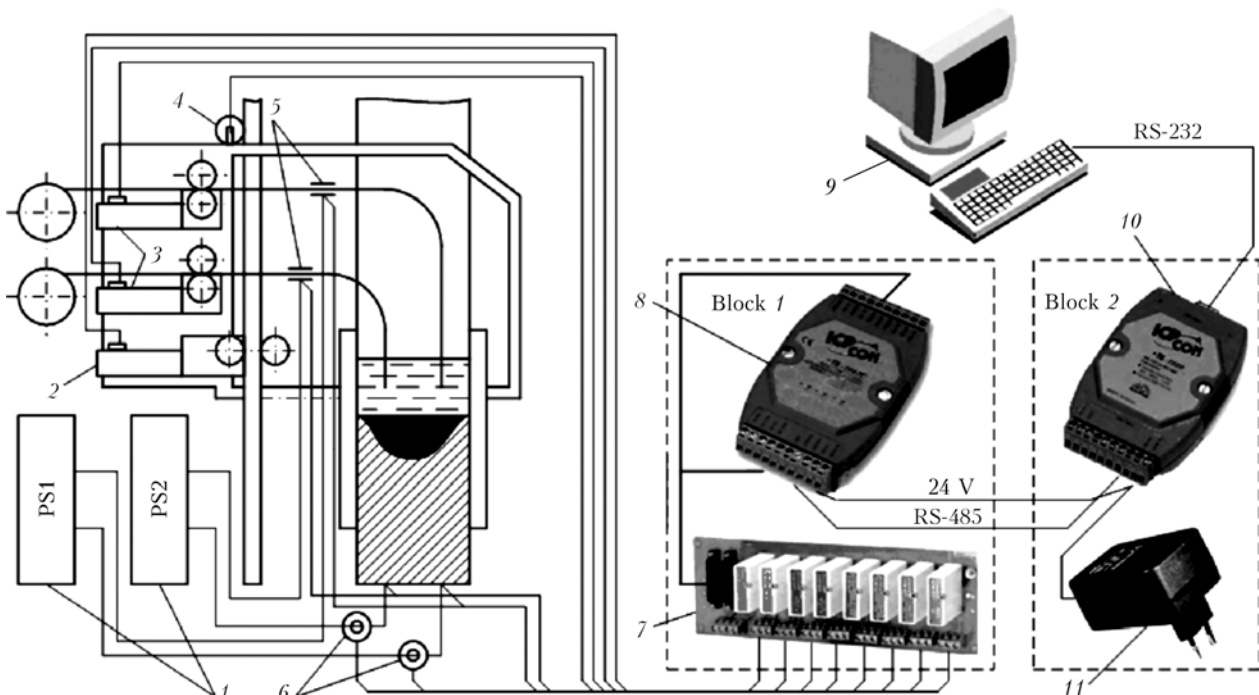


Figure 1. Block-diagram of the data acquisition system: 1 — welding power sources; 2 — carriage motor; 3 — motors (drives) of electrode wire feed; 4 — carriage displacement drive; 5 — current supplies; 6 — welding current sensors; 7 — sensor signal normalizers; 8 — module of analog-digital converter (ADC); 9 — computer; 10 — interface converter module; 11 — power source

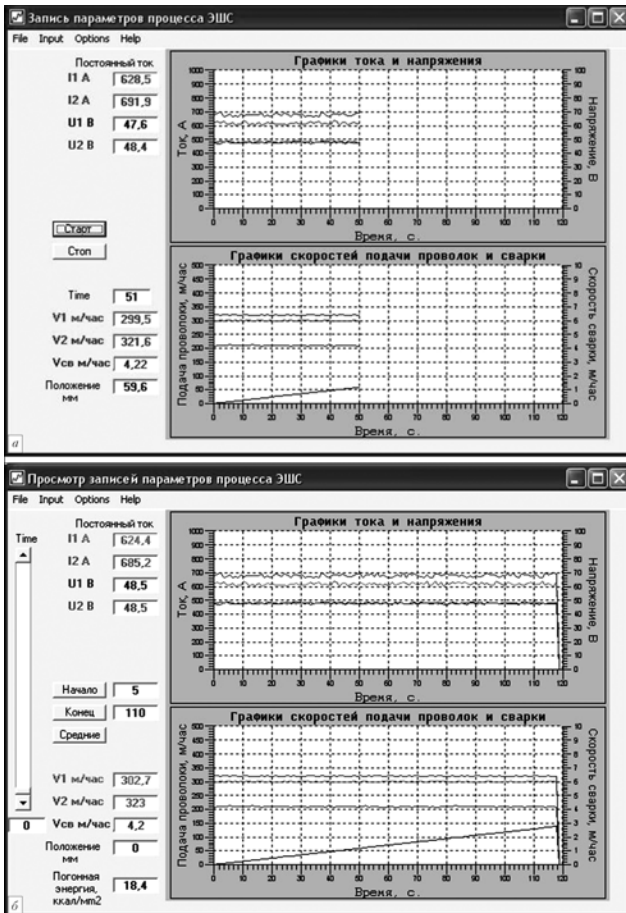


Figure 2. Screens of control and displaying of the data in the mode of recording of the measured ESW parameters during welding (a) and viewing the files of recorded ESW parameters (b)

sensors 6 with the lowest values of output voltage. In DC welding this is usually the shunt for current measurement. Thus, it is possible to eliminate additional amplifiers, setting the module input range at ± 150 mV. Signals of the controlled parameter sensors come to the inputs of module I-7017 through signal normalizers (see Figure 1, position 7). In our case these are just voltage dividers and simplest RC-filters with a time constant equal to 1 s. Voltages of tachometric bridges are used for measurement of the motor rotation speed. Carriage position is determined using a potentiometer (Figure 1, position 4).

Measurement module I-7017 is connected to module I-7520 by two strand pairs (see Figure 1, position 10) — two power leads and two wires of serial interface RS-485. Module I-7520 and power source 11 of both the modules are in block 2 located near computer 9. Module I-7520 is used for conversion of the industrial serial interface RS-485 into a computer standard interface RS-232, for which the cable length should not exceed several meters. In its turn RS-485 interface provides a reliable connection with the transfer rate of up to 115.2 kbaud for up to 1.2 km distance. This is more than enough for system application not only in the laboratory, but also on the shop floor. ADC module I-7017 can be connected to the computer without any wires at all, which is sometimes necessary, for instance in welding in site. For this purpose, the

Figure 3. Screen for entering the initial welding parameters

interface conversion module I-7520 is replaced by a radiomodem of SST-900EXT type manufactured by the same company, which has the communication range of up to 800 m. In this case, however, the system cost increases 2 times.

For saving the experimental data into a file «New» option is selected from «File» menu (Figure 2, a). In the opened dialogue panel the current date is automatically saved in the file name for its identification. If required, the file name can be changed manually. Recording is started by pressing «Start» button.

Results of any experiment saved in the data file can be viewed by loading it using «File Open» command from «File» menu. All the plots are automatically displayed on the computer screen (Figure 2, b). Any measurement is chosen using the scroll band «Time». Numerical values of all the parameters are displayed. «Start» and «End» buttons can be used to specify any selected measurement as the start or end of ESW process parameter averaging range. When «Average» button is pressed the average values of ESW parameters in the selected interval are calculated and displayed, and the welding heat input is calculated by the following formula and displayed:

$$W_{h,i} = \frac{0.24(U_{1\text{av}}I_{1\text{av}} + U_{2\text{av}}I_{2\text{av}})\eta}{v_w S}$$

where η is the ESW efficiency, dependent on thickness S of the metal being welded*. All these data are automatically recorded into the file of the welding process protocol. Naturally, if average values of ESW process parameters in different averaging ranges are determined for one experiment, the automatically set file name has to be corrected manually.

The window for entering ESW parameters is called from «Input» menu (Figure 3). ESW parameters, comments and remarks are entered into the respective character windows from the keyboard. Scroll band is

* Yushchenko, K.A., Lychko, I.I., Sushchuk-Slyusarenko, I.I. (1999) Effective techniques of electrosag welding and prospects for their application in welding production. In: *Welding and Surfacing Rev.*, Vol. 12, Pt 2. Kiev: E.O. Paton Electric Welding Institute. 108 p.



PROTOCOL	
Date 11-01-2006	Time 16:01:23
Tyukalov V.G., Moskalenko A.A. Welding with current switching. Switching frequency 1 Hz	
Sample being welded	
Material:	10KhSND steel
Thickness	32 mm
Gap bottom	28 mm
Gap top	28 mm
Joint type and groove shape: Butt U-shaped	
Wire	
Grade:	Sv10NMA
Diameter	3 mm
Quantity	2
Dry extension	90 mm
Flux	
Grade:	AN-8
Slag pool depth	50 mm
Baking 20 h at the temperature of 400 deg	
Power	
Source:	TShS-1000-3
Kind of current:	alternating
Polarity	–
Welding parameters averaged when making the weld between 5.8 and 128.4 mm	
Start of welding this weld section 5 s, end – 110 s	
Current of electrode #1	624.4 A
Current of electrode #2	685.2 A
Voltage on electrode #1	48.5 V
Voltage on electrode #2	48.5 V
Feed rate of 1st wire	302.7 m/h
Feed rate of 2nd wire	323 m/h
Welding speed	4.2 m/h
Specific heat input	18.4 kcal/cm ²

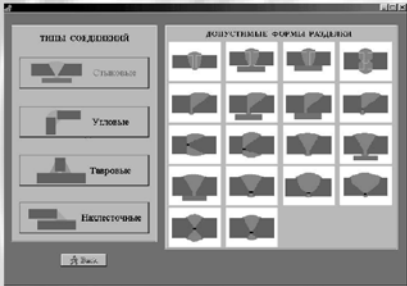
Figure 4. Welding process protocol

used to select joint type and groove shape in the list window. A graphic image of the butt with the groove is shown on the right of the groove list window (Figure 3). «Save» option in «File» menu is used (Figure 2, b) to save the entered data into the protocol file, the name of which is assigned automatically and coincides with the data file name, differing only by

the extension. When «Print» option is pressed, the protocol is printed out (Figure 4).

The kind of current of ESW power sources is selected in «Options» menu. The graphs are taken to the printer by selecting «Print UI» or «Print V» from «File» menu in «ESW parameter recording» and «ESW parameter viewing» windows.

COMPUTER SYSTEM TO DESIGN TECHNOLOGIES FOR WELDING LIGHT ALLOYS



Purpose. The computer system is intended for design of technologies for electric arc welding of light alloys with different alloying systems. It allows selection of shape of the weld groove, welding consumables, welding method and parameters depending upon the geometric features of a welded joint, base metal grade and other welding conditions. To make an optimal decision, a user is given an information support in the form of comparative characteristics of welding methods by 10 indicators, as well as information on welding-technological characteristics of non-consumable electrodes. Result of operation of the system has the form of a flow sheet.

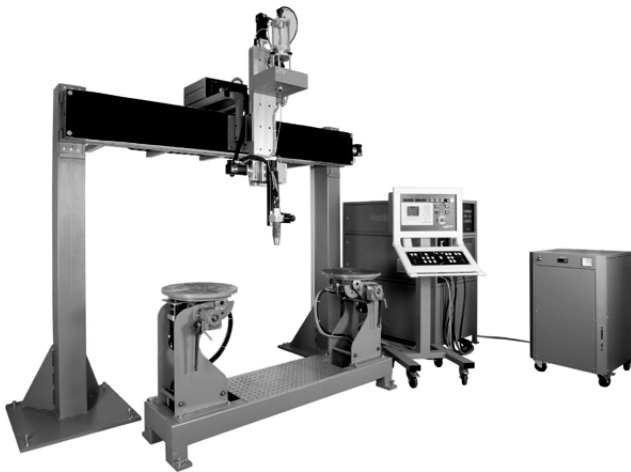
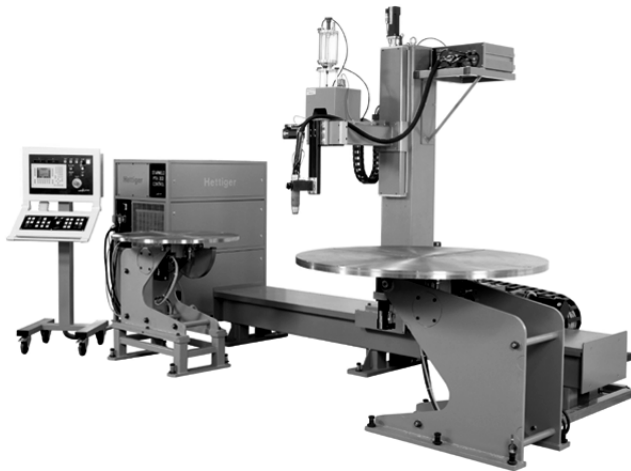
Application. The system can be applied at machine building enterprises, technology and design bureaus, as well as at higher education institutions for training welding engineers.

Contacts: Prof. Makhnenko V.I.
E-mail: d34@paton.kiev.ua



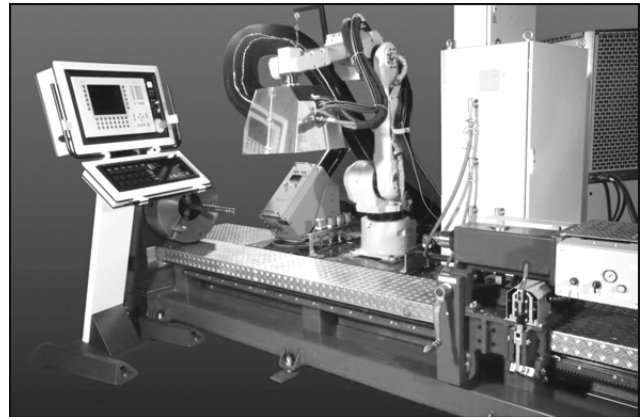
NEW JOINT VENTURE IN DELORO STELLITE GROUP ---- DS URAL

DS Ural (Krasnokamsk, Perm Territory, Russia) ---- the twelfth link in system of the Deloro Stellite Group enterprises ---- started its working history.

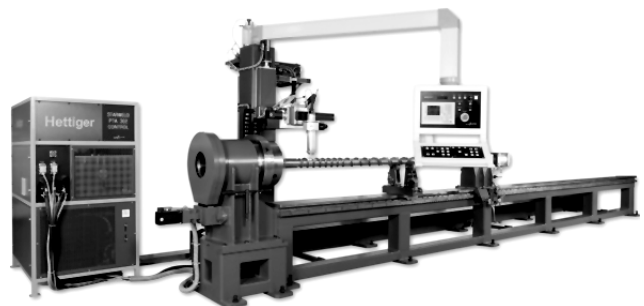


DS Ural was conceived as a joint venture and established by the known Perm Oil Machine-Building Company (Perm), New Machine-Building Plants (Perm), Technological Center TENA (Moscow), and Deloro Stellite Holding GmbH and Co KG (Koblenz, Germany). This enterprise is specialized in fulfillment of orders on surfacing and spraying of special-purpose parts of industrial equipment for the purpose of ensuring their high wear resistance and longer service life. The bay of gas-flame spraying is already commissioned, and launching of the installation for supersonic

(Jet Kote®) and plasma spraying, which meets state-of-the-art requirements of the world market, is at the final stage. For surfacing and spraying the Deloro Stellite original materials are used, which are known all over the world by trade marks Stellite® and Trib-alloy ---- cobalt-base alloys, Deloro®, Nistell® ---- nickel-base, and other resistant to wear, corrosion and high temperature alloys.



State-of-the-art technologies and spraying materials, proposed by the DS Ural enterprise, will allow machine-builders of the region and Russia as a whole and customers from the near and far abroad to fabricate their specialized equipment according to the highest world standards. DS Ural will provide with reliable long-lasting items producers and consumers in such fields as oil production and processing, power engineering and engine-building, mining, chemical, paper, food, metallurgical, glass, and other industries.



DS Ural has intellectual, technical and economic potential, which allows producing high-quality products at the top state-of-the-art technical level.

STEEL-REINFORCED CONCRETE CONSTRUCTION WITH TECHNOLOGY OF WELDING FLEXIBLE STOPS

The main peculiarity of new efficient structures is ideal combination of several different building materials. Advantageous combination of steel with its high tensile strength and plasticity and concrete with its high compression strength and good corrosion resistance has been recognized since long in the building industry. Application of steel-reinforced concrete structures in construction allows combining positive features of steel and concrete. It means that steel frame of the structure is integrated with concrete parts in such way that the effect of joint work is created.



Steel beams take tensile forces, and concrete elements — compression forces and, in addition, they ensure protection against fire. Application of cold-forged stops enables development of large-scale steel-reinforced concrete construction. Main advantages of steel-reinforced concrete construction are as follows:

- reliability and safety in static and dynamic loads;
- mechanical connection of steel and concrete, prevention of break-off of a concrete slab;
- high plasticity and significant increase of the load-carrying capacity due to consideration in the design of plastic stage of the work;
- anchoring of steel parts in concrete, which allows withstanding loads, applied in different directions, and absence of cracking caused by mechanical fixing;
- individual design solutions on reinforcement by preliminary location of steel elements in the concrete;
- strong welded joints of flexible stops in case of insignificant deformation of the metal.

Present steel-reinforced concrete bridges would be inconceivable without dowel stops. In big bridges several hundred thousand stops are often used, which ensure long-lasting connection between load-carrying steel structures and reinforced concrete slabs of the traffic area. Designing of steel-reinforced concrete bridges with application of cold-forged flexible stops started in Ukraine comparatively recently. In particu-

lar, Podol-Voskresenka bridge passage over the Dnepr river (Kiev) and bridge passage over the Dnepr river (Zaporozhie) have such design. Similar steel-reinforced concrete design has bridge passage over river Prut in Ivano-Frankovsk oblast. On this object the enterprise «Ukrspetsterm» Ltd. performed the welding of flexible stops to steel beams.

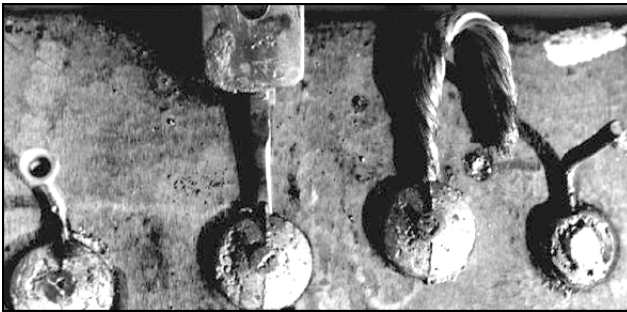


According to the design flexible stops of 200 mm length and 22 mm diameter in amount of 5488 pieces were welded. Welding was performed with application of ceramic rings, which ensured protection and formation of a weld according to DIN EN ISO 14555. Quality of the flexible stop welding depends not just upon precise observance of the welding procedure, but also on correct functioning of the acting mechanism (for example, a welding gun), state of the components, auxiliary equipment, and power supply. The whole complex of works, connected with welding of the stops, was fulfilled within 12 days, taking into account marking and cleaning of the beams under mounting and unstable weather conditions. The welding was performed by the U1151 single-gun installation, produced at «Ukrspetsterm» Ltd. On average about 500 stops per shift were welded. Welding technology was corrected, taking into account specific conditions, depending upon places in the structure, in which welding was performed.



THERMIT WELDING OF ECP OUTLETS TO HIGH PRESSURE PIPELINES

The known thermit (exothermal) welding process is a simple and safe method, which does not require for application of the external power source for producing copper-copper, copper-steel joints or welding of the steel parts functioning as electric conductors. For welding of the electrochemical protection (ECP) outlets to the pipeline reusable graphite crucible-mould of TFT grade or disposable ceramic cartridges are used. Surface of the pipe is carefully cleaned of residues of insulation, soil and dust. End of the conductor and the place of welding on the pipe are cleaned by a file up to the metal gloss.



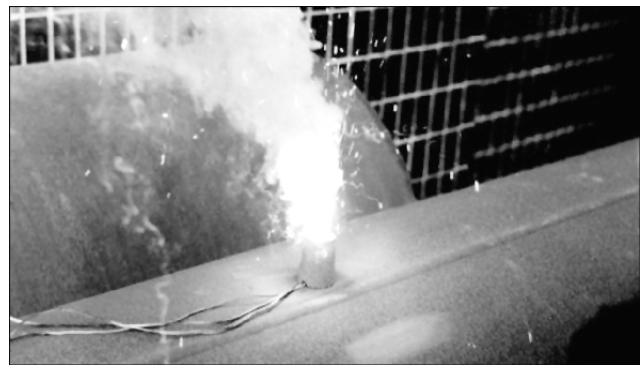
On bottom of combustion chamber of the crucible-mould a copper membrane is placed. The thermit mixture is carefully mixed and poured into the crucible. Ignition of the thermit mixture is performed by the thermit match, installed through the ignition hole of the crucible-mould.

After one minute elapses, the welder removes the mould, and the welded contact is cleaned of slag. After cooling down the section of the pipe with the welded contact is insulated.

Thermit welding ensures the best contact of the conductor with the pipe, not subjected to corrosion.

In the process of welding maximal temperature on the pipe surface does not exceed 100 °C, and at the depth of 2 mm --- 450 °C, whereby such thermal action lasts several seconds, which can not be ensured in arc methods of welding.

Thermit welding is a permitted and preferable method of welding of the ECP outlets to high-pressure pipelines, officially registered in respective departmental normative documents.



The exothermal method of welding optimizes cathode anticorrosion protection due to improved and reliable connection of the system components. This method ensures production of reliable, corrosion-resistant compounds.

For construction of anticorrosion protection using this method it is possible to welding each to other the following components: copper cable of 2.5--200 mm² and higher section; solid copper conductors of any shape of up to 250,000 mm², and welding of copper or steel conductors to any metal structures, including high pressure pipelines.

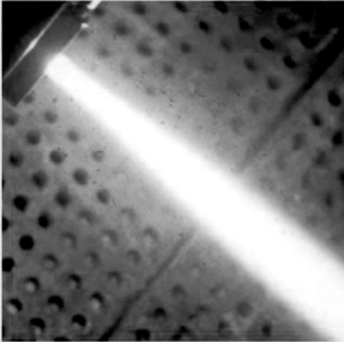
CASPSP-3.12 SOFTWARE FOR COMPUTER SIMULATION OF PLASMA SPRAYING PROCESS

At the E.O. Paton Electric Welding Institute of NASU a package of applied programs for computer simulation of turbulent plasma jets, used in plasma application of coatings, and for modeling of the movement and heating of the particles being sprayed, has been developed. It allows rather quick quantitative estimating spatial distribution of temperatures and speed of plasma in the jet; trajectories, speeds and thermal condition of the particles being sprayed, depending upon parameters of the spraying process. This software is useful for specialists, post-graduate students and students, dealing with the plasma spraying issues.

CASPSP-3.12 is a new version of the software and contains two interconnected modules: CASPSP --- Simulation of Plasma Jet, and CASPSP --- Simulation of Spray Particles.

This software has user-friendly interface (English language), which includes the following systems for each module: management menu, input-output and data processing system; system of graphic presentation and printing-out of the simulation result; help system.

The first module is designed for simulation of the turbulent plasma jets created by the plasmatron with a smooth channel, escaping into the environment at



CASPSP
 Software Package for
 Computer Aided Simulation
 of Plasma Spraying Process
 Version 3.12

Developed by
 Prof. Yu.S. Borisov
 Dr. I.V. Krivtsun and
 Mr. A.F. Muzhichenko

Licensed to: BNTU
 (serial # 3.12/0010)

Copyright © 1996-2005 E.O. Paton Electric Welding Institute

Second module is designed for simulating behavior of the particles being sprayed in the plasma jet with preliminary calculated distributions of plasma temperatures and speeds. A respective computer program is based on the mathematical model of heating and acceleration of the particle being sprayed, which is described by the non-linear equation of heat conductivity and equation of a spherical particle movement in the plasma flow. This module allows calculating and representing trajectory of movement, speed and temperature field of the particle being sprayed, depending upon the material and initial diameter of the particle and conditions of its introduction into the plasma jet.

atmospheric pressure. A respective computer program is based on the mathematical model of gas dynamics and heat exchange in thermal arc plasma, described by the system of MHD-equations in approximation of the turbulent boundary layer. This module allows calculating, presenting and printing-out spatial distributions of temperatures and speeds of the plasma jet, allowing for the electric arc processes proceeding in the plasmatron depending upon size of its anode-nozzle, arc current, composition, and flow rate of the plasma gas.

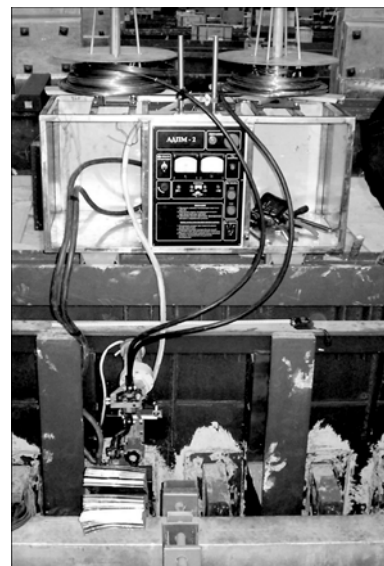
New version of the software allows choosing different measurement units in entry and output data: sizes (µm | in), temperature (K | °F | °C), gas flow rate (SLPM | SCFH), powder consumption (kg/hr | lb/hr), plasma gas (Ar, N₂, Ar + H₂, Ar + He), material of the particles (Al, Cu, Mo, Ni, Ti, Al₂O₃, Cr₂O₃, Fe₃O₄, TiO₂, ZrO₂, Cr₃C₂, TiC, WC, CaF₂, chromic cast iron).

The software was already purchased by a number of companies of USA, Canada, Germany, Belarus, Ukraine, RF, Sweden, Italy, and Switzerland.

AUTOMATIC ARC WELDING BY EMBEDDED ELECTRODE OF COMPACT SECTION COMPONENTS UNDER ERECTION CONDITIONS

In 2006 at Irkutsk aluminium plant (Shelekhov, Irkutsk oblast, RF) a new development of PWI --- electric arc welding by embedded electrode of the compact section components --- was tested. The work was connected with welding of plates with flexible chutes to steel cathode blooms of 80 × 220 mm section in construction of the series 5-1 of IrkAP (two workshops with 104 electrolytic furnaces, designed for the 330 kA current, in each). According to the design it is required to weld in each electrolytic furnace 80

joints (40 on each side), i.e. all together more than 6 thou joints in both workshops. For fulfillment of this large-scale work the PWI specialists developed a new technology, a specialized equipment (the ADPM-2 device), and welding consumables (PP-ANPM1 wire and ANPM-8 embedded electrodes), which allowed ensuring required productivity and quality of the





welded joints. The main difficulty in solution of this task consisted in constrained conditions, under which the erection works had to be carried out, and negative temperatures (up to $-40\text{ }^{\circ}\text{C}$). The developed equipment --- the ADPM-2 welding device complete with the technological fitting-out for assembly of the joint and formation of the weld --- is characterized by compactness, which is especially important under erection

conditions. The device has two modifications --- for welding of the right and the left blooms. The «Selma» VDU-1250 welding rectifier is used as the welding current source. Machine time of the joint with 16--18 mm desired gap is 10--12 min, due to which productivity of one device up to 15 joints per a shift is achieved.

TURBOATOM IS ON THE RISE

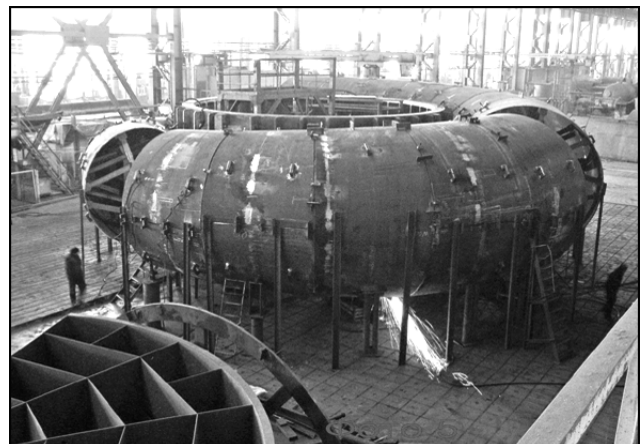
«Turboatom» Ltd. (Kharkov, Ukraine) constantly increases rate of fabrication of power engineering equipment for nuclear, heat and hydraulic power plants of Ukraine and countries of near and far abroad. For example, timely and in full volume orders on manufacturing of equipment for hydroelectric power station «El Kahon» (Mexico) and for NPP «Kaiga» and «Ragistan» (India) were fulfilled. One K-325 turbine was fabricated for heat power station «Aksu» (Kazakhstan) and fabrication of the other one is in final stage.



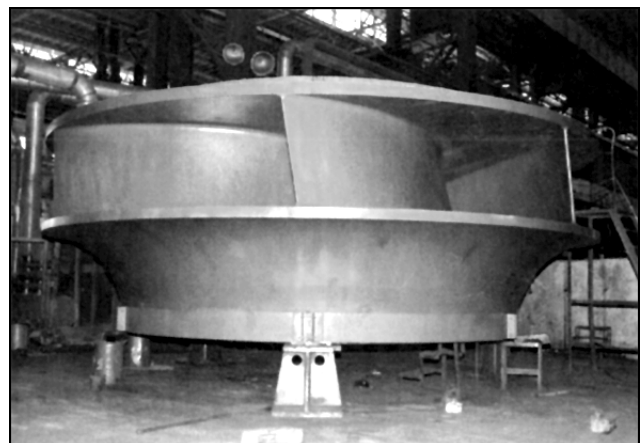
Several turbines were also fabricated for Kama hydroelectric power station (Russia). Fabrication of the turbine and its units for the Dnestr pumped storage station, the design of which is original and has not analogues in the world, is over. Stage-by-stage modernization of hydroelectric power stations of the Dnestr cascade, which includes Dneprodzerzhinsk, Kakhovka, Kiev, Kanev and other stations, continues. Their modernization will allow replacing outdated equipment, the service life of which is over, for new, highly efficient, environmentally clean one, increasing efficiency and total power of the cascade of hydroelectric power stations by 350 MW, and ensuring increased reliability of operation of hydraulic units by application of new structural and functional materials, improving diagnostic system of the power engineering equipment, and increasing export of electric power.

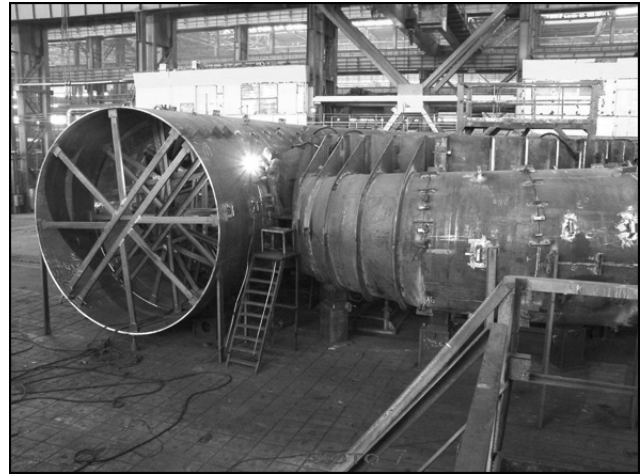
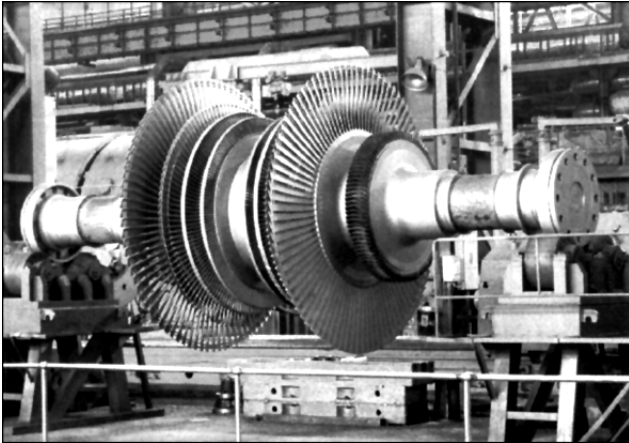
A large-scale technical re-equipment and modernization of the production equipment is underway at the enterprise. New resource-conservation technolo-

gies are being introduced. Welding operations constitute a significant share in fabrication of the power-engineering equipment. It is planned to replace outdated power sources, automatic and semiautomatic welding machines for state-of-the-art ones and introduce new welding technologies for improving quality characteristics of the fabricated products. Taking into account increasing requirements to reliability of the fabricated turbine units and increase of their power with simultaneous reduction of their specific consumption of materials, new equipment is purchased for destructive and non-destructive quality control.



In 2006 «Turboatom» Ltd. won in bitter competition the tender, arranged in India, on modernization of the power-generating unit of NPP «Narora». Positive decision in the tender was ensured due to state-





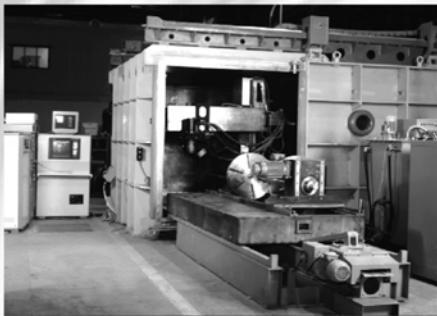
of-the-art level of production, high skill of the engineering services, marketing service, efficient work of the managerial personnel, and improved executive labor discipline.

Within 2006 volume of production increased by 15 % and net profit constituted UAH 22.2 mln, which exceeded planned parameters. Availability of the current assets allowed updating the production equipment, financing scientific-research works, and carrying out socially oriented programs. Average monthly salary of employees of the enterprise increased by 70 % and equals at present UAH 1325, and that of the piece-workers increased by 94 % and equals UAH 2410. Salary increase and solution of different

social tasks ensured reduction of the labor turnover and inflow into the enterprise of young workers, which are provided, if necessary, with hostels. Within 2006 more than 100 working places were organized. Courses for training of workers of the main occupations are organized: welders, machine operators, and metallurgists.

For 2007 further growth of the production volumes is planned in comparison with the previous year, achievement of which under conditions of well thought-out organization of production is deemed quite realistic.

UNIVERSAL MACHINE FOR ELECTRON BEAM WELDING MODEL 102



- Universal production machine for EBW of a wide range of cylindrical and flat workpieces.
- PC and programmable controllers are used.
- Real-time seam tracking and monitoring of EBW process by RASTR-3 system on the basis of secondary electron emission.
- Power source with the electron tube flashless system.
- Mobile type 15, 30 or 60 kW electron beam gun at 60 kV.

Machine design

The work chamber has two sliding doors. For loading and unloading, the workpiece table is moved out of the work chamber onto the runout platform. This is especially necessary for welding of large heavy workpieces with commensurately large clamping devices. The table accommodates the universal rotator with horizontal or vertical axis, and back centre. The EB gun 3-axis-manipulator has the travelling distance in X-direction — 2000 mm, in Y-direction — 800 mm and in Z-direction — 800 mm. Precision of the guidance and drive systems equals that of the precision machine tools operation with tolerances in the hundredth-of-a-millimeter range.

The gun can be mounted in any spatial position and has an independent turbomolecular pumping system. The cathode area is isolated by a vacuum valve to keep the gun under vacuum when the work chamber is vented.

Application. Welding and repair in turbine engine fabrication; selection of welding technology for a wide range of workpieces.

Contacts: Prof. Nazarenko O.K.
E-mail: nazarenko@technobeam.com.ua